



Synthesis and Properties of Metal Oxide Thin Films by Liquid-Phase Deposition(LPD)

青井, 芳史

(Degree)

博士 (工学)

(Date of Degree)

1997-03-31

(Date of Publication)

2008-03-25

(Resource Type)

doctoral thesis

(Report Number)

甲1652

(JaLCD0I)

<https://doi.org/10.11501/3129762>

(URL)

<https://hdl.handle.net/20.500.14094/D1001652>

※ 当コンテンツは神戸大学の学術成果です。無断複製・不正使用等を禁じます。著作権法で認められている範囲内で、適切にご利用ください。



博士論文

Synthesis and Properties of Metal Oxide Thin Films
by Liquid-Phase Deposition (LPD)

液相析出法による金属酸化物薄膜の合成およびその物性

平成9年1月

神戸大学大学院自然科学研究科

青井 芳史

Acknowledgment

The study represented in the present thesis has been carried out under the guidance of Professor Shigehito Deki. The author is greatly indebted to Professor Shigehito Deki for his kind guidance and valuable discussions for this study.

The author also wishes to thank Professor Itaru Motooka and Professor Yoji Kawamoto for their valuable comments and advice.

The author wishes to express his sincere thanks to Dr. Yukio Kanaji, Professor Emeritus of Kobe University, Staff Assistants Akihiko Kajinami and Minoru Mizuhata for guidance, helpful discussions, precious comments, and hearty encouragement.

The author would like to express sincere thanks to Dr. Keisuke Oguro and Ms. Yasuko Ehara of Hydrogen Energy Section of Osaka National Research Institute, AIST for XPS measurement.

The author would like to express sincere thanks to Professor Ikuichiro Izumi and Mr. Yasuyuki Ohnishi of Nara National College of Technology for XPS measurement.

The author also would like to express sincere thanks to Dr. Hiroaki Tada of NSG Techno-Research Co. Ltd. for XPS measurement.

The author wishes to thank for the considerable assistance to Mr. O. Hiroi, Mr. A. Gotoh, Ms. J. Ikenaga, Ms. Y. Miyake, Mr. H. Kishimoto, Mr. Y. Asaoka, Mr. H. Yanagimoto, Mr. K. Akamatsu, Mr. K. Ishii, Mr. S. Yamahira, Ms. Y. Matsuura, Ms. N. Iwashita, Ms. S. Miyano, Mr. M. Uemura, Ms. T. Ebisutani, Ms. Hnin Yu Yu Ko, and all members of the Laboratory of Inorganic Applied Chemistry, Department of Chemical Science & Engineering, Kobe University.

Finally the author wishes to express his greatest gratitude to his parents and sisters for their continuous encouragement, without which the present work would be impossible to be finished.

Yoshifumi Aoi

Kobe, January 1997

要 旨

金属酸化物は、電氣的、光学的に種々の機能性を有しており、現在様々な分野において幅広く利用されている。これら機能性酸化物は、薄膜という形態で用いられることが多く、これまでその製膜法として種々の方法が開発・提案されている。それらは物理的製膜法と、化学的製膜法に大別され、前者としては気相法である蒸着法、スパッター等が、後者としては、気相法であるCVD、液相法であるsol-gel法等がよく知られている。これらの方法は、種々の酸化物および複合酸化物薄膜の合成に適用され、既に一部実用されている。

近年、これらの方法とは異なる新しいタイプの湿式製膜法として、液相析出(LPD)法が、 SiO_2 薄膜の合成法として開発された。この方法は、水溶液中での配位子置換(加水分解)平衡反応を利用して、酸化物薄膜を反応溶液中に浸漬した基板上に直接合成する製膜法である。この製膜法は、基板の形状の制約を受けず、比較的低温で、均一かつ緻密な薄膜を合成し得る新しい方法である。これまで、 SiO_2 薄膜に関しては、製膜条件の検討、析出機構、得られた薄膜の応用等の研究がなされているが、他の酸化物に対する研究は見られない。

本研究では、この液相析出法により、種々の酸化物薄膜および複合酸化物薄膜の合成を試み、その製膜条件の検討、反応機構の検討、そして得られた薄膜のキャラクタリゼーション、および、電氣的・光学的特性の評価を行った。

第1章(序論)では、本研究の背景について述べた。既存の様々な酸化物薄膜合成法について、その問題点について言及し、液相析出法の特色について概説した。また、現在までになされている液相析出法に関する研究を紹介し、本論文の取り扱っている内容について述べた。

第2章では、酸化チタン薄膜の合成を試み、得られた薄膜の光電氣化学的特性について検討した。 $(\text{NH}_4)_2\text{TiF}_6$ と H_3BO_3 の混合溶液中に基板を浸漬し数十時間反応させることによりアナターゼ型酸化チタン薄膜が得られた。反応溶液中の $(\text{NH}_4)_2\text{TiF}_6$ 濃度が低い領域では白色薄膜が、高い領域では干渉色を示す透明膜が得られた。この薄膜は、熱処理により結晶性が向上することが明らかとなった。得られた薄膜について、 $1 \text{ mol dm}^{-3} \text{ Na}_2\text{SO}_4$ 水溶液中で光電氣化学的特性について検討したところ、水分解による明瞭な光電流が観測され、薄膜の熱処理温度の増加に伴う光電流の増加が見られた。

第3章では、QCM法により、液相析出法による酸化チタン薄膜の析出過程をモニタリングし、遊離F⁻、 $(\text{NH}_4)_2\text{TiF}_6$ 、 H_3BO_3 濃度の析出速度に及ぼす効果について検討した。反応の初期段階においては、遊離F⁻が優先的に H_3BO_3 と反応し、析出の誘導期間が見られた。この誘導期間は、反応溶液中の遊離F⁻濃度に依存することを明らかにした。薄膜の析出速度は、 H_3BO_3 濃度の増加に伴い増加し、誘導

期間は減少した。また、 $(\text{NH}_4)_2\text{TiF}_6$ 濃度の増加と共に、析出速度が減少することを明らかにした。

第4章では、バナジウム酸化物薄膜の液相析出法による製膜を試みた。 $(\text{V}_2\text{O}_5\text{-HF})$ 水溶液と、金属Alとの反応により基板上に茶褐色の薄膜が得られた。析出直後の薄膜は非晶質であり、4価のバナジウムイオンから構成されていることが、IR、ESR測定より明らかとなった。この薄膜を空气中で熱処理することにより、 300°C では V_3O_7 および V_2O_5 の2つの相からなる薄膜が、 400°C では V_2O_5 薄膜をそれぞれ製膜することが出来た。反応溶液の可視吸収スペクトルより、バナジウムイオンは反応溶液中で4価のイオンとして存在していることが明らかとなり、 $[\text{VOF}_n]^{2-n}$ の加水分解反応によりバナジウム酸化物薄膜が形成されると結論した。

得られた薄膜の、 $1\text{ mol dm}^{-3}\text{ LiClO}_4/\text{PC}$ 溶液中でのエレクトロクロミック特性について検討し、 300°C 以上での熱処理膜では、Liイオンの挿入、脱離に対応した薄膜の色調変化、エレクトロクロミック特性を見出した。

第5章では、 $(\text{V}_2\text{O}_5\text{-HF})$ 水溶液と、金属Alとの反応により得られた薄膜を窒素雰囲気中で熱処理することにより VO_2 薄膜の合成を試みた。その結果、 400°C 以上での熱処理により VO_2 薄膜を得た。得られた VO_2 薄膜についてその半導体-金属転移挙動についての検討を試み、薄膜の電気伝導度の温度変化を測定した。 70°C 付近において明瞭な電気伝導度の増加を見出し、得られた VO_2 薄膜が半導体-金属転移を生じることを示した。その転移温度、転移前後における電気伝導度の比等の転移挙動は、薄膜の製膜条件(反応時間・熱処理温度)により異なる事を見出し、結晶性、 VO_2 以外の他の酸化物成分の存在等が転移挙動の違いの原因であると結論した。

第6章では、鉄酸化物薄膜の製膜を試みた。 $\text{FeOOH-NH}_4\text{FHF}$ と H_3BO_3 の混合水溶液中に、基板を浸漬し数十時間反応させることにより、結晶性の $\beta\text{-FeOOH}$ 薄膜を得た。反応溶液の H_3BO_3 濃度により、得られた $\beta\text{-FeOOH}$ 薄膜の結晶配向に違いが認められ、低 H_3BO_3 濃度時にはランダム配向性の、高 H_3BO_3 濃度時には $[211]$ 方向に優先配向した薄膜を得た。得られた薄膜を熱処理することにより、 $\beta\text{-FeOOH}$ 薄膜は非晶質相を経て 600°C で完全に $\alpha\text{-Fe}_2\text{O}_3$ 薄膜となった。 $\beta\text{-FeOOH}$ 薄膜は鉄イオンのフルオロ錯体 $([\text{FeF}_6]^{3-})$ もしくは一部加水分解されたイオン種 $([\text{FeF}_{6-n}(\text{OH})_n]^{3-})$ の配位子置換平衡反応(加水分解反応)により析出すると考えられた。

液相析出法は、水溶液中での反応を利用した製膜法であるが故に、多成分の酸化物薄膜の合成が容易であるという特徴を有している。そこで、第7章では、金超微粒子の分散した酸化チタン薄膜の製膜を試みた。 $(\text{NH}_4)_2\text{TiF}_6$ と H_3BO_3 の混合溶液に HAuCl_4 水溶液を添加し、そこに基板を浸漬することにより金イオンを含有する酸化チタン薄膜が得られた。XPS測定より、析出直後の薄膜中で金は Au^{III}

イオンとして存在していることが明らかとなった。薄膜中の金含有量は、添加する HAuCl_4 量により容易に制御可能であった。この薄膜に熱処理、もしくは、光照射処理を施すことにより Au^{III} イオンを還元し金超微粒子分散酸化チタン薄膜を得た。200°C 以上での熱処理により薄膜中に金超微粒子が生成し、可視吸収スペクトルに表面プラズマ共鳴に帰属される吸収が確認された。熱処理温度の増加による吸収ピーク位置の、長波長側への大きなシフトが認められた。これは、熱処理温度の増加によりマトリックスの結晶化が進行し、それによるマトリックスの誘電率の上昇が原因であると結論した。TEM 観察より薄膜中の金微粒子の粒径は約 15nm であった。また、析出直後の薄膜を光照射することによっても Au^{III} イオンは還元され、金微粒子が生成した。光照射時間の増加と共に表面プラズマ共鳴に帰属される吸収は増加し、その吸収位置は高波長側へシフトした。この結果より、光照射時間と共に薄膜中の金微粒子が増加し、その粒径が大きくなることが明らかとなった。この事は、TEM 観察からも確認した。

以上のように、液相析出法により種々の酸化物薄膜の合成を試み、得られた薄膜の評価、そして、その電氣的・光学的特性について検討した。これより、種々の遷移金属酸化物薄膜が、水溶液から非常にマイルドな条件下で析出させることが可能であるという事を明らかにした。

Contents

Abstract (in Japanese)	v
1 General Introduction	1
2 Titanium Oxide Thin Films Prepared by Liquid-Phase Deposition	9
2.1 Introduction	10
2.2 Experimental	10
2.2.1 Liquid-phase deposition process	10
2.2.2 Characterization of the deposited films	11
2.2.3 Photoelectrochemical properties of the deposited films	11
2.3 Results and Discussion	11
2.3.1 Characterization of the deposited films	11
2.3.2 Photoelectrochemical properties of the deposited films	15
2.4 Conclusion	18
3 Monitoring for Growing Process of Titanium Oxide Thin Films from Aqueous Solution by the Quartz Crystal Microbalance	21
3.1 Introduction	22
3.2 Experimental	22
3.2.1 Treatment solutions for the LPD method	22
3.2.2 QCM technique	22
3.3 Results and Discussion	23
3.3.1 Monitoring the growth of thin films with QCM	23
3.3.2 Deposition of titanium oxide thin film by LPD method	24
3.3.3 Effects of the concentration of free F ⁻ in the treatment solution	26
3.3.4 Effects of the concentration of H ₃ BO ₃ in the treatment solution	27
3.3.5 Effects of the concentration of (NH ₄) ₂ TiF ₆ in the treatment solution	28
3.4 Conclusion	29

4	Vanadium Oxide Thin Films Prepared by Liquid-Phase Deposition	31
4.1	Introduction	32
4.2	Experimental	32
4.2.1	Liquid-phase deposition process	32
4.2.2	Characterization of the deposited films and the treatment solutions	33
4.2.3	Measurements of electrochromic properties	33
4.3	Results and Discussion	34
4.3.1	Preparation and characterization of the films	34
4.3.2	Mechanism of the film deposition	40
4.3.3	Electrochromic properties of the deposited films	41
4.4	Conclusion	44
5	Vanadium Dioxide Thin Films Prepared by Liquid-Phase Deposition	47
5.1	Introduction	48
5.2	Experimental	48
5.2.1	Liquid phase deposition process	48
5.2.2	Characterization of the deposited films	49
5.2.3	Electrical properties of the deposited thin films	49
5.3	Results and Discussion	49
5.3.1	Preparation and characterization of the deposited films	49
5.3.2	Electrical properties of the LPD-VO ₂ films	51
5.4	Conclusion	53
6	Iron Oxide Thin Films Prepared by Liquid-Phase Deposition	55
6.1	Introduction	56
6.2	Experimental	56
6.2.1	Liquid-phase deposition process	56
6.2.2	Characterization of the deposited films	57
6.3	Results and Discussion	57
6.4	Conclusion	64
7	Gold-Dispersed Titanium Oxide Thin Films Prepared by Liquid-Phase Deposition	67
7.1	Introduction	68
7.2	Experimental	69
7.2.1	Liquid-phase deposition process	69

7.2.2	Characterization of the deposited films	69
7.3	Results and Discussion	70
7.3.1	Heat treatment of the deposited films	71
7.3.2	Photoirradiation of the deposited films	76
7.4	Conclusion	82
8	Summary	85
	Publication list	91
	Oral presentation list	93

Chapter 1

General Introduction

Metal oxides were used from old times for inorganic materials such as fireproof materials, building materials, pigments, glasses, catalysts, and so on. There are a large number of research work with respect to the preparation, structure, and properties.

Recently, transition metal oxides and/or multi-component oxides have attracted interests as functional inorganic materials in the fields of electrically and optically application. They possess various electrical and optical properties, because they contain an element in more than one valence state, and electron transition from low valence state ion to high valence state ion is occurred. Such materials are used as thin films in many cases. At present, these metal oxide and/or multi-component oxide thin films were widely used for semiconducting materials, dielectric materials, sensor, electrode materials, catalysts, optical logic devices, and so on.

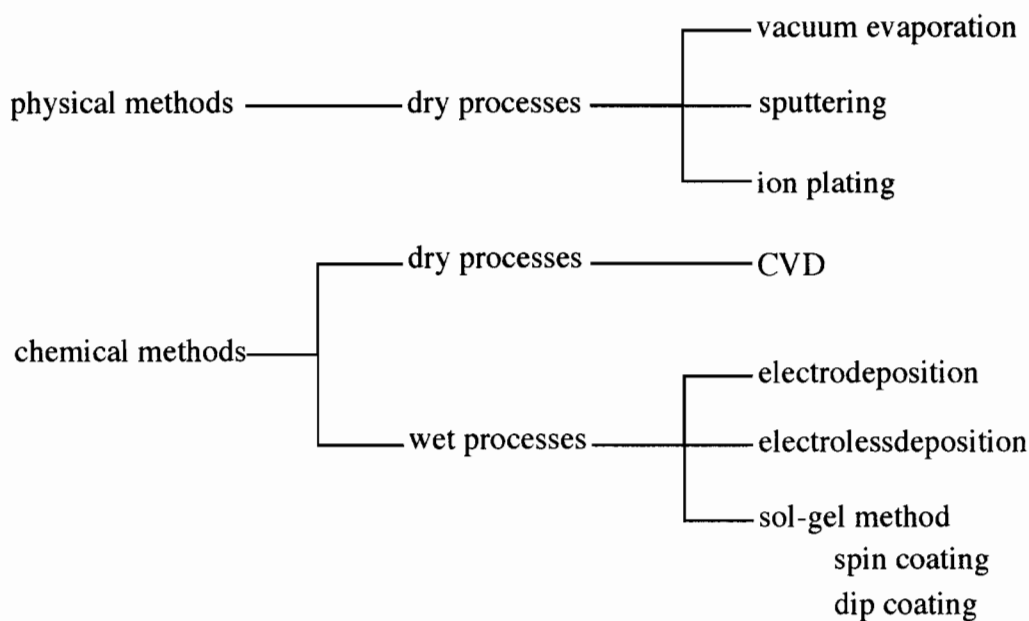


Figure 1.1. Classification of preparing methods of thin films.

Generally, methods for preparing thin films can be classified into physical method and chemical method. Physical method includes dry processes such as vacuum evaporation and sputtering. And chemical methods includes dry process such as chemical vapor deposition (CVD), and wet processes such as electrodeposition, electrolessdeposition, dipping and spin coating of sol-gel regents (Fig. 1.1). Both types of processes are widely applied to prepare many kinds of metal oxides and have been studied in detail. However, there are several problems associated with these pro-

Methods	Advantages	Problems
Vacuum evaporation	<ul style="list-style-type: none"> • Most popular process. • Thickness control is easy. 	<ul style="list-style-type: none"> • Require special apparatus and high energy. • Disqualification for high-melting point materials.
Sputtering	<ul style="list-style-type: none"> • Possible for high-melting point materials. 	<ul style="list-style-type: none"> • Require special apparatus and high energy.
Chemical vapor deposition (CVD)	<ul style="list-style-type: none"> • Possible for various kinds of compounds. 	<ul style="list-style-type: none"> • Require special apparatus and high energy.
Electro-deposition	<ul style="list-style-type: none"> • Low-temperature process. • Homogeneous thin films are formed. 	<ul style="list-style-type: none"> • Restricted to electrical conductive substrates.
Sol-gel method	<ul style="list-style-type: none"> • Operation and composition control are easy. • Dose not require special apparatus. 	<ul style="list-style-type: none"> • Require heat-treatment. • Difficult to preparation on complex morphologies. • Sol-gel regents are expensive.

Table 1.1. Characteristics of methods for preparing thin films.

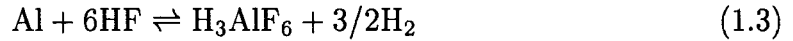
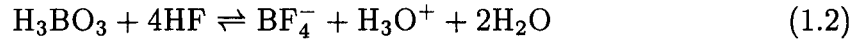
cesses. Physical processes are difficult to control the precise composition of metal oxides. Dry processes require special apparatuses for deposition of films, and they are not suitable for the preparation of thin films on substrates with large surface areas because they need vacuum or low pressure in operation. Vapor deposition is disqualification for materials which have high melting point. For wet processes, substrates are restricted to electrical conductive materials for electrodeposition method, and for the sol-gel method, it is difficult to preparation of thin films on substrate with complex morphologies.

In 1988, a novel wet process has been developed for the preparation of SiO_2 thin films [1]. This process is called Liquid-Phase Deposition (LPD) method. In this process, it is possible to form SiO_2 thin films directly on the substrate immersed in a mixed solution of hydrofluorosilicic acid (H_2SiF_6) supersaturated with silica gel and boric acid (H_3BO_3) or metal aluminum [1, 2]. SiO_2 thin film is formed by means of ligand-exchange (hydrolysis) equilibrium reaction of $[\text{SiF}_6]^{2-}$ and F^- consumptive reactions by boric acid or aluminum metal as F^- scavenger. In the solution, following ligand-exchange (hydrolysis) equilibrium reaction of H_2SiF_6 is

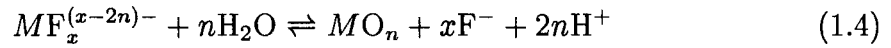
presumed:



The equilibrium reaction (1.1) is shifted to the right-hand side by the addition of boric acid or aluminum metal, which react readily with F^- ions and form stable complex ions as follows:



More generally, Eq. (1.1) is represented as follows:



It suggests that the LPD method can be applied to other metal oxides.

The LPD method is very simple process and does not require any special equipment such as vacuum system. It is, moreover, readily to apply to various kinds of substrates with large surface areas and complex morphologies, and multi-component oxide thin films can be formed readily by the addition of the objective metal ions to the treatment solution, because the LPD method is performed in aqueous solution system which is typical homogeneously mixing system.

Since Nagayama *et al.* [1] firstly reported the formation of SiO_2 thin films by the LPD method in 1988, the LPD method has attracted interests as soft and mild process to preparation of thin films. Until now, several studies have been made with respect to the formation of SiO_2 thin films by the LPD method. Preparation and characterization of SiO_2 thin films by the LPD method were made by Hishinuma *et al.* [2], Homma *et al.* [3], and Yeh *et al.* [4, 5, 6, 7]. Nitta and Kimura [8] applied to the LPD method to preparation of SiO_2 thin films on stainless steel substrate, and Suzuki *et al.* [9, 10] and Nagamura *et al.* [11] prepared dye doped SiO_2 thin films by the LPD method. Huang *et al.* [12] studied the photoirradiation effects on the deposition rate of SiO_2 . Growth mechanisms of the SiO_2 thin films by the LPD method were studied by Awazu *et al.* [13] and Chou *et al.* [14]. Applications of the deposited SiO_2 thin films by the LPD method for metal-oxide-semiconductor capacitor or transistor [15, 16, 17, 18], interlayer dielectric films in ULSI [19, 20, 21], and solar cell [22] were supposed.

Although several studies have been made with respect to the SiO_2 thin films as mentioned above, the extension of the LPD method to the other metal oxide thin films have never been studied. The purpose of the present work is preparation and characterization of various kinds of metal oxide and multi-component oxide thin

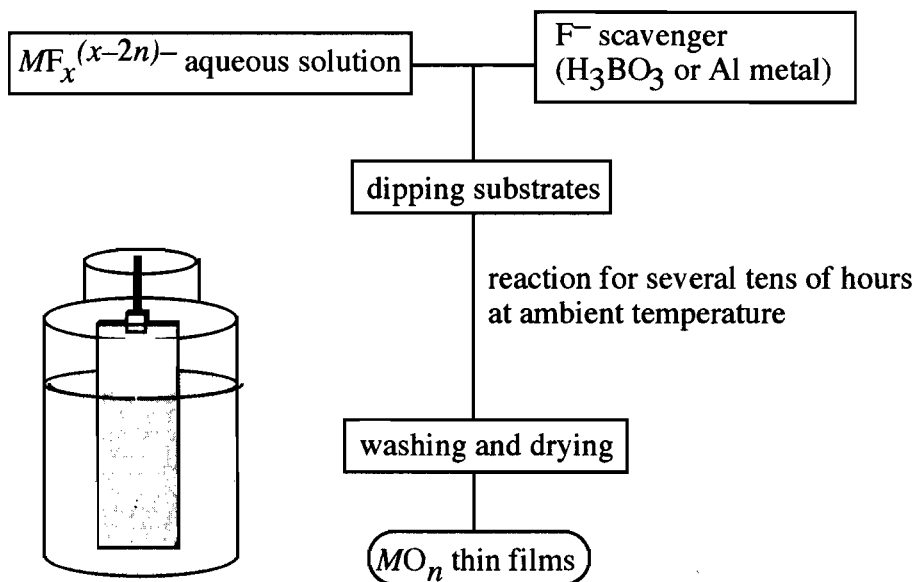


Figure 1.2. Preparation of MO_n thin films by the LPD method and schematic diagram of reaction cell.

films by the LPD method. Mechanisms of the deposition of the films were also discussed.

The present thesis consists of following eight chapters.

In Chapter 1, a general introduction was given, and the purpose and construction of present thesis were described.

The experimental, results and discussions were mentioned in detail in the following six chapters.

In Chapter 2, the preparation of titanium oxide thin films by the LPD method was described. Formed films were characterized by X-ray diffraction (XRD), IR absorption spectroscopy, and scanning electron microscope (SEM) observation. Photoelectrochemical properties of the deposited films were also investigated.

In Chapter 3, the quartz crystal microbalance (QCM) technique was applied to investigate formation of titanium oxide thin films by the LPD method. This is the first attempt to monitor the thin film formation by the LPD method with the QCM method. The concentration effects of reactants on film deposition rate were discussed.

In Chapter 4, the LPD method was applied to the preparation of vanadium oxide thin films. The formed films were characterized by XRD, IR absorption spec-

troscopy, thermal analysis, electron spin resonance (ESR), and SEM observation. Optical absorption spectra of the treatment solutions were also measured in order to investigate the dissolving species, and deposition mechanism was discussed. Electrochemical and optical properties related to electrochromism were also investigated.

In Chapter 5, preparation of vanadium dioxide by the LPD method was described. Electrical properties with respect to semiconductor-to-metal phase transition behavior of the obtained VO₂ thin films were investigated.

In Chapter 6, preparation of iron hydroxide and oxide thin films by the LPD method was described. The formed films were characterized by XRD, IR absorption spectroscopy, and SEM observation. Deposition mechanism was discussed.

In Chapter 7, preparation of Au-dispersed titanium oxide thin films by the LPD method and subsequent heat treatment or ultraviolet photo-irradiation was described. Optical properties of the formed films were discussed.

In Chapter 8, the summary of the present thesis was given.

References

- [1] H. Nagayama, H. Honda, and H. Kawahara, *J. Electrochem. Soc.* **135**, 2013 (1988).
- [2] A. Hishinuma, T. Goda, M. Kitaoka, S. Hayashi, and H. Kawahara, *Appl. Surf. Sci.* **48/49**, 405 (1991).
- [3] T. Homma, T. Katoh, Y. Yamada, and Y. Murao, *J. Electrochem. Soc.* **140**, 2410 (1993).
- [4] C. F. Yeh and C. L. Chen, *J. Electrochem. Soc.* **142**, 3579 (1995).
- [5] C. F. Yeh, C. L. Chen, W. Lur, and P. W. Yen, *Appl. Phys. Lett.* **66**, 938 (1995).
- [6] C. F. Yeh and S. S. Lin, *J. Non-Cryst. Solids* **187**, 81 (1995).
- [7] C. F. Yeh, S. S. Lin, and W. Lur, *J. Electrochem. Soc.* **143**, 2658 (1996).
- [8] S. Nitta and Y. Kimura, *J. Soc. Mat. Sci., Jpn.* **43**, 1437 (1994).
- [9] S. Suzuki, N. Tokou, T. Mabuchi, T. Nakajima, J. Ino, K. Takemura, and H. Kawahara, *Bull. Chem. Soc. Jpn.* **68**, 1275 (1995).
- [10] T. Usui, S. Suzuki, M. Kojima, T. Nakajima, J. Ino, and K. Takemura, *Mol. Cryst. Liq. Cryst. A* **276**, 215 (1996).

- [11] T. Nagamura and H. Shimizu, *Mol. Cryst. Liq. Cryst. A* **267**, 169 (1995).
- [12] C. T. Huang, P. H. Chang, and J. S. Shie, *J. Electrochem. Soc.* **143**, 2044 (1996).
- [13] K. Awazu, H. Kawazoe, and K. Seki, *J. Non-Cryst. Solids* **151**, 102 (1992).
- [14] J. S. Chou and S. C. Lee, *J. Electrochem. Soc.* **141**, 3214 (1994).
- [15] C. F. Yeh, S. S. Lin, and T. Y. Hong, *IEEE Electron Device Lett.* **16**, 316 (1995).
- [16] C.F. Yeh, S.S. Lin, and T. Y. Hong, *Microelectronic Engineering* **28**, 101 (1996).
- [17] W. S. Lu and J. G. Hwu, *IEEE Trans. Electron Device Lett.* **17**, 172 (1996).
- [18] J. S. Chou and S. C. Lee, *IEEE Trans. Electron Devices* **43**, 599 (1996).
- [19] T. Homma and Y. Murao, *Thin Solid Films* **249**, 15 (1994).
- [20] T. Homma, *J. Non-Cryst. Solids* **187**, 49 (1995).
- [21] T. Homma, *Thin Solid Films* **278**, 28 (1996).
- [22] Y. P. Shen and J. G. Hwu, *IEEE Photonics Technology Lett.* **8**, 420 (1996).

Chapter 2

Titanium Oxide Thin Films Prepared by Liquid-Phase Deposition

2.1 Introduction

Transition metal oxide thin films, which have various kinds of optical and electrical properties, are very widely used as inorganic functional materials in the fields of application. Generally, these metal oxide thin films were prepared by some dry processes such as sputtering and C. V. D., and some wet processes such as sol-gel method. Recently, a new wet process to prepare metal oxide thin films has been developed. This process is called Liquid-Phase Deposition (LPD) process [1]. In this process, metal oxide thin films could be deposited on the immersed substrates by using chemical equilibrium reaction between metal fluoro-complex ion and metal oxide in an aqueous solution system. This process is easy to apply to any kinds of substrates with large surface areas and/or complex morphologies without special equipment at ambient temperature.

There has been much interest in the use of semiconducting oxide electrodes to accomplish the photoelectrolysis of water. A great number of studies have been carried out on especially TiO_2 of n-type semiconductor, since Fujishima *et al.* [2] found that TiO_2 (rutile) single crystal decompose water with assistance of illumination. This photo-assisted electrolysis of water has also been observed for polycrystalline TiO_2 . Moreover, it has been suggested that TiO_2 (anatase) has a stronger catalytic activity for water decomposition than TiO_2 (rutile) [3], and it can decompose water without any application of external bias [4]. From these point of view, TiO_2 (anatase) is advantageous to use as photo-sensitive electrode for solar energy converter. To use for TiO_2 electrode for large-scale energy converter, it is advantageous that polycrystalline TiO_2 film electrode which has large area is utilized in place of TiO_2 single crystal one. There are many proposal to prepare such polycrystalline TiO_2 film. For example, CVD [5], anodic oxidation and thermal oxidation of Ti metal [6, 7, 8], and sol-gel method [9].

In this chapter, the author reports the preparation and characterization of titanium oxide thin films by using the LPD method. Photoelectrochemical properties of the deposited films were also described.

2.2 Experimental

2.2.1 Liquid-phase deposition process

As parent solutions, hexafluorotitanate ammonium [$(\text{NH}_4)_2\text{TiF}_6$; Kishida Chemical Co. Ltd.] and boric acid (H_3BO_3 ; Nacalai Tesque Inc.) were dissolved in distilled water at concentrations of 0.5 mol dm^{-3} . These solutions were mixed at various

compositions and used as the treatment solution for deposition. Non-alkali glass (Corning, # 7059) was used as the substrate. After being degreased and washed ultrasonically, the substrate was immersed in the treatment solution and suspended therein vertically. Temperature of the treatment solution was kept at 25 °C. After appropriate reaction time, the substrate was removed from the treatment solution, washed with distilled water and dried at ambient temperature. Some of the deposited films were heat-treated at various temperatures in an air flow.

2.2.2 Characterization of the deposited films

X-ray diffraction (XRD) studies of the deposited films were measured with a Rigaku RINT 2100 diffractometer, using Cu K α radiation (40 kV, 40 mA). IR absorption spectra of the deposited films were measured with an IR spectrophotometer A-302 (Japan Spectroscopic Co. Ltd.). The surface morphologies of the films were observed with a scanning electron microscope (SEM; Hitachi, S-2500). The film thickness of the deposited transparent films, which showed interference color, were derived from the visible spectra of the films by interference method.

2.2.3 Photoelectrochemical properties of the deposited films

In order to study photoelectrochemical properties, the films were formed on indium tin oxide (ITO) coated glass substrates. The ITO film layer is transparent conductor with sheet resistance of 30 Ω sq.⁻¹, and copper wire was connected to this layer.

Electrochemical measurements were performed in a 0.1 mol dm⁻³ Na₂SO₄ solution using a potentiostat (Hokuto Denko Ltd., PS-5000) and a function generator (NF Circuit Design Block Co. Ltd., FG-106T) with a three-electrode system. Pt plate electrode and saturated calomel electrode (SCE) were used as a counter and a reference electrode, respectively. The deposited TiO₂ film electrode was illuminated through a quartz window in the cell wall using a 100 W high-pressure mercury lamp USH-102D (Ushio Denki Co.) with a power supply HB-101A (Ushio Denki Co.).

2.3 Results and Discussion

2.3.1 Characterization of the deposited films

After reaction for several tens of hours, hazy or transparent films were deposited on the substrates. These films showed strong adherence to the substrate.

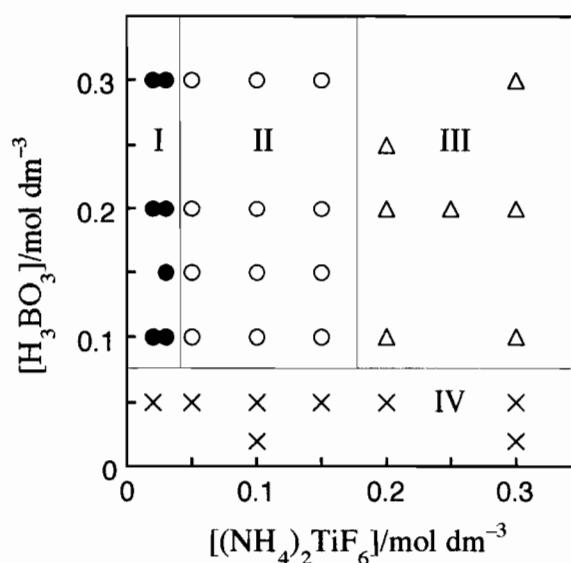


Figure 2.1. Relationship between aspect and chemical composition of the deposited film and the concentrations of $(\text{NH}_4)_2\text{TiF}_6$ and H_3BO_3 . ●: hazy anatase, ○: transparent anatase, △: NH_4TiOF_3 , ×: no deposition. Reaction time: 40 h.

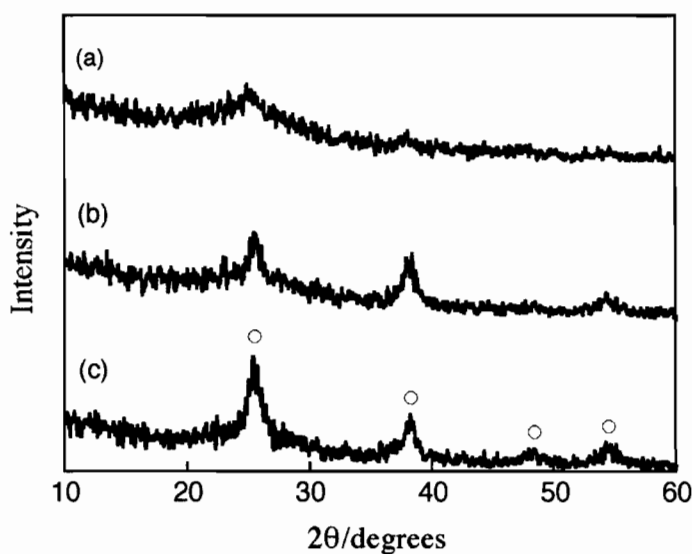


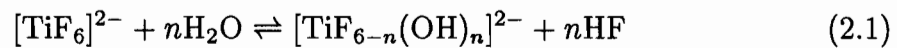
Figure 2.2. X-ray diffraction patterns of the deposited films heat-treated at various temperatures. (a): As-deposited film, (b): heat-treated at 400 and (c): 500 °C. ○: TiO_2 (anatase). Concentration of $(\text{NH}_4)_2\text{TiF}_6$: 0.10 mol dm^{-3} and of H_3BO_3 : 0.20 mol dm^{-3} . Reaction time: 40 h.

According to the aspects of the deposited films, the concentration range of $(\text{NH}_4)_2\text{TiF}_6$ and H_3BO_3 is classified into four groups (Figure 2.1). From XRD studies of the deposited films, it was found that the deposited film was hazy anatase at

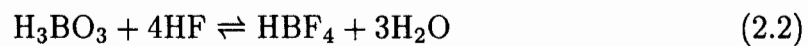
the region I, and that at the region II was transparent anatase. Peak intensity of the diffraction of anatase for the film deposited at region II was larger than that for the region I film. At the region III, micro-crystalline of NH_4TiOF_3 was formed on the substrate. At the region IV, any deposition was not recognized. Crystallinity of the deposited films were improved by heat treatment, but the diffraction peaks of rutile were not observed after heat treatment above $600\text{ }^\circ\text{C}$ (Fig. 2.2). When another substrates such as alumina ceramic plate or stainless steel were used, similar results were obtained.

In IR absorption spectrum of the as-deposited film, absorption bands at 3200 , 1620 , and 1400 cm^{-1} were observed. Absorption bands at 3200 and 1620 cm^{-1} are assigned to an O-H stretching mode and H-O-H deformation mode, respectively. These bands are assigned to the physically and chemically adsorbed water molecules. The LPD process is performed in an aqueous solution system, water molecules were absorbed and adsorbed readily. Absorption band at 1400 cm^{-1} is assigned to N-H deformation mode of NH_4^+ . NH_4^+ which were contained in $(\text{NH}_4)_2\text{TiF}_6$, which is one of the source materials for deposition, were enclosed in the deposited oxide film during the reaction. These bands disappeared by the heat treatment above $300\text{ }^\circ\text{C}$ completely.

For the ligand-exchange (hydrolysis) of $[\text{TiF}_6]^{2-}$ ion in aqueous solution, the following equilibrium scheme has been proposed by Schmitt *et. al.* [10].



However, under the law of mass action, the equilibrium can be shifted to the right-hand side by the addition of H_3BO_3 as F^- scavenger into the solution. H_3BO_3 readily reacts with F^- ions and forms stable complex ion as follows [11]:



The addition of H_3BO_3 leads to the consumption of non-coordinated F^- ions and accelerates the ligand-exchange (hydrolysis) reaction. From the results of XRD studies, which showed the deposited film was TiO_2 , it is considered that the deposition of TiO_2 thin film arose through the dehydration reaction among $[\text{Ti}(\text{OH})_6]^{2-}$, which was generated by the ligand-exchange (hydrolysis) reaction of $[\text{TiF}_6]^{2-}$. In the region III, added H_3BO_3 was insufficient for the ligand-exchange (hydrolysis) to be completed because the concentration of $(\text{NH}_4)_2\text{TiF}_6$ is high; consequently, titanium oxy-fluoride was supersaturated and deposited on the substrate.

Figure 2.3 shows relationship between film thickness and reaction time. The film thickness of the film deposited at region II increased linearly with reaction time

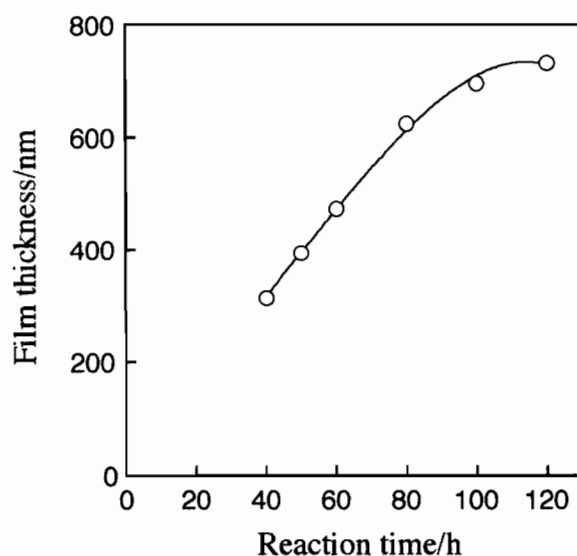


Figure 2.3. Dependence of film thickness on reaction time. Concentration of $(\text{NH}_4)_2\text{TiF}_6$: 0.1 mol dm^{-3} and of H_3BO_3 : 0.2 mol dm^{-3} .

up to 80 h. The deposition rate was reduced, when reaction time was more than 80 h. It can be said that the decreasing of the concentration of the reactant led to decreasing of the deposition rate. The deposited film was peeled off when reaction time was more than 130 h. The deposition rate of the film was depended on the concentration of added H_3BO_3 as F^- scavenger (Figure 2.4). The deposition rate

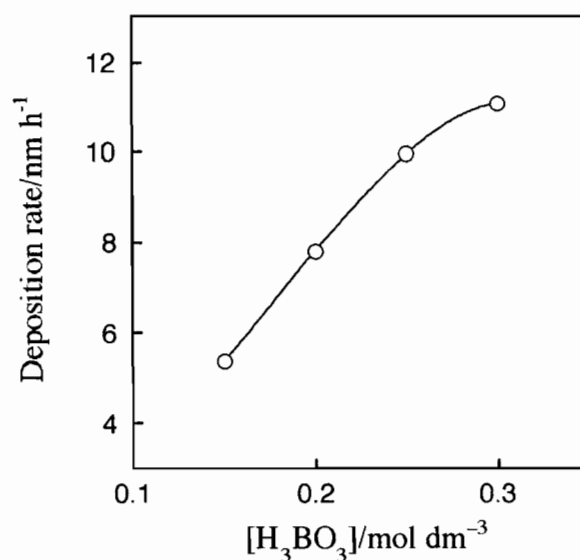


Figure 2.4. Relationship between the deposition rate and the concentration of H_3BO_3 . Concentration of $(\text{NH}_4)_2\text{TiF}_6$: 0.1 mol dm^{-3} .

increased linearly with concentration of H_3BO_3 up to 0.25 mol dm^{-3} . This indicates that the rate-determining step of the TiO_2 thin film formation by the LPD method is F^- consuming reaction by H_3BO_3 .

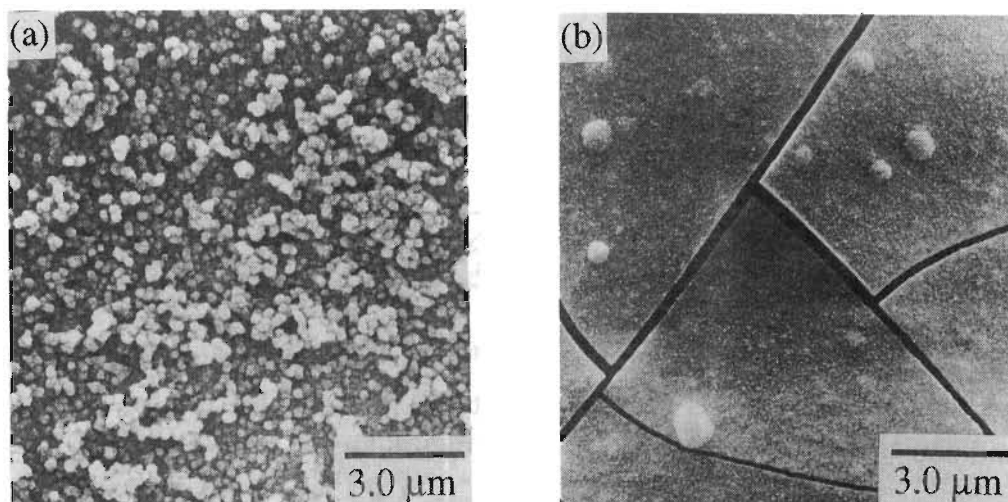


Figure 2.5. SEM photographs of the deposited films. (a): Region I and (b): region II.

Figure 2.5 shows SEM photographs of the films which were formed at the region I and II. The films were constructed of small particles. Constructed particles of region I film are several hundreds of nanometers which diffuse visible ray, thus, the region I film was hazed. On the other hand, constructed particles of region II film are less than 20 nm, which are smaller than wavelength of visible ray; therefore, the film formed at the region II was transparent. Some cracks were also observed for the region II film. It is considered that these cracks were generated by internal stress of the film due to contract of the film by dissociation of water on drying procedure.

2.3.2 Photoelectrochemical properties of the deposited films

For the measurements of the photoelectrochemical properties, the films formed in the region I, that is TiO_2 (anatase) films were used. Figure 2.6 shows photocurrent-potential curves of the region I films heat-treated at various temperatures. The as-deposited film did not show photoelectrochemical behavior. For the films formed in the region II, similar results were obtained. For all samples, dark current were very small, so only photocurrents were represented in the figure. The anodic current due to the decomposition of water was observed from *ca.* -0.6 V under illumination. The photocurrents of the films heat-treated at 400 and 500 °C increased in two steps and show almost constant above *ca.* 0 V . The two step increasing is also observed

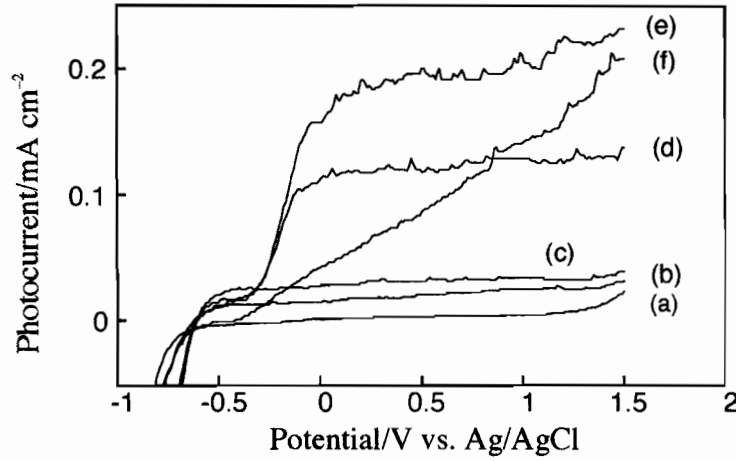
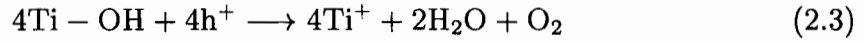
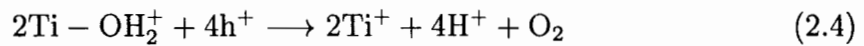


Figure 2.6. Photocurrent-potential curves of the deposited films heat-treated at various temperatures. Films heat-treated at 100 (a), 200 (b), 300 (c), 400 (d), 500 (e), and 600 °C (f).

by Displat [12] for the TiO₂ (rutile) single crystal and Yoko *et al.* [4] for the sol-gel TiO₂ (anatase) film. They suggest that oxygen generation on TiO₂ electrode occur through the two step reaction. Yoko *et al.* [4] proposed that the first anodic current is due to the reaction,



and the second anodic current due to the reaction.



The same explanation will be applied to the LPD-TiO₂ thin films. As shown in Fig. 2.6, the saturation of the photocurrent was not observed for the film heat-treated at 600 °C, although it observed for the film which heat-treated below 600 °C. Figure 2.7 shows the photocurrent at 0, 0.5, and 1.0 V as a function of heat-treatment temperature. The photocurrent increases with increasing heat-treatment temperature until 500 °C, it markedly, however, decreases for the film heat-treated at 600 °C. For an n-type semiconductor, the most simplest model which estimates the photocurrent-potential curve is expressed as follows [13]:

$$J_p = qI_0[1 - \exp(-\alpha W)/(1 + \alpha L)] \quad (2.5)$$

where, J_p is the photocurrent density, q is the electronic charge, I_0 is the intensity of the irradiation light, α is the absorption coefficient, W is the depletion layer width,

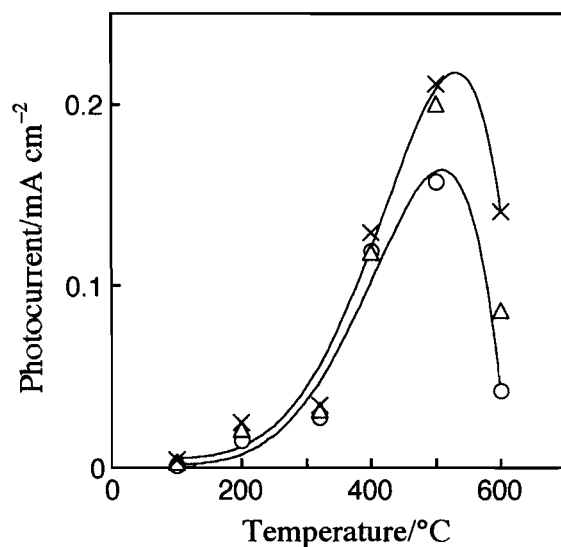


Figure 2.7. Variations of the photocurrent with heat-treatment temperature. ○: at 0 V, △: at 0.5 V, and ×: at 1.0 V.

and L is the diffusion length for holes in the bulk of semiconductor. This equation shows that the photocurrent density increases, if α , W , and L is large. Here, the depletion layer width is given by [14]

$$W = 2\epsilon_0\epsilon(V - V_{fb})/qN_d^{1/2} \quad (2.6)$$

where ϵ_0 is the permittivity of free space, ϵ is the relative permittivity, V is the bias potential, V_{fb} is the flatband potential, q is the electronic charge, and N_d is the donor concentration of the semiconductor. As shown in Eq. (2.6), depletion layer width is dependent upon the bias potential, V , and donor concentration, N_d (in case of TiO_2 , Ti^{III} acts as donor). Therefore, if donor concentration decrease, depletion layer width will narrow. On the other hand, the electric field in the depletion layer is expressed by [14]

$$F = (V - V_{fb})/W \quad (2.7)$$

where F is the electric field in the depletion layer. Therefore, the electric field in the depletion layer decreases with increasing the depletion layer width.

As stated above, the increase in photocurrent with increasing the heat treatment temperature until 500 °C can be considered as follows. Ti^{III} as donors in TiO_2 are oxidized to Ti^{IV} upon heat treatment in an air flow. Therefore, the donor concentration of the film decreases, and the depletion layer width increases according to the Eq. (2.6). Consequently, the photocurrent increases as shown in Eq. (2.5). Moreover increase of the crystallinity causes increasing the photocurrent, because

the diffusion length for holes, L , increases with increasing crystallinity. On the other hand, the decrease in photocurrent for the TiO_2 film heat-treated at $600\text{ }^\circ\text{C}$ might be attributed to the decrease of the electric field in the depletion layer which decreases with the increase of the depletion layer width according to Eq. (2.7). As a result of the decrease in the electric field in the depletion layer, recombination of the electron-hole pairs generated by irradiated photon increases, because the electric field in the depletion layer is available for the electron-hole separation. Therefore, the photocurrent decreases for the film heat-treated at $600\text{ }^\circ\text{C}$. In short, with regard to the variations of the photocurrent with heat-treatment temperature, it may be said that the increase in the depletion layer width due to the decrease in donor concentration is predominant for the TiO_2 film heat treated below $600\text{ }^\circ\text{C}$, and the decrease in the electric field in the depletion layer due to the increase in the depletion layer width is predominant for the TiO_2 film heat treated at $600\text{ }^\circ\text{C}$.

As shown in Fig. 2.6, saturation of the photocurrent were observed for the TiO_2 film heat-treated below $600\text{ }^\circ\text{C}$. It indicates that almost electrons generated by the irradiated photon move to the TiO_2 surface according to electric field in the depletion layer without recombination. On the contrary, it can be considered that the saturation of the photocurrent was not observed for the TiO_2 film heat treated at $600\text{ }^\circ\text{C}$, since the electron-hole pairs were recombination in the depletion layer. These results support to the above consideration.

2.4 Conclusion

Titanium (IV) oxide (anatase) thin films were prepared on the substrates by the LPD method by using ligand-exchange (hydrolysis) reaction of $[\text{TiF}_6]^{2-}$ accelerated by the addition of H_3BO_3 as F^- scavenger. The aspects and chemical compositions of the deposited films were different according to the concentrations of $(\text{NH}_4)_2\text{TiF}_6$ and H_3BO_3 . At low concentration range of $(\text{NH}_4)_2\text{TiF}_6$, hazy or transparent anatase TiO_2 thin films were formed. At high concentration range of $(\text{NH}_4)_2\text{TiF}_6$, thick films of micro-crystalline NH_4TiOF_3 were formed. Thickness of the deposited TiO_2 film increased linearly with reaction time and the deposition rate of transparent TiO_2 film depended on the concentration of added H_3BO_3 . The as-deposited film was amorphous and it crystallized upon heat treatment. Rutile phase was not observed even after heat treatment above $600\text{ }^\circ\text{C}$.

The heat-treated films showed photoelectrochemical behavior. The photocurrent due to the decomposition of water increased with increasing heat-treatment temperature until $500\text{ }^\circ\text{C}$ and it decreased for the film heat-treated at $600\text{ }^\circ\text{C}$. The

saturation of the photocurrent was not observed for the films heat-treated at 600 °C.

References

- [1] H. Nagayama, H. Honda, and H. Kawahara, *J. Electrochem. Soc.* **135**, 2013 (1988).
- [2] A. Fujishima and K. Honda, *Nature* **238**, 37 (1972).
- [3] C. D. Jaeger and A. J. Bard, *J. Phys. Chem.* **84**, 3146 (1979).
- [4] T. Yoko, K. Kamiya, and S. Sakka, *Nihon Kinzoku Gakkai Kaihou* **28**, 176 (1989).
- [5] Y. Takahashi, K. Tsuda, and K. Sugiyama, *J. Chem. Soc. Faraday Trans. I* **77**, 1051 (1981).
- [6] J. Augustynski, J. Hinder, and C. Stalder, *J. Electrochem. Soc.* **124**, 1063 (1977).
- [7] Y. Matsumoto, J. Kurimoto, Y. Amagasaki, and E. Soto, *J. Electrochem. Soc.* **127**, 2148 (1980).
- [8] K. H. Yoon and S. O. Yoon, *Jpn. J. Appl. Phys.* **23**, 1137 (1984).
- [9] T. Yoko, A. Yuasa, K. Kamiya, and S. Sakka, *J. Electrochem. Soc.* **138**, 2279 (1991).
- [10] R. H. Schmitt, E. L. Grove, and R. D. Brown, *J. Am. Chem. Soc.* **82**, 5292 (1960).
- [11] C. A. Wamser, *J. Am. Chem. Soc.* **73**, 409 (1951).
- [12] J. Dispat, *J. Appl. Phys.* **47**, 5102 (1976).
- [13] W. W. Gätnner, *Phys. Rev.* **116**, 84 (1959).
- [14] K. H. Yoon and J. S. King, *J. Phys. Chem.* **90**, 6488 (1986).

Chapter 3

Monitoring for Growing Process of Titanium Oxide Thin Films from Aqueous Solution by the Quartz Crystal Microbalance

3.1 Introduction

The quartz crystal microbalance (QCM) is an extremely sensitive sensor capable of measuring mass change in the nanogram range because its oscillating frequency is changed by deposition of substances on the crystal surface [1]. It has been used as a mass sensitive detector in aqueous solution system as well as in vacuum or gas phase system. The QCM in solution system have been applied to the study of electrodeposition [2, 3, 4], ion fluxes in polymer films [5, 6], intercalation phenomena [7], and other interfacial phenomena.

The change in oscillating frequency of the quartz crystal (Δf) is proportional to the change in mass (Δm) per unit area (A) of the deposits on the crystal. The equivalence is expressed as follows [1, 8]:

$$\Delta f = -f_0^2 \Delta m / (\rho_q N A) \quad (3.1)$$

where f_0 is the fundamental frequency of the crystal, N is the frequency constant (1.670×10^5 cm Hz for an AT-cut quartz), and ρ_q is the density of quartz (2.648 g cm⁻³).

In the present chapter, growth of the titanium oxide thin films by the LPD method was monitored with the QCM technique in order to clarify the film formation mechanism. This is the first attempt to monitor the thin film formation by the LPD method with QCM technique. The author discusses the dependence of the thin film formation on concentrations of solutes in the treatment solution.

3.2 Experimental

3.2.1 Treatment solutions for the LPD method

As parent solutions for the treatment solution of the LPD method, $(\text{NH}_4)_2\text{TiF}_6$ (Kishida Chemical Co. Ltd.) and H_3BO_3 (Nacalai Tesque Inc.) were dissolved in distilled water at concentrations of 0.5 mol dm⁻³, respectively. These solutions were mixed at various compositions and used as the treatment solution for deposition. In order to investigate the concentration effect of free F^- in the treatment solution, NH_4F (Nacalai Tesque Inc.) aqueous solution was added to the treatment solution at various concentrations.

3.2.2 QCM technique

The quartz crystals used in this study were biplanar, circular AT-cuts with 13 mm diameter. The crystal has a fundamental frequency of 3.58 MHz, and the approxi-

mate sensitivity for the frequency change is $35 \text{ ng cm}^{-2} \text{ Hz}^{-1}$ (from Eq. (3.1)). The surface of the crystal which contact with the solution was coated with gold metal thin film (*ca.* 100 nm) by vacuum evaporation. The crystal was mounted on a holder by using silicon sealant so as to expose one side of the crystal to the solution.

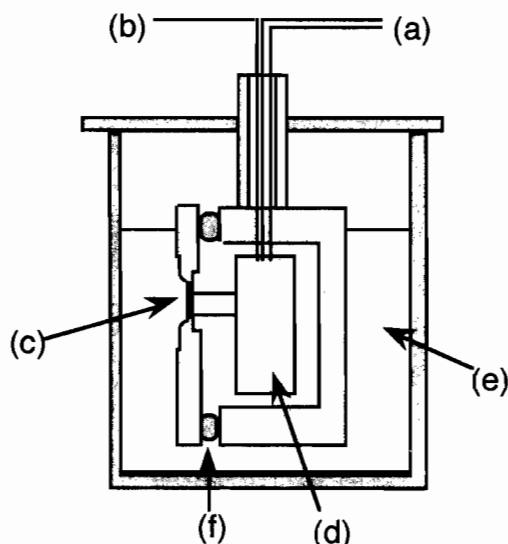


Figure 3.1. Schematic diagram of the cell and quartz crystal apparatus. (a): Frequency counter, (b): d. c. power source, (c): quartz crystal oscillator, (d): oscillating circuit, (e): treatment solution, and (f): o-ring.

A schematic diagram of the cell and quartz crystal apparatus is shown in Fig. 3.1. The cell was made of acrylic resin. The quartz crystal apparatus was immersed into the treatment solution for deposition, and the resonant frequency was measured by a frequency counter (Advantest Inc., TR5823H) at intervals of 15 min at 30 °C.

3.3 Results and Discussion

3.3.1 Monitoring the growth of thin films with QCM

Figure 3.2 shows the relationship between the thickness of the deposited films by the LPD method determined by SEM observation (t_{SEM}) and that measured by QCM technique (t_{QCM}). The t_{QCM} were calculated using following equation.

$$t_{\text{QCM}} = \Delta m \frac{1}{A} \frac{1}{d} \quad (3.2)$$

where Δm is obtained from Eq. (3.1), A is the area of the QCM, and d is the density of TiO_2 (anatase) (3.90 g cm^{-3}). As shown in Fig. 3.2, a good linear relationship

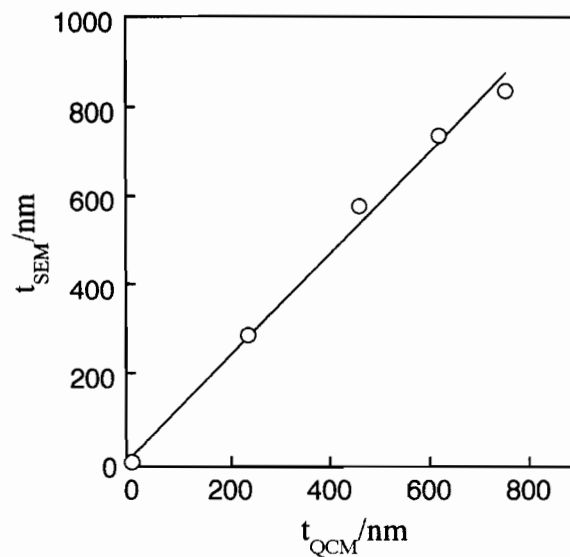


Figure 3.2. Relationship between film thickness determined from QCM (t_{QCM}) and SEM (t_{SEM}).

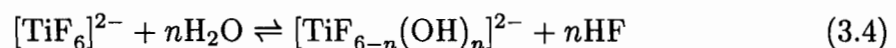
was observed between t_{SEM} and t_{QCM} . It can be said that the QCM technique is suitable for monitoring the growth of thin films by the LPD method. The t_{QCM} was expressed as follows:

$$t_{\text{QCM}} = 0.85t_{\text{SEM}} \quad (3.3)$$

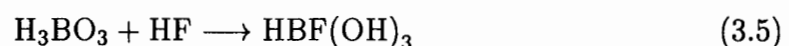
The value of t_{QCM} was lower than t_{SEM} because of the value of d which using in Eq. (3.2) is larger than that of actual value since the crystallinity of the deposited film is low.

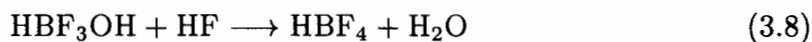
3.3.2 Deposition of titanium oxide thin film by LPD method

The depositing reaction in the LPD method consists of the ligand-exchange (hydrolysis) equilibrium reaction of metal-fluoro complex ion and F^- consumptive reaction by H_3BO_3 as F^- scavenger. For the ligand-exchange (hydrolysis) of $[\text{TiF}_6]^{2-}$ ion in an aqueous solution, the following equilibrium scheme has been proposed [9, 10].



The value of n is small, and the degree of hydrolysis decreases with increasing the concentration of the $[\text{TiF}_6]^{2-}$ [9, 10]. On the other hand, H_3BO_3 readily reacts with F^- as follows [11, 12, 13]:





The reactions (3.5) to (3.7) are rapid and the reaction (3.8) is slow [11, 12, 13]. The addition of H_3BO_3 to the $(\text{NH}_4)_2\text{TiF}_6$ solution accelerates the ligand-exchange (hydrolysis) reaction (3.4), that is, the reaction (3.4) is shifted to the right-hand side, owing to the reaction of H_3BO_3 with F^- . Consequently titanium oxide thin films form on the substrates upon the dehydration reaction among $[\text{Ti}(\text{OH})_6]^{2-}$ species which are generated by the hydrolysis reaction of $[\text{TiF}_6]^{2-}$.

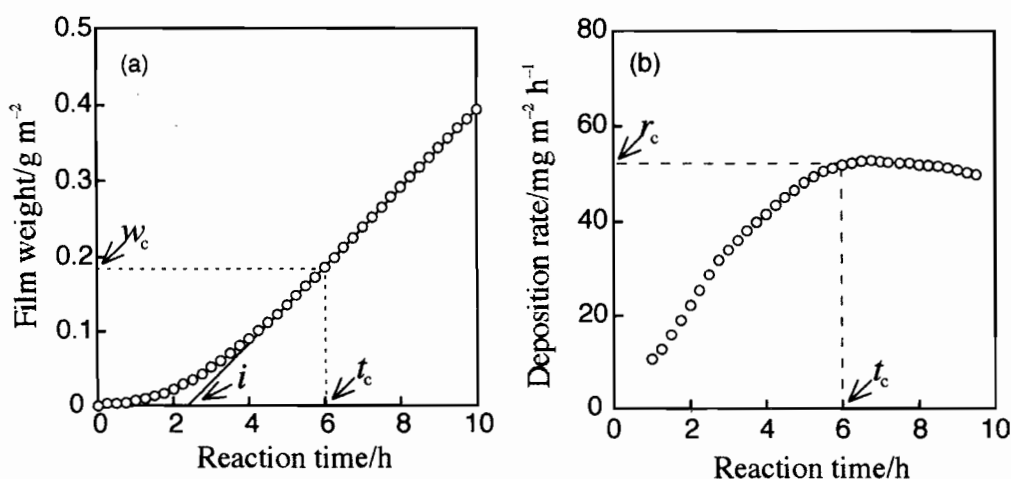


Figure 3.3. Dependence of deposited film weight (a) and deposition rate (b) on reaction time. Concentration of $(\text{NH}_4)_2\text{TiF}_6$: 100 mmol dm^{-3} and of H_3BO_3 : 150 mmol dm^{-3} .

Figure 3.3 (a) shows the relationship between the deposited film weight (w) and the reaction time. Figure 3.3 (b) shows the variation of the deposition rate (r) with reaction time. The deposition rates (r) was determined from the gradient of Fig. 3.3 (a). In this case, the deposition rate increased with reaction time up to 6 h, was constant to 9 h, and then decreased gradually. As shown in Fig. 3.3 (b), there are three steps for the deposition rate; (i) increasing in deposition rate with time, (ii) constant region, and (iii) decreasing with time. From SEM observation of the deposited film, several nuclei were observed on the substrate at the step (i), and the number of the nuclei increased with reaction time. At the steps (ii) and (iii), growing of the nuclei were observed. The decreasing of the deposition rate at step (iii) is presumably due to the decrease of the reactant content. Here we introduce several parameters. The reaction time at which the deposition rate was constant is

t_c . The deposited film weight at t_c is w_c . The deposition rate at t_c is defined as the film formation rate, r_c . The induction period for deposition (i) is defined as follows:

$$i = t_c - \frac{w_c}{r_c} \quad (3.9)$$

These parameters were indicated on Fig 3.3.

3.3.3 Effects of the concentration of free F^- in the treatment solution

In the solution, $[TiF_6]^{2-}$ ions partially hydrolyse and release F^- , although the value of n of Eq. (3.4) is small. Thus free F^- ions may exist in the solution at the initial stage. It is considered that the H_3BO_3 as F^- scavenger preferentially react with such free F^- at the initial stage of the deposition reaction, therefore the induction period may be strongly correlated with the initial content of free F^- . In order to investigate the effects of the concentration of free F^- , NH_4F solution was added to the treatment solution. As NH_4F dissociates to NH_4^+ and F^- , the concentration of free F^- in the treatment solution could be controlled by the addition of NH_4F . Fig. 3.4 (a)

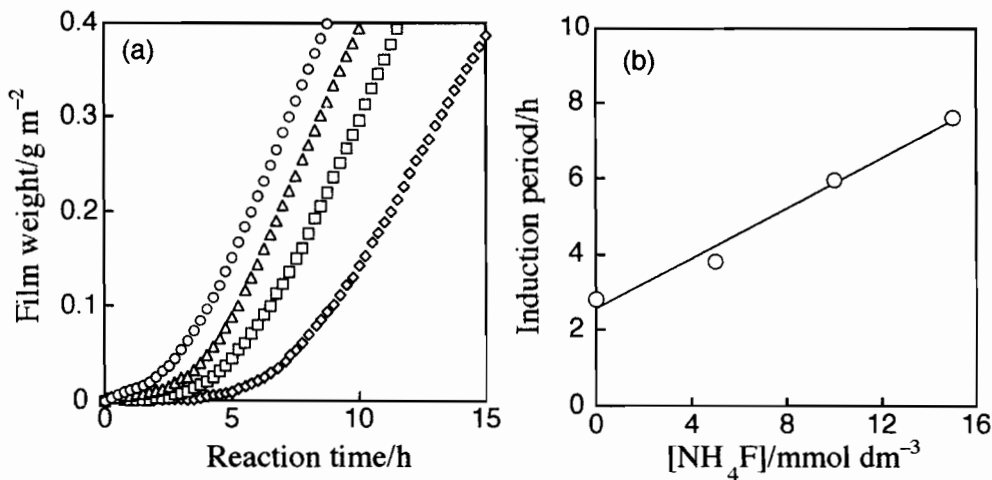


Figure 3.4. (a): Relationships between deposited film weight on reaction time. Concentration of NH_4F : \circ : 0, \triangle : 5.0, \square : 10.0, and \diamond : 15.0 $mmol\ dm^{-3}$. (b): Variation of induction period with concentration of NH_4F . Concentration of $(NH_4)_2TiF_6$: 100 $mmol\ dm^{-3}$ and of H_3BO_3 : 150 $mmol\ dm^{-3}$.

shows the relationships between reaction time and the deposited film weight with various concentrations of NH_4F in the treatment solution. The deposited film weight decreased and the induction period increased with increasing the concentration of NH_4F , that is free F^- concentration, whereas the film formation rates were almost

constant. The variation of induction period with the concentration of NH_4F is shown in Fig. 3.4 (b). The induction period increased linearly with increasing the concentration of NH_4F . Based on these data, we concluded that free F^- ions react with H_3BO_3 in the initial stage of the deposition reaction, that is the induction period. After that, F^- ions coordinated to $[\text{TiF}_{6-n}(\text{OH})_n]^{2-}$ are reacted with H_3BO_3 , and then titanium oxide deposition arises. The film formation rate does not depend on the concentration of free F^- .

3.3.4 Effects of the concentration of H_3BO_3 in the treatment solution

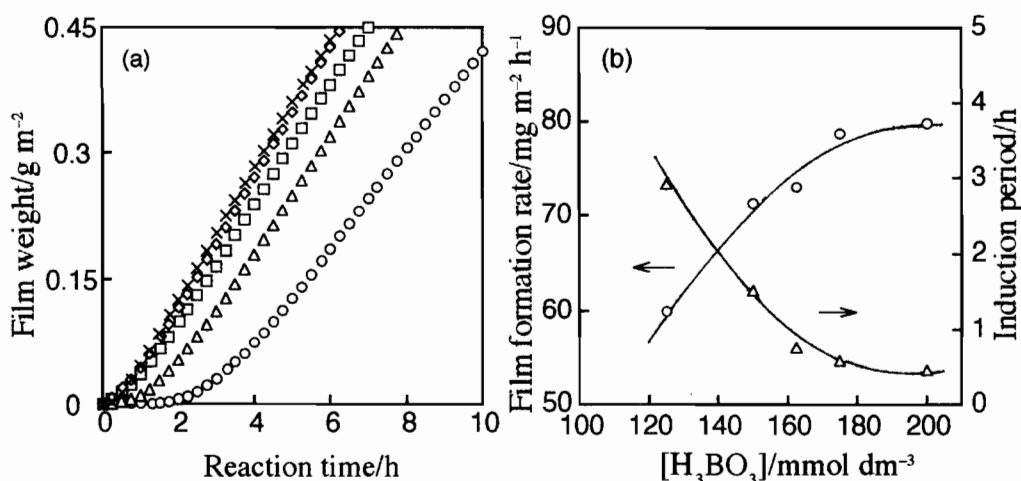


Figure 3.5. (a): Relationships between deposited film weight and reaction time. Concentration of $(\text{NH}_4)_2\text{TiF}_6$: $50.0 \text{ mmol dm}^{-3}$. Concentration of H_3BO_3 : ○: 125.0 , △: 150.0 , □: 162.5 , ◇: 175.0 , and ×: $200.0 \text{ mmol dm}^{-3}$. (b): Variations of deposition rate (○) and induction period (△) with concentration of H_3BO_3 .

Figure 3.5 (a) shows the relationship between the deposited film weight and reaction time. Concentration of $(\text{NH}_4)_2\text{TiF}_6$ was constant to 100 mmol dm^{-3} and that of H_3BO_3 was varied from 125.0 to $200.0 \text{ mmol dm}^{-3}$. The deposited film weight increased with increasing the concentration of H_3BO_3 . The film formation rate and the induction period are shown in Fig. 3.5 (b) as a function of the concentration of H_3BO_3 . As shown in Fig. 3.5 (b), the film formation rate increased and the induction period decreased with increasing the concentration of H_3BO_3 . Variation of the film formation rate was contrasted with that of the induction period.

As stated in Section 3.3.3, free F^- ions exist in the $[\text{TiF}_6]^{2-}$ aqueous solution with equilibrium concentration at the initial stage. These free F^- ions react with

H_3BO_3 in the induction period, and then F^- ions coordinated to $[\text{TiF}_{6-n}(\text{OH})_n]^{2-}$ complex ion react with H_3BO_3 . The concentrations of free F^- are constant for every solution in Fig. 3.5 since the concentrations of $(\text{NH}_4)_2\text{TiF}_6$ are constant, thus the induction period decreased with increasing the concentration of H_3BO_3 . The decreasing of the induction period slowed down when the concentration of H_3BO_3 was more than $162.5 \text{ mmol dm}^{-3}$. As mentioned in Section 3.3.2, consuming reaction of F^- ions with H_3BO_3 could be divided into rapid steps (Eqs. (3.5) to (3.7)) and slow step (Eq. (3.8)). It could be considered that when concentration of H_3BO_3 is higher than $162.5 \text{ mmol dm}^{-3}$, free F^- ions were consumed on rapid steps, therefore the induction period decreased gradually. On the other hand, the film formation rate increased remarkably with the concentration of H_3BO_3 up to $162.5 \text{ mmol dm}^{-3}$, and then increased gradually. The film formation rate is controlled by the consuming reaction of F^- ions coordinated to $[\text{TiF}_{6-n}(\text{OH})_n]^{2-}$. It is considered that F^- coordinated to $[\text{TiF}_{6-n}(\text{OH})_n]^{2-}$ were consumed by H_3BO_3 on slow step (Eq. (3.8)) when concentration of H_3BO_3 is lower than $162.5 \text{ mmol dm}^{-3}$, on the other hand, those were consumed on rapid steps (Eqs. (3.5) to (3.7)) when concentration of H_3BO_3 is higher than $162.5 \text{ mmol dm}^{-3}$. Therefore dependency of the film formation rate on the concentration of H_3BO_3 varied with the concentration range of H_3BO_3 .

3.3.5 Effects of the concentration of $(\text{NH}_4)_2\text{TiF}_6$ in the treatment solution

Figure 3.6 (a) shows relationships between the deposited film weight and reaction time for various concentrations of $(\text{NH}_4)_2\text{TiF}_6$. The concentration of H_3BO_3 was constant to 200 mmol dm^{-3} . The deposited film weight decreased with increasing the concentration of $(\text{NH}_4)_2\text{TiF}_6$. The t_c values were almost constant at 3 h. Figure 3.6 (b) shows the film formation rate and induction period as a function of the concentration of H_3BO_3 . The film formation rate decreased monotonously with increasing the concentration of $(\text{NH}_4)_2\text{TiF}_6$. On the other hand, the induction period slightly increased with increasing the concentration of $(\text{NH}_4)_2\text{TiF}_6$. The change of the induction period was smaller than that when the concentration of H_3BO_3 was constant (Fig. 3.5).

As shown in Section 3.3.2, degree of hydrolysis of $[\text{TiF}_6]^{2-}$ decreases with increasing the concentration of $(\text{NH}_4)_2\text{TiF}_6$ [9]. The change of concentration of free F^- on concentration of $(\text{NH}_4)_2\text{TiF}_6$ may be small. Thus, the dependence of induction period and t_c on the concentration of $(\text{NH}_4)_2\text{TiF}_6$ were small. On the other hand, concentration of partially hydrolyzed species of $[\text{TiF}_6]^{2-}$ decreased with increasing the concentration of $(\text{NH}_4)_2\text{TiF}_6$, causing the decrease of the film formation rate

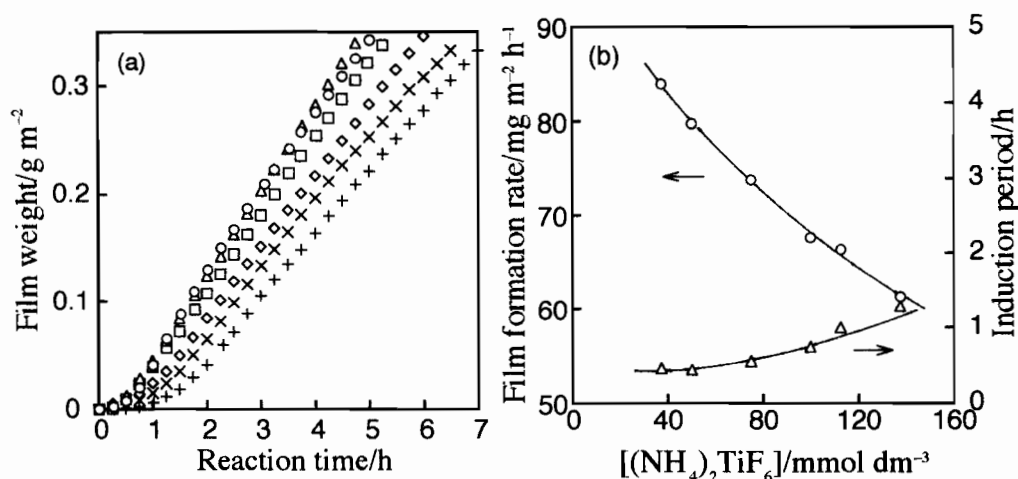


Figure 3.6. (a): Relationships between deposited film weight and reaction time. Concentration of H_3BO_3 : 200 mmol dm^{-3} . Concentration of $(\text{NH}_4)_2\text{TiF}_6$: \circ : 37.5, \triangle : 50.0, \square : 75.0, \diamond : 100.0, \times : 112.5, and $+$: 137.5 mmol dm^{-3} . (b): Relationships between deposition rate (\circ) and induction period (\triangle) with concentration of $(\text{NH}_4)_2\text{TiF}_6$.

with increasing the concentration of $(\text{NH}_4)_2\text{TiF}_6$.

3.4 Conclusion

The QCM technique was applied to the monitoring the growth of titanium oxide thin films by the LPD method. The effects of the concentrations of free F^- , $(\text{NH}_4)_2\text{TiF}_6$, and H_3BO_3 in the treatment solution on the film formation were studied.

In the induction period, the initial stage of the reaction, free F^- ions in the treatment solution preferentially react with H_3BO_3 . The induction period increased linearly with increasing the concentration of added NH_4F , indicating that the induction period depends on the concentration of free F^- . The film formation rate, however, independent on the concentration of free F^- . The film formation rate increased and the induction period decreased with increasing the concentration of H_3BO_3 . When the concentration of H_3BO_3 was more than $162.5 \text{ mol dm}^{-3}$, the increasing of the film formation rate and the decreasing of the induction period slowed down, suggesting that the consuming reaction of F^- by H_3BO_3 occurred on slow step when the concentration of H_3BO_3 was low, on the other hand that occurred on rapid steps when the concentration of H_3BO_3 was high. The film formation rate decreased with increasing the concentration of $(\text{NH}_4)_2\text{TiF}_6$, and the dependency of the induction period on the concentration of $(\text{NH}_4)_2\text{TiF}_6$ was small.

The QCM technique may be useful in monitoring the formation of thin films by the LPD method for characterizing the kinetics of the growth of the films.

References

- [1] G. Sauerbrey, *Z. Phys.* **155**, 206 (1959).
- [2] M. Seo, K. Yoshida, H. Takahashi, and I. Sawamura, *J. Electrochem. Soc.* **139**, 3108 (1992).
- [3] R. Beck, U. Pittermann, and K. G. Weil, *J. Electrochem. Soc.* **139**, 453 (1992).
- [4] M. R. Deakin and O. R. Melroy, *J. Electrochem. Soc.* **136**, 349 (1989).
- [5] J. H. Kaufman, K. K. Kanazawa, and G. B. Street, *Phys. Rev. Lett.* **53**, 2461 (1984).
- [6] D. Orata and D. A. Buttry, *J. Am. Chem. Soc.* **109**, 3574 (1987).
- [7] H. K. Park and W. H. Smyrl, *J. Electrochem. Soc.* **141**, L25 (1994).
- [8] K. K. Kanazawa and J. G. Gordon II, *Anal. Chim. Acta* **175**, 99 (1985).
- [9] R. H. Schmitt, E. L. Grove, and R. D. Brown, *J. Am. Chem. Soc.* **82**, 5292 (1960).
- [10] Y. A. Buslaev, D. S. Dyer, and R. O. Ragsdale, *Inorg. Chem.* **6**, 2208 (1967).
- [11] C. A. Wamser, *J. Am. Chem. Soc.* **70**, 1209 (1948).
- [12] R. E. Mesmer, K. M. Palen, and C. F. Baes, Jr., *Inorg. Chem.* **12**, 89 (1973).
- [13] C. A. Wamser, *J. Am. Chem. Soc.* **73**, 409 (1951).

Chapter 4

Vanadium Oxide Thin Films Prepared by Liquid-Phase Deposition

4.1 Introduction

Vanadium oxide is one of the functional inorganic materials used widely in the application fields such as catalyst [1, 2], cathode material for lithium ion secondary battery [3, 4], and electrochromic display device [5, 6]. Especially, V_2O_5 and related oxides have attracted interests as host materials for Li^+ intercalation. They are able to intercalate Li^+ ions electrochemically accompanied with reversible electrochromic effect. As thin film, it has high potentialities for use in electrochromic display devices, color filters, and other optical devices.

Usually, vanadium oxide thin films have been prepared by dry processes such as vacuum evaporation [7] and sputtering [5, 8], and by conventional wet processes such as electrochemical deposition [9] and sol-gel method [6].

In the present chapter, the author reports on the LPD method for preparing vanadium oxide thin films and the characterization of the deposited films. Electrochemical and optical properties of the deposited films related to electrochromism were also described.

4.2 Experimental

4.2.1 Liquid-phase deposition process

Vanadium (V) oxide (Nacalai Tesque Inc.) was dissolved in 5 % hydrofluoric acid aqueous solution (Hashimoto Chemical Corp.) at a concentration of vanadium ion was $0.384 \text{ mol dm}^{-3}$. This solution was diluted to 0.15 mol dm^{-3} with distilled water, and then supplied for the treatment solution for deposition. Non-alkali glass (Corning, # 7059), soda lime glass (Matsunami Glass Ind., Ltd.), and alumina ceramic plate were used as the substrates. After being degreased and washed ultrasonically, the substrate was immersed in the treatment solution and suspended therein vertically. Then aluminum metal plate, of which purity is 99.98 %, that acts as F^- ion scavenger was set around the suspended substrate. Then the reaction cell was kept at $30 \text{ }^\circ\text{C}$ for 20–40 h. The substrate was then removed from the solution, washed with distilled water and dried at ambient temperature. Some of samples were heat-treated at various temperatures for 1 h in a muffle furnace in an air flow.

4.2.2 Characterization of the deposited films and the treatment solutions

X-ray diffraction (XRD) studies of the deposited films were carried out on a Rigaku RINT-2100 diffractometer with thin film attachment, using Cu-K α radiation (40 kV, 40 mA). The measurements were made at an X-ray incidence angle of 1°. Infrared (IR) absorption spectra of the deposited films were measured with an A-302 IR spectrophotometer (Japan Spectroscopic Co. Ltd.) in the range of 5000–330 cm⁻¹. Thermogravimetric analysis (TG) and differential thermal analysis (DTA) for the precipitated powder were carried out with a Rigaku Type 8085 at a heating rate of 10 °C min⁻¹ in the air. Electron spin resonance (ESR) spectra of the precipitated powder were recorded at ambient temperature on an X-band spectrometer JES-FE3X (JEOL Ltd.). The g-values were determined from Mn²⁺ standard marker. Surface morphologies of the deposited films were observed by a scanning electron microscope (SEM, Hitachi, S-2500).

Optical absorption spectra of the treatment solutions were measured with a UVIDEC 660 (Japan Spectroscopic Co. Ltd.) in the range of 910–300 nm.

4.2.3 Measurements of electrochromic properties

In order to investigate electrochromic properties, the films were formed on indium tin oxide (ITO) coated glasses. The ITO film layer is a transparent conductor with a sheet resistance of 30 Ω sq.⁻¹. A copper wire was connected to this layer.

Cyclic voltammograms of the deposited films were measured in 1.0 mol dm⁻³ LiClO₄-propylene carbonate (PC) solution, using a potentiostat (Hokuto Denko Ltd., PS-5000) and a function generator (NF Circuit Design Block Co. Ltd., RW-101T) with a three-electrode system. Pt plate electrode and saturated calomel electrode (SCE) were used as the counter and reference electrodes, respectively.

Figure 4.1 shows the electrochromic device cell schematically. The electrolyte (1.0 mol dm⁻³ LiClO₄-PC solution) is sandwiched between the sample and an ITO coated glass by using a spacer. Optical absorption spectra were measured by a UVIDEC 660 (Japan Spectroscopic Co. Ltd.) over controlled charge transfer using coulometer (Hokuto Denko Ltd., HF 201). A constant voltage (2 V) was applied to the electrochromic device cell.

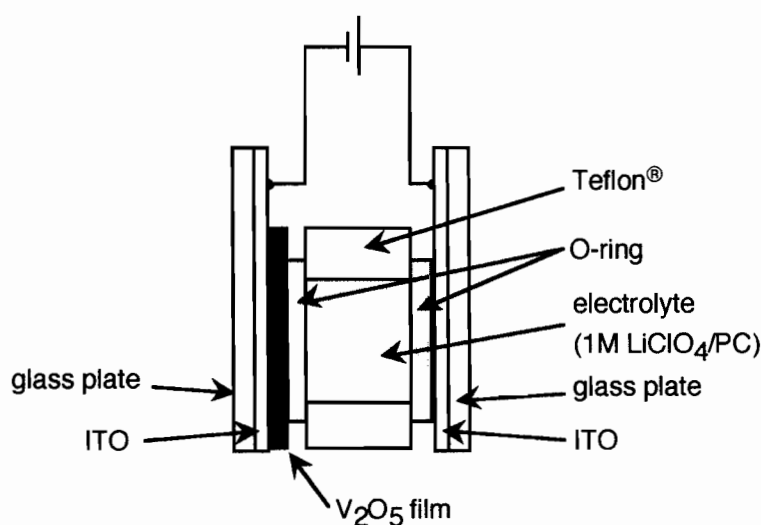


Figure 4.1. Schematic diagram of the electrochromic device cell.

4.3 Results and Discussion

4.3.1 Preparation and characterization of the films

After treatment for several tens of hours, brownish and transparent films were formed on the substrates. The deposited film showed strong adherence to the substrate. On the bottom of the reaction cell, there was brownish powder similar to the deposited film. The colors of the films changed with heat treatment. The films heat-treated at 100, 200, 300, and 400 °C were moss green, dark green, yellowish green, and yellow, respectively. These changes in color on the heat treatment suggest that the valence state of the vanadium ion in the films changed from IV to V during heat treatment in an air flow.

XRD patterns of the deposited films which were heat-treated at various temperatures are shown in Fig. 4.2. The as-deposited film and the films heat-treated at 100 and 200 °C were amorphous without any significant diffraction peak. However, the films heat-treated above 300 °C were crystallized. While diffraction peaks assigned to mixture of V_3O_7 and V_2O_5 were observed for the film heat-treated at 300 °C, only diffraction peaks of V_2O_5 were observed for the film heat-treated at 400 °C. V_3O_7 is a mixed oxide and one of the intermediates of oxidizing from V^{IV} to V^V oxide. It consists of VO_2 and V_2O_5 . From the XRD studies, it is concluded that the deposited film is crystallized and oxidized through the heat treatment.

The TG-DTA curves of the precipitated powder of the by-product are shown in

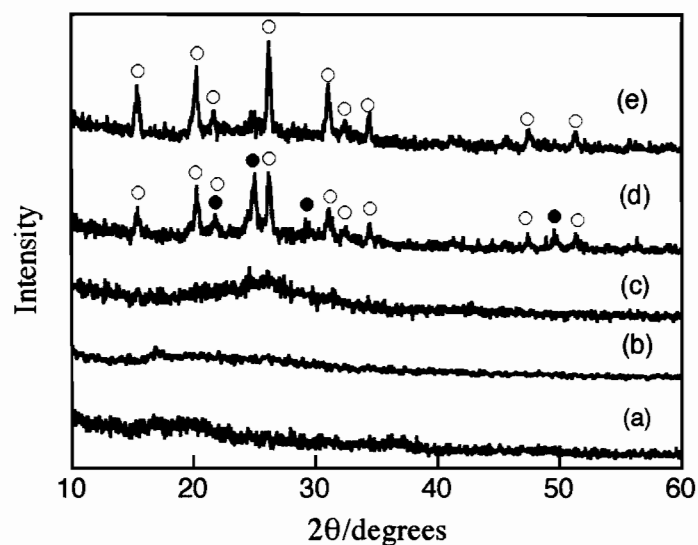


Figure 4.2. X-ray diffraction patterns of the deposited films heat-treated at various temperatures for 1 h in an air flow. \circ : V_2O_5 , \bullet : V_3O_7 . (a): As-deposited film, (b) to (e): films heat-treated at 100, 200, 300, and 400 °C, respectively.

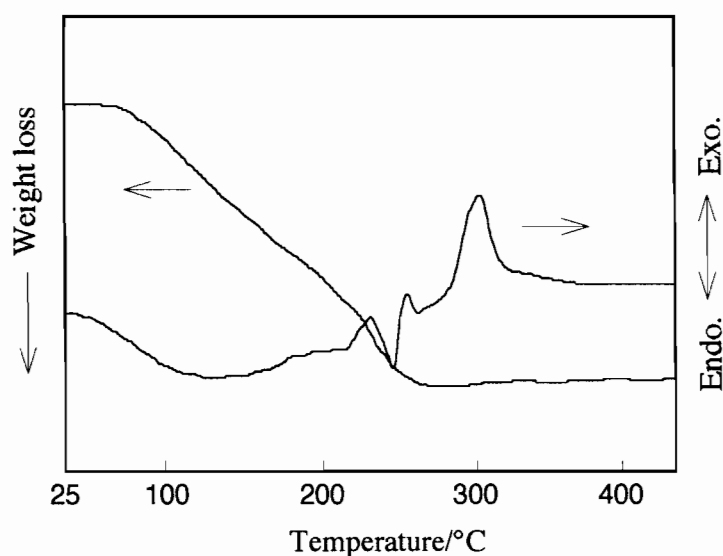


Figure 4.3. TG-DTA curves of the precipitated powder. Heating rate: $10\text{ }^\circ\text{C min}^{-1}$

Fig. 4.3. A broad endothermic peak was observed over the temperature range from room temperature to *ca.* 220 °C, and a sharp endothermic peak was observed at *ca.* 250 °C, accompanied by a weight loss in TG curve. The first and second endothermic peaks presumably correspond to the dissociation of physically and chemically bonded water molecules, respectively. Since the LPD process is performed in an aqueous

solution system, the deposited film encloses some water molecules as adsorbed or bound water. An exothermal peak at *ca.* 300 °C corresponds to the crystallization. The TG curve showed a little weight gain above 300 °C. It is presumably assigned to oxidation of vanadium ions.

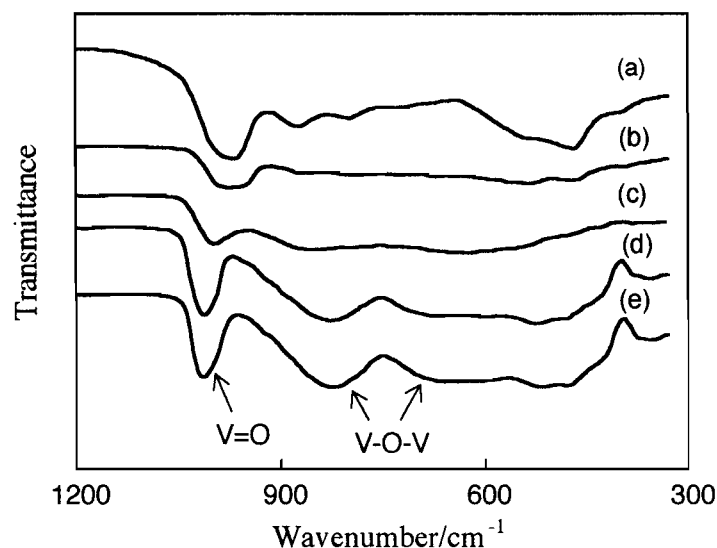


Figure 4.4. IR absorption spectra of the deposited films heat-treated at various temperatures for 1 h in an air flow. (a): As-deposited film, (b) to (e): films heat-treated at 100, 200, 300, and 400 °C, respectively.

Figure 4.4 shows IR absorption spectra of the deposited films. Absorption bands were all broad for the as-deposited film and the films heat treated at 100 and 200 °C. These bands were sharpened by the heat treatment above 300 °C. IR absorption spectrum of the as-deposited film showed absorption band at 970 cm⁻¹. This band shifted towards higher energies, that is higher wavenumbers, with increasing heat-treatment temperature. For the films heat-treated at 300 and 400 °C, the shifted band was observed at 1020 cm⁻¹, which is assigned to V=O stretching mode of V₂O₅ [10, 11]. These results indicate that the V=O bond length of the as-deposited film and the films heat-treated at low temperatures are longer than that of the films heat-treated at 300 and 400 °C. IR absorption spectra of the films heat-treated at 300 and 400 °C also showed absorption bands at 820 and 620 cm⁻¹, which are assigned to V-O-V deformation mode of V₂O₅ [10, 11]. The broadenings of the absorption bands for the as-deposited film and the films heat-treated at 100 and 200 °C indicate that the distributions of the bond lengths between the vanadium ion and the oxygen are broad. Based on these results, it is concluded that the valence state of vanadium ion in the as-deposited film and the films heat-treated at 100 and 200 °C is lower

than V^V , that is V^{IV} . Absorption bands at 3400 and 1620 cm^{-1} , which are assigned to an O-H stretching mode and an H-O-H deformation mode, respectively, were also observed for the as-deposited film and the films heat-treated at 100 and $200\text{ }^\circ\text{C}$. These bands completely disappeared after the heat treatment above $300\text{ }^\circ\text{C}$.

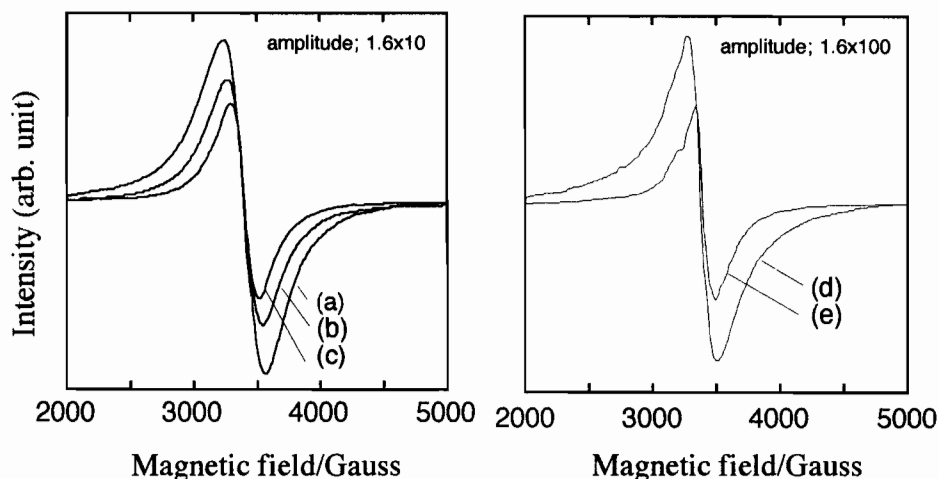


Figure 4.5. ESR spectra of the precipitated powders. (a): As-deposition, (b) to (e): heat-treatment at 100 , 200 , 300 , and $400\text{ }^\circ\text{C}$, respectively.

ESR spectra of the deposited powder which were heat-treated at various temperatures are shown in Fig. 4.5. As shown in Fig 4.5, a broad singlet band was observed for every sample. The g -values for these ESR bands were 1.97 of same constant values. These ESR bands were assigned to the V^{IV} ion, because V^{IV} ion has an unpaired electron [12]. Any hyperfine structure (hfs) due to the electron spin–nuclear spin coupling was not observed, even though the vanadium ion predominantly consists of ^{51}V , natural abundance is 99.75% , with a nuclear spin of $7/2$. Reasons why any hfs was not observed are following. (i) The dipole broadening due to the interaction among neighboring paramagnetic species owing to many V^{IV} species existing in the samples [13]. (ii) The electron delocalization occurred over several vanadium nuclei causing to the absence of hfs [13], because the measurements were carried out at ambient temperature. The intensity and line width of ESR signals decreased with increasing heat-treatment temperature. Furthermore, the signals for the samples heat-treated at 300 and $400\text{ }^\circ\text{C}$ are much weaker than that of the as-deposited film and that of the films heat-treated at 100 and $200\text{ }^\circ\text{C}$.

These data indicate that the as-deposited vanadium oxide thin film formed by the LPD method is amorphous and consists of V^{IV} ions, and it crystallized and oxidized upon the heat treatment in an air flow.

SEM photographs of the deposited films on non-alkali glass and alumina ceramic

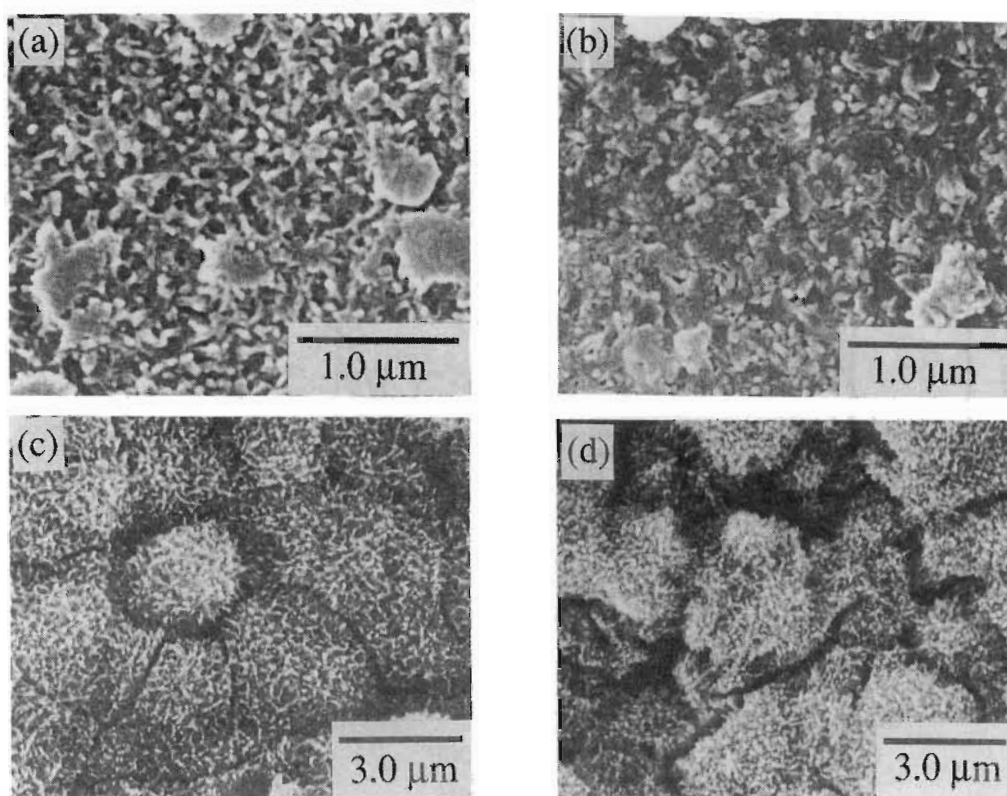


Figure 4.6. SEM photographs of the deposited films on non-alkali glass (a), (b) and on alumina ceramic plate (c), (d). (a), (c): As-deposited films, (c), (d): films heat-treated at 400 °C.

plate are shown in Fig. 4.6. It was found that the film was made up of small particles. These particles agglomerated on the heat treatment. As shown in Fig. 4.6 (c), (d), the deposited film completely covered over complicated surface of alumina ceramic plate. This is one of the good points of the LPD method.

When soda lime glass was used as the substrate, sodium vanadium bronze ($\text{Na}_{0.33}\text{V}_2\text{O}_5$) was formed. As-deposited film was brownish and comparatively transparent, it is very similar to the film formed on non-alkali glass. From XRD studies, the as-deposited film formed on the soda lime glass was amorphous as same as the film formed on non-alkali glass. Figure 4.7 shows XRD pattern of the films formed on soda lime glass heat-treated at 400 °C. This XRD pattern is different from that of the film formed on non-alkali glass, and showed that the film is $\text{Na}_{0.33}\text{V}_2\text{O}_5$ (sodium vanadium bronze). It is well-known that V_2O_5 exhibits a layered structure, the $[\text{V}_2\text{O}_5]$ layers being built up from VO_5 square pyramids sharing edges and corners [14]. It has been possible to to dope the V_2O_5 network by intercalation of alkali metal cations between the layers by electrochemically [15, 16] and chemically [17]. These facts suggest that the soda lime glass as substrate is etched by fluorine ions in the treatment solution during deposition reaction, and sodium ions were taken

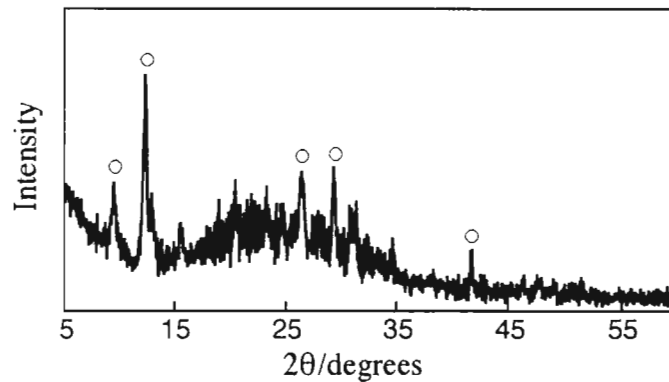


Figure 4.7. X-ray diffraction patterns of the deposited films on soda lime glass heat-treated at 400 °C for 1 h in an air flow. ○: $\text{Na}_{0.33}\text{V}_2\text{O}_5$.

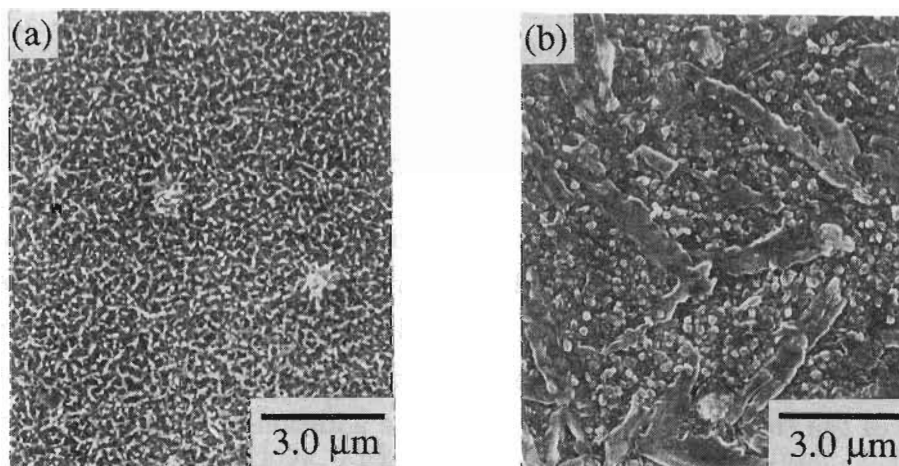


Figure 4.8. SEM photographs of the deposited films on soda lime glass. (a): As-deposited films and (b): films heat-treated at 400 °C.

into the deposited vanadium oxide. Then such sodium ions were intercalated during crystallization on heat treatment. It can be, also, considered that the diffusion of sodium ions from the substrate to the deposited film upon the heat treatment.

SEM photographs of the films formed on soda lime glass are shown in Fig. 4.8. The as-deposited film was made up of small particles. These are similar to those of the film on alumina ceramic plate. The morphology of the film changed obviously upon the heat treatment. The particles which composed the film grew into scale-like structure. It is considered that this structure reflecting layered structure.

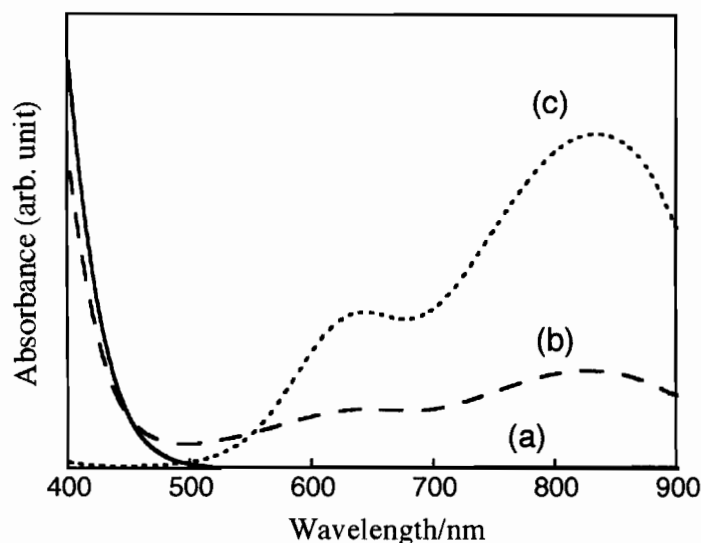
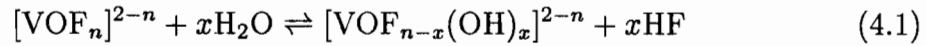


Figure 4.9. Optical absorption spectra of the treatment solutions. (a): Before the addition of aluminum metal. (b): After 2.5 and (c): 15 min of the addition of aluminum metal.

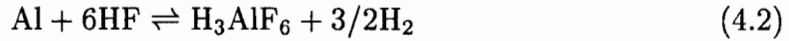
4.3.2 Mechanism of the film deposition

The treatment solution was yellowish in color before the addition of aluminum metal, but turned a bluish color just after adding aluminum. In order to clarify the dissolving species in the treatment solution, optical absorption spectra of the treatment solution before and after addition of aluminum metal were measured (Fig. 4.9). The spectrum of the treatment solutions before the addition of aluminum metal has an absorption edge which raises from 500 nm, and no other absorption bands were observed. The absorption band below 500 nm was assigned to a charge transfer band of the complex ion of V^V [18]. In the treatment solution, V^V exists as VO_2^+ , which may be partly coordinated by fluorine ions such as $[VO_2F_n]^{1-n}$. After the addition of aluminum metal, the spectrum obviously changed. The absorption band below 500 nm decreased gradually with time and disappeared completely after 15 min, and two kinds of absorption bands were observed in VIS region. The absorption bands at 630 and 830 nm were assigned to the ${}^2B_2 \rightarrow {}^2B_1$ transition and ${}^2B_2 \rightarrow {}^2E(I)$ transition of vanadyl ion, VO^{2+} [19], respectively, where vanadium ion has a valence of IV. From these results, it is concluded that the vanadium ion in the initial solution was V^V and it was reduced to V^{IV} by the addition of aluminum metal. In the solution, V^{IV} normally exists as VO^{2+} which is the most stable species in aqueous solution. It is considered that the VO^{2+} is coordinated by fluorine ions, and forms a fluoro-oxy complex ion, $[VOF_n]^{2-n}$ ($n \leq 5$), in the treatment solution.

The LPD process consists of ligand-exchange (hydrolysis) equilibrium reaction of the metal-fluoro complex ion, and F^- consuming reaction by aluminum metal as F^- scavenger. From experimental results, which showed the deposited film was vanadium oxide that consisted of V^{IV} ion, the author proposes following deposition mechanism similar to that for SiO_2 thin film deposition [20, 21]. V^{IV} ion exists as $[VOF_n]^{2-n}$ in the treatment solution and following F^- ion releasing reaction proceeds on the film depositing process:



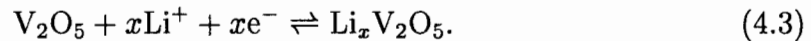
The ligand-exchange (hydrolysis) equilibrium reaction (4.1) is shifted to the right-hand side under the low of mass action by the addition of aluminum metal which reacts with F^- ions as follows:



The addition of aluminum leads to consumption of non-coordinated F^- ions and accelerates the ligand-exchange (hydrolysis) of $[VOF_n]^{2-n}$ (Eq. (4.1)). Then, the dehydration reaction occurs among $[VO(OH)_n]^{2-n}$ species, which are generated in the process of ligand-exchange reaction of $[VOF_n]^{2-n}$, near or on the surface of the substrate. Vanadium oxide deposition proceeds continuously with the reactions (4.1) and (4.2).

4.3.3 Electrochromic properties of the deposited films

It has been shown in previous works that V_2O_5 electrodes are able to intercalate lithium ions according to the following electrochemical reaction. This reaction is accompanied with reversible electrochromic effect [5, 8].



Cyclic voltammograms of the deposited films heat-treated at 300 and 400 °C are shown in Fig. 4.10. The film heat-treated at 400 °C showed quasi-reversible cyclic voltammogram similar to that reported for sputtered [5] or spin-coated V_2O_5 films [6]. Cathodic reduction and anodic oxidation peaks are attributed to Li^+ insertion and extraction, respectively. The color of the film changed from yellow to green on the cathodic sweep, and from green to yellow on the anodic sweep. The film heat-treated at 300 °C gave a different cyclic voltammogram from that of the film heat-treated at 400 °C. Although, the anodic oxidation peaks at *ca.* 0.5 and *ca.* 0.6 V, and the cathodic reduction peaks at *ca.* 0.4 and *ca.* 0 V were quite similar to that of

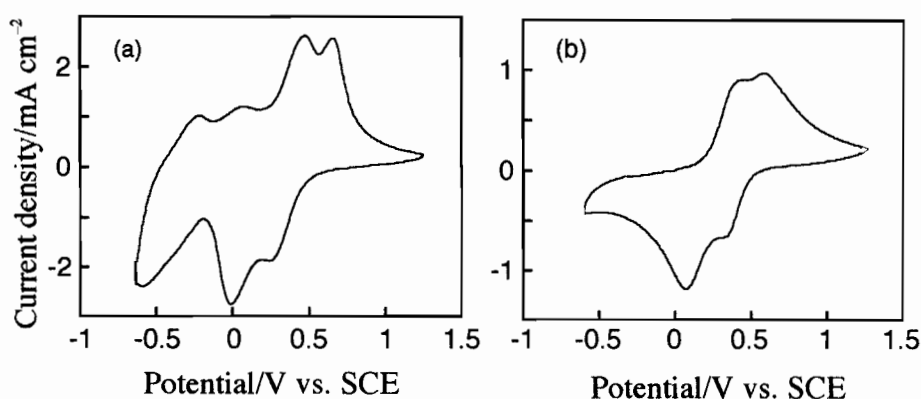


Figure 4.10. Cyclic voltammograms of the deposited films heat-treated at (a) 300 °C and (b) 400 °C. Sweep rate: 50 mV s⁻¹.

the film heat-treated at 400 °C, anodic oxidation current below 0.2 V and cathodic reduction current below -0.1 V newly appeared in the voltammogram. The color of the film changed from yellowish-green to grayish-blue for the cathodic sweep. From the XRD studies, two crystalline phases of V₂O₅ and V₃O₇ were observed for the film heat-treated at 300 °C, while only one crystalline phase of V₂O₅ was observed for the film heat-treated at 400 °C. On the basis of these results, it is considered that the redox reactions occur independently in the V₂O₅ and V₃O₇ phases for the film heat-treated at 300 °C, and it causes the differences in voltammograms and change of the colors of films between the films heat-treated at 300 and 400 °C.

Because the deposited film without heat treatment behaved insulator, electrochemical properties could not be measured. Broadened cyclic voltammograms with low current densities were obtained for the films heat-treated at 100 and 200 °C. The colors of these films did not change during potential cycles. Incomplete of oxidation and crystallization may be causes of the absence of electrochromism.

Figure 4.11 shows the optical absorption spectra of the heat treated film and the colored film. The absorption spectra of the films were measured by using electrochromic device cell (Fig. 4.1). The heat-treated film was yellow and it changed gradually to green with the injected charges by applying an external voltage with the polarity of the V₂O₅ film negative. As shown in Fig. 4.11, on injected charge the absorption edges of the films are shifted to higher energies and the absorption in the region above 650 nm increased. Since the absorption in the region above 650 nm increase, the color of the film changed to green. Figure 4.12 shows the change of absorbance at 800 nm as a function of the electric charges injected and extracted. The scale of abscissa of this figure indicates the injected charges for the coloring process and the differences between the whole injected charges and the extracted

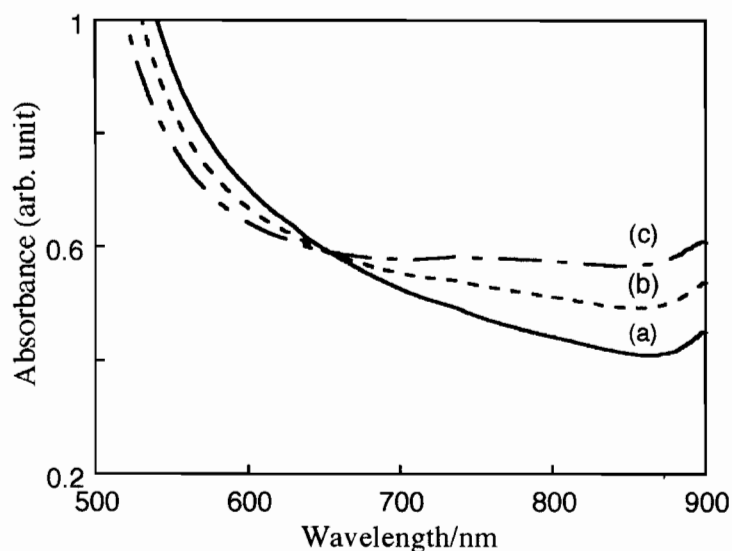


Figure 4.11. Optical absorption spectra of the films heat-treated at 400 °C. (a): As heat-treated film (0 mC cm^{-2}); (b): colored film (12 mC cm^{-2}); (c): colored film (24 mC cm^{-2}).

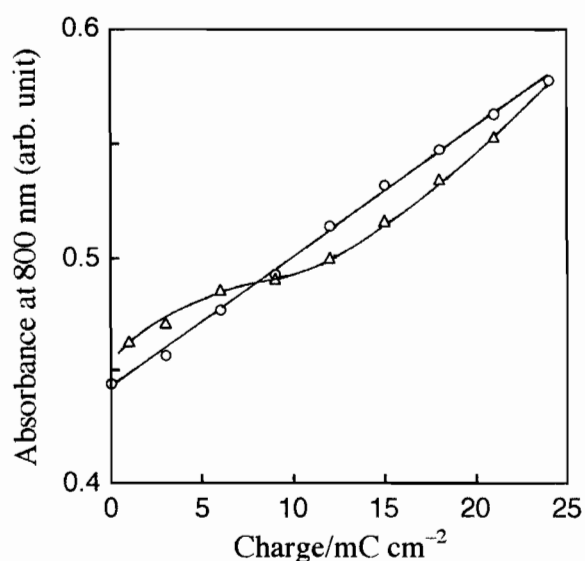


Figure 4.12. The change of absorbance at 800 nm for the films heat-treated at 400 °C as correlated with the electric charge injected and extracted. ○: Charge injection (coloring process); △: charge extraction (bleaching process).

charges for the bleaching process. The absorbance at 800 nm was increased linearly with charge injection, and it decreased gently with charge extraction. As shown in

Fig. 4.12, although the whole injected charges extracted from the colored film, the absorbance was not agree with that of the initial state. It suggests that the positive charges which do not act the coloring process are extracted during the bleaching process. However the origins of these positive charges are not identify.

4.4 Conclusion

The LPD method was applied to the preparation of vanadium oxide thin films. This process uses ligand-exchange (hydrolysis) equilibrium reaction in ($V_2O_5 - HF$) solution with the addition of aluminum metal as F^- scavenger which is able to shift the ligand-exchange equilibrium. The as-deposited film was amorphous and it consisted of reduced state vanadium ions, that is V^{IV} . On heat treatment in an air flow, the film was oxidized and crystallized. By the XRD studies, it was found that the film heat-treated at 300 °C was mixed oxide of V_3O_7 and V_2O_5 , and the film heat-treated at 400 °C was V_2O_5 . IR absorption spectra of the deposited films and ESR spectra of the deposited precipitate also indicated that the as-deposited film consisted of reduced state vanadium ion, V^{IV} , and it oxidized upon the heat treatment in an air flow.

The author proposed the following reaction mechanism for the deposition of vanadium oxide thin films by the LPD method. The film was formed through the ligand-exchange (hydrolysis) reaction of $[VOF_n]^{2-n}$ with H_2O . In the initial treatment solution, vanadium ions existed as $[VO_2F_n]^{1-n}$ which is the most stable species of V^V in an aqueous solution. By the addition of aluminum metal to the treatment solution, they were reduced to V^{IV} and form $[VOF_n]^{2-n}$ which is the most stable species of V^{IV} in an aqueous solution. Aluminum metal as F^- scavenger consumed F^- ions simultaneously, and accelerated the ligand exchange of $[VOF_n]^{2-n}$. Then, the dehydration reaction occurs among $[VO(OH)_n]^{2-n}$. Consequently, vanadium oxide formed on the immersed substrate.

The crystallized film showed electrochromism. The color changed from yellowish-green to grayish-blue for the film heat-treated at 300 °C and yellow to green for the film heat-treated at 400 °C when lithium ions were electrochemically injected and ejected. On injected charge by applying an external voltage with the polarity of the V_2O_5 film negative, the absorption edges of the films are shifted to higher energies and the optical absorption above 650 nm increased. The absorbance at 800 nm was increased linearly with charge injection, and it decreased gently with charge extraction. Although the whole injected charges extracted from the colored film, the absorbance was not agree with that of the initial state. It suggests that the

positive charges which do not act the coloring process are extracted during the bleaching process.

References

- [1] B. C. Bond, J. Sarkany, and G. D. Parfitt, *J. Catal.* **57**, 476 (1979).
- [2] S. Yoshida, *Catalyst* **10**, 90 (1968).
- [3] N. Machida, R. Fuchida, and T. Minami, *J. Electrochem. Soc.* **136**, 2133 (1989).
- [4] H. Park and W. H. Smyrl, *J. Electrochem. Soc.* **141**, L25 (1994).
- [5] S. F. Cogan, N. M. Nguyen, S. J. Perrotti, and R. D. Rauh, *J. Appl. Phys.* **66**, 1333 (1989).
- [6] K. Nagase, Y. Shimizu, M. Miura, and N. Yamazoe, *Appl. Phys. Lett.* **60**, 802 (1992).
- [7] Y. Fujita, K. Matazaki, and C. Tatsuyama, *Jpn. J. Appl. Phys.* **24**, 1082 (1985).
- [8] D. Wruck, S. Ramamurthi, and M. Rabin, *Thin Solid Films* **182**, 79 (1989).
- [9] T. Yoshino, N. Baba, and Y. Kouda, *Jpn. J. Appl. Phys.* **26**, 782 (1987).
- [10] L. D. Frederickson, Jr. and D. M. Hausen, *Anal. Chem.* **35**, 818 (1963).
- [11] T. R. Gilison, O. F. Bizri, and N. Cheetham, *J. Chem. Soc. Dalton Trans.* **3**, 291 (1973).
- [12] H. Takahashi, M. Shiotani, H. Kobayashi, and J. Sohma, *J. Catal.* **14**, 134 (1969).
- [13] J. Livage, P. Pineau, M. C. Leroy, and M. Michand, *phys. stat. sol. (a)* **39**, 73 (1977).
- [14] H. G. Bachmann, F. R. Ahmed, and W. H. Barnes, *Z. Kristallogr.* **115**, 110 (1961).
- [15] S. Hub, A. Trauchant, and R. Messina, *Electrochem. Acta.* **33**, 997 (1988).
- [16] A. Trauchant, J. M. Blengino, J. Farcy, and R. Messina, *J. Electrochem. Soc.* **139**, 1243 (1992).

-
- [17] D. W. Murphy, P. A. Christian, F. J. DiSalvo, and J. V. Waszczak, *Inorg. Chem.* **18**, 2800 (1979).
- [18] N. Gharbi, C. Sanchez, J. Livage, J. Lemerle, L. Néjem, and J. Lefebvre, *Inorg. Chem.* **21**, 2758 (1982).
- [19] C. J. Ballhausen and H. B. Gray, *Inorg. Chem.* **1**, 111 (1962).
- [20] H. Nagayama, H. Honda, and H. Kawahara, *J. Electrochem. Soc.* **135**, 2013 (1988).
- [21] A. Hishinuma, T. Goda, M. Kitaoka, S. Hayashi, and H. Kawahara, *Appl. Surf. Sci.* **48/49**, 405 (1991).

Chapter 5

Vanadium Dioxide Thin Films Prepared by Liquid-Phase Deposition

5.1 Introduction

VO₂ is known to have a reversible thermally-induced semiconductor-to-metal phase transition around 68 °C. Electrical conductivity and IR reflectivity increased abruptly when going through the transition temperature [1, 2]. The crystal of VO₂ undergoes a first-order phase transition from a low-temperature monoclinic structure to a high-temperature tetragonal structure [3]. In order to avoid the deterioration by volume change during the transition, the use of VO₂ in the form of thin film is proposed [4]. Thin films of VO₂ have been prepared by a variety of techniques such as reactive sputtering [5, 6], reactive evaporation [7], chemical vapor deposition [4, 8, 9], and sol-gel process [8, 10, 11]. In these processes, precise control of the deposition atmosphere is necessary to obtain the exact composition VO₂ film, because VO₂ gives the narrow stability range of the phase [12].

As described in the previous chapter, amorphous vanadium oxide thin films which consist of reduced state vanadium ions, that is V^{IV}, can be formed by the LPD method. It is considered that the crystalline VO₂ thin films can be obtained by heat treatment of the deposited films by the LPD method under inert atmosphere.

In this chapter, the author reports on the preparation and characterization of thin films of VO₂ by the LPD method. Electrical properties with respect to the thermally-induced semiconductor-to-metal phase transition of the obtained VO₂ films are also described.

5.2 Experimental

5.2.1 Liquid phase deposition process

Vanadium (V) oxide (Nacalai Tesque Inc.) was dissolved in 5 % hydrofluoric acid aqueous solution (Hashimoto Chemical Corp.) at a concentration of vanadium ion was 0.384 mol dm⁻³. This solution was diluted to 0.15 mol dm⁻³ with distilled water, and then supplied for the treatment solution for deposition. Non-alkali glass (Corning, # 7059) was used as the substrate. After being degreased and washed ultrasonically, the substrate was immersed in the treatment solution and suspended therein vertically. Then aluminum metal plate, of which purity is 99.98 %, that acts as F⁻ scavenger was set around the suspended substrate. Then the reaction cell was kept at 30 °C for several tens of hours. The substrate was then removed from the solution, washed with distilled water and dried at ambient temperature. Heat treatment of the deposited films were carried out at various temperatures in an N₂ atmosphere.

5.2.2 Characterization of the deposited films

X-ray diffraction (XRD) studies of the deposited films were measured on a Rigaku RINT-2100 diffractometer with thin film attachment, using Cu-K α radiation (40 kV, 40 mA). The measurements were made at an X-ray incidence angle of 1°. Surface morphologies of the deposited films were observed by a scanning electron microscope (SEM, Hitachi S-2500).

5.2.3 Electrical properties of the deposited thin films

The transition behaviors in electrical conductivity of the deposited VO₂ films were measured using a conventional two-probe method. Silver paste was coated in a coplanar geometry as electrodes. The sample was located on a temperature controlled electric heater plate, and it was heated at a rate of 2 °C min⁻¹ in a heating cycle. In a cooling cycle, spontaneous decrease in the temperature was adopted. The transition temperature (T_t) is taken as the temperature at which the midpoint of the conductivities at 40 and 90 °C in a heating cycle after cycling 3–4 times through T_t .

5.3 Results and Discussion

5.3.1 Preparation and characterization of the deposited films

It is considered from mentioned in the previous chapter that VO₂ film can be obtained by heat treatment of the deposited film under inert atmosphere. When the deposited film was heat-treated in an N₂ atmosphere, greenish film was obtained. Figure 5.1 shows the XRD patterns of the deposited films which were obtained by the heat-treatment at various temperatures in N₂ atmosphere for 1 h. The monoclinic VO₂ phase was observed for the film heat-treated above 400 °C in N₂ atmosphere. Other crystalline phases can not be detected from XRD patterns even the film heat-treated at 600 °C. Peak intensity became large and full-width at half-maximum of the diffraction peaks of VO₂ became narrow with increasing heat-treatment temperature. The diffraction from (011) plane of monoclinic VO₂ is particularly intense compared with a randomly oriented powder of VO₂. It indicates that the deposited VO₂ thin film is partially oriented to the [011] direction. Similar phenomenon is observed for the VO₂ thin films prepared by other methods, such as chemical vapor deposition [8] and sol-gel method [10].

SEM photographs of the deposited films heat-treated in N₂ atmosphere are shown in Fig. 5.2. The films were constructed of particles. The particle sizes were several

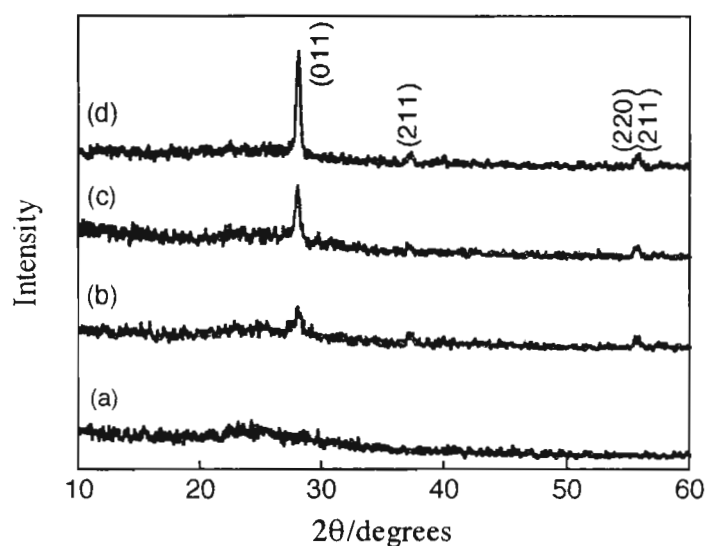


Figure 5.1. X-ray diffraction patterns of the deposited films heat-treated at various temperatures for 1 h in N_2 atmosphere. (a): As-deposited film, (b) to (d): films heat-treated at 400, 500, and 600 °C, respectively.

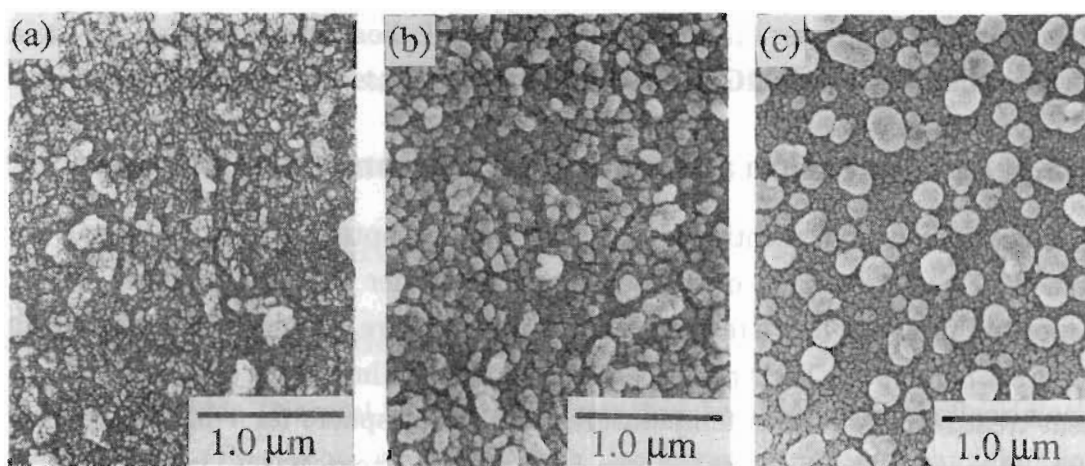


Figure 5.2. SEM photographs of the deposited films heat-treated at various temperatures for 1 h in N_2 atmosphere. Films heat-treated at 400 (a), 500 (b), and 600 °C (c).

tens of nanometers in diameter for the film heat-treated at 400 °C and around one hundred nanometer for that heat-treated at 500 °C. Agglomeration of the constructed particles was observed for the film heat-treated at 500 °C. The surface microstructure of the film heat-treated at 600 °C is different from the others, large particles which are 150–300 nm in diameter were observed on the small particles. SEM photographs of the cross-section of the deposited film heat-treated at 500 °C

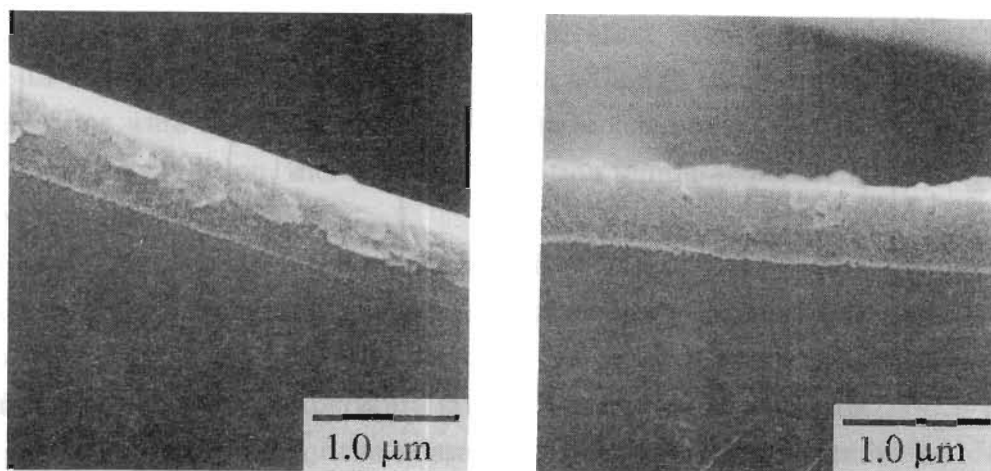


Figure 5.3. SEM photographs of the cross-section of the deposited film heat-treated at 500 °C for 1 h in N₂ atmosphere.

in N₂ atmosphere is shown in Fig. 5.3. The film exhibits a homogeneous flat surface and the thickness is *ca.* 500 nm.

5.3.2 Electrical properties of the LPD-VO₂ films

Electrical measurements were performed on the VO₂ films obtained by the heat treatment at 400 and 500 °C in N₂ atmosphere. The film obtained by the heat treatment at 600 °C showed very high resistivity more than 30 MΩ sq.⁻¹, which is too high to measure the resistivity. It is suggested for the film heat-treated at 600 °C that the formation of some insulator phases, although the XRD study of the film showed only the diffraction peaks of VO₂, and/or the resistance of this sample was dominated by high resistance of the crystallite boundaries.

Typical transition behaviors in the electrical resistivity are shown in Fig. 5.4. The resistivities were dropped abruptly around 70 °C. The heating-cooling hysteresis of *ca.* 10 °C were observed. The change in resistivity with temperature of the film obtained by the heat treatment at 500 °C was sharper than that obtained by the heat treatment at 400 °C. The transition temperatures (T_t), the ratios of the conductivities at 90 and 40 °C, and the activation energies of conduction for below and above T_t for the films obtained under several preparing conditions are summarized in Table 5.1. The transition temperatures of the films obtained by the heat treatment at 400 °C were lower than those obtained by the heat treatment at 500 °C, and the ratios of the conductivities of the films obtained by the heat treatment at 400 °C were smaller than those obtained by the heat treatment at 500 °C. Begishev *et al.* [13] and Griffiths *et al.* [12] indicate that the transition behavior depends on both structural and compositional factors. The broadening

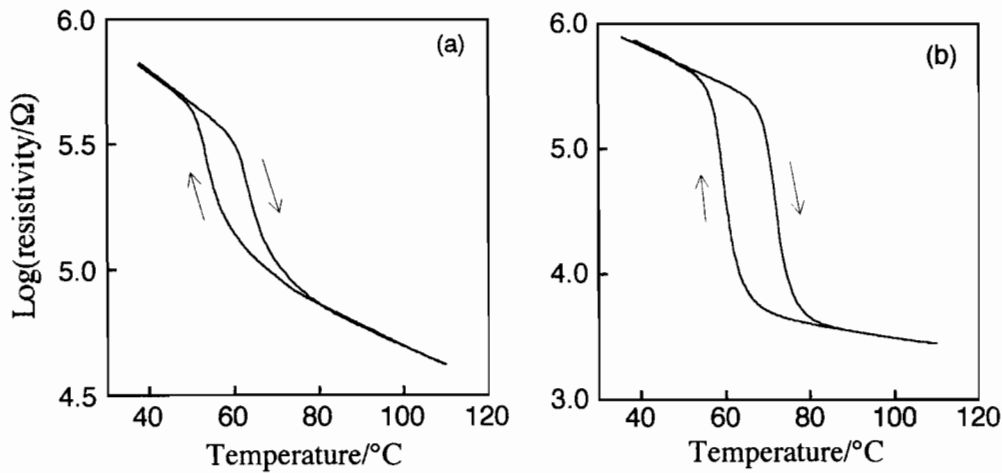


Figure 5.4. Typical transition behaviors in electrical resistivity of the LPD-VO₂ films. Films heat-treated at 400 (a) and 500 °C (b).

Table 5.1. Preparation conditions of the LPD-VO₂ films and the electrical conductivity data.

reaction time/h	heat treatment temperature/°C	transition temperature/°C	σ_{90}/σ_{40}	activation energy/eV	
				$T < T_t$	$T > T_t$
40	400	65.2	10	0.26	0.22
70	400	66.2	90	0.29	0.14
40	500	72.4	200	0.32	0.14
70	500	76.4	450	0.34	0.12

of the transition behavior of the film obtained by the heat treatment at 400 °C is attributed to an inhomogeneous distribution of transition temperature in the film because of the spatial inhomogeneity in the distribution of the factors for the change in transition temperature [13]. The film obtained by the heat treatment at 400 °C was deficient in crystallinity in comparison with that obtained by the heat treatment at 500 °C, thus it remained much amorphous phase. The existence of the much amorphous phase caused the broadening of the transition behavior. The crystal imperfection also affects the transition temperature. It is clear from Table 5.1, the transition temperatures of the films obtained by the heat treatment at 400 °C were lower *ca.* 10 °C than those obtained by the heat treatment at 500 °C. This is also explained by the differences in crystallinity between the films obtained by the heat treatment at 400 and 500 °C. In addition, compositional factors are also considered to explain the differences in the transition temperatures. The non-stoichiometry of the material, which is, for example, caused by the presence of V^{III}

or V^V ions, has influence on the transition temperature. It is reasonable to consider that the LPD- VO_2 films are non-stoichiometric, although exact compositions of the deposited films were not determined. The non-stoichiometry of the film depends on the preparing condition, therefore the transition temperature changes due to the preparing condition of the film.

In the high-temperature state, single crystals of VO_2 or high quality oriented VO_2 films exhibit positive temperature coefficients of resistivity, characteristic of metallic behavior [1, 7, 14]. In the LPD- VO_2 films, the temperature coefficients of resistivity were all negative in high-temperature state. It indicated that the LPD- VO_2 films were non-stoichiometric and/or the existence of some another semiconductor phases of vanadium oxide. In the low-temperature state, that is, semiconductor state, the linear Arrhenius behavior was observed, which provides a measure of the activation energy of conduction. The values of the activation energies of conduction, which is reported to be sensitive to the film stoichiometry [15, 16], for the LPD- VO_2 films are in the range 0.26–0.34 eV which is consistent with the range of reported values [14, 17].

5.4 Conclusion

The LPD method was applied to the preparation of vanadium dioxide thin films. Vanadium oxide thin films have been formed on the immersed substrates from the aqueous solution system of (V_2O_5 -HF aq.) with the addition of aluminum metal by the LPD method. The as-deposited film was amorphous and it consisted of V^{IV} ions. Monoclinic VO_2 phase was obtained when the deposited film was heat-treated above 400 °C in an N_2 atmosphere. The obtained VO_2 film was partially oriented to the [011] direction. No other phases were detected from XRD studies.

The obtained VO_2 film exhibited metal-to-semiconductor transition behavior around 70 °C accompanied with heating-cooling hysteresis *ca.* 10 °C. The transition temperature and sharpness of the transition behavior was depended on the preparation condition of the film. The transition temperature of the film obtained by the heat treatment at 500 °C was higher than that obtained at 400 °C, and the ratio of the conductivities below and above the transition temperatures for the film heat-treated at 500 °C was larger than that heat-treated at 400 °C.

References

- [1] F. J. Morin, *Phy. Rev. Lett.* **3**, 34 (1959).

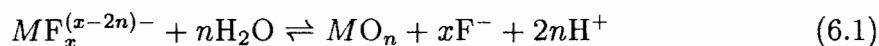
- [2] A. S. Barker Jr., H. W. Verleur, and H. J. Guggenheim, *Phy. Rev. Lett.* **17**, 1286 (1966).
- [3] J. B. Goodenough, *J. Solid State Chem.* **3**, 490 (1971).
- [4] C. B. Greenberg, *Thin Solid Films* **110**, 73 (1983).
- [5] G. A. Rozgonyi and D. H. Hensler, *J. Vac. Sci. Tech.* **5**, 194 (1969).
- [6] P. Jin and S. Tanemura, *Jpn. J. Appl. Phys. Part 1* **33**, 1478 (1994).
- [7] J. P. De Natale, P. J. Hood, and A. B. Harker, *J. Appl. Phys.* **66**, 5844 (1989).
- [8] Y. Takahashi, M. Kanamori, H. Hashimoto, Y. Moritani, and Y. Masuda, *J. Mater. Sci.* **24**, 192 (1989).
- [9] T. Maruyama and Y. Ikuta, *J. Mater. Sci.* **28**, 5073 (1993).
- [10] G. Guzman, R. Morineau, and J. Livage, *Mater. Res. Bull.* **29**, 509 (1994).
- [11] K. R. Speck, H. S. Hu, M. E. Sherwin, and R. S. Potember, *Thin Solid Films* **165**, 317 (1988).
- [12] C. H. Griffiths and H. K. Eastwood, *J. Appl. Phys.* **45**, 2201 (1974).
- [13] A. R. Begishev, G. B. Galiev, A. S. Ignat'ev, V. G. Mokerov, and V. G. Poshin, *Sov. Phys. Solid State* **20**, 951 (1978).
- [14] C. N. Berglund and A. Jayaraman, *Phys. Rev.* **185**, 1034 (1969).
- [15] N. Kimizuka, M. Ishii, I. Kawada, M. Saeki, and M. Nakahira, *J. Solid State Chem.* **9**, 69 (1974).
- [16] M. Fukuma, S. Zembutsu, and S. Miyazawa, *Appl. Opt.* **22**, 265 (1983).
- [17] C. N. Berglund and H. J. Guggenheim, *Phys. Rev.* **185**, 1022 (1969).

Chapter 6

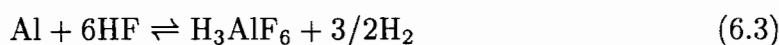
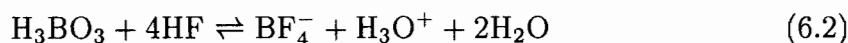
Iron Oxide Thin Films Prepared by Liquid-Phase Deposition

6.1 Introduction

Recently, a novel wet process has been developed for the preparation of thin metal oxide films. This process is called Liquid-Phase Deposition (LPD) process [1, 2]. In this process, it is possible to form metal oxide or metal hydroxide thin films onto the substrate which is immersed into the treatment solution for deposition. Metal oxide or hydroxide thin film is formed by means of ligand-exchange equilibrium reaction (hydrolysis) of metal-fluoro complex ionic species and F^- consumptive reaction by boric acid or aluminum metal as F^- scavenger [1, 2]. In aqueous solution, following ligand-exchange (hydrolysis) equilibrium reaction of metal-fluoro complex ion ($MF_x^{(x-2n)-}$) is presumed:



The equilibrium reaction (6.1) is shifted to the right-hand side by addition of boric acid or aluminum metal of F^- scavenger, which readily react with F^- and form stable complex ions as follows:



The LPD method is very simple process and does not require any special equipment such as vacuum system. It is, moreover, easy to apply to various kinds of substrates with large surface areas and/or complex morphologies, because the LPD method is performed in an aqueous solution system.

This chapter deals with the preparation and characterization of iron oxyhydroxide and iron oxide thin films by the LPD method. β -FeOOH (akageneite) thin film was formed from aqueous solution system of FeOOH-NH₄F·HF with addition of H₃BO₃ solution. The deposited film was transformed into α -Fe₂O₃ (haematite) by heat treatment.

6.2 Experimental

6.2.1 Liquid-phase deposition process

FeOOH-NH₄F·HF solution was used as a parent solution for deposition. FeOOH was precipitated by the hydrolysis of Fe(NO₃)₂ (Nacalai Tesque Inc.) with addition of NH₃ aq. (Nacalai Tesque Inc.). After the filtration of the precipitate, it was washed repeatedly and dried at ambient temperature. Then the precipitate was dissolved

in 1.0 mol dm⁻³ NH₄F·HF (Nacalai Tesque Inc.) solution at a concentration of 0.07 mol dm⁻³, and it was used for the parent solution. H₃BO₃ (Nacalai Tesque Inc.) was dissolved in distilled water at a concentration of 0.5 mol dm⁻³ and used as F⁻ scavenger. FeOOH–NH₄F·HF and H₃BO₃ solutions were mixed at various compositions and used as the treatment solution for deposition.

Non-alkali glass (Corning, # 7059) was used as the substrate. After being degreased and washed ultrasonically, the substrate was immersed in the treatment solution and suspended therein vertically. Reaction was carried out at 30 °C for 20 h. The substrate was then removed from the solution, washed with distilled water and dried at ambient temperature. Heat treatment of the deposited films were carried out in an air flow for 1 h at different temperatures ranging from 100 to 600 °C.

6.2.2 Characterization of the deposited films

X-ray diffraction (XRD) studies of the deposited films were carried out on a Rigaku RINT-2100 diffractometer with thin film attachment, using Cu-K α radiation (40 kV, 40 mA). The measurements were made at X-ray incidence angle of 1°. Crystallite sizes of the deposited films were calculated using Scherrer's equation, $L = 0.94\lambda/\beta \cos \theta$, where L is the mean dimension of the crystallites, β is the full width in radians subtended by the half maximum intensity width of the diffraction peak, θ is the diffraction angle, and λ is the wavelength of the Cu-K α radiation (1.54 Å) [3]. In order to calculate the crystallite size, the intensities were accumulated by repeating the measurement 20 times. Infrared (IR) absorption spectra of the deposited films were measured with an A-302 IR spectrophotometer (Japan Spectroscopic Co. Ltd.) in the range of 5000–330 cm⁻¹. Fluorine and iron contents of the deposited films were determined by an X-ray photoelectron spectroscopy (XPS, PHI, XPS-5600ci). Surface morphologies of the films were observed by a scanning electron microscope (SEM, Hitachi S-2500).

6.3 Results and Discussion

After reaction for 20 h, transparent orange film was formed on the substrate. The deposited film showed strong adherence to the substrate. As shown in Fig. 6.1, there was deposition region according to the concentrations of FeOOH and H₃BO₃ in the treatment solution. At the low concentration of H₃BO₃, any deposition was not observed. XRD patterns of the films formed at each point which are indicated in Fig. 6.1 are shown in Fig. 6.2. The diffraction peaks of every film are assigned to

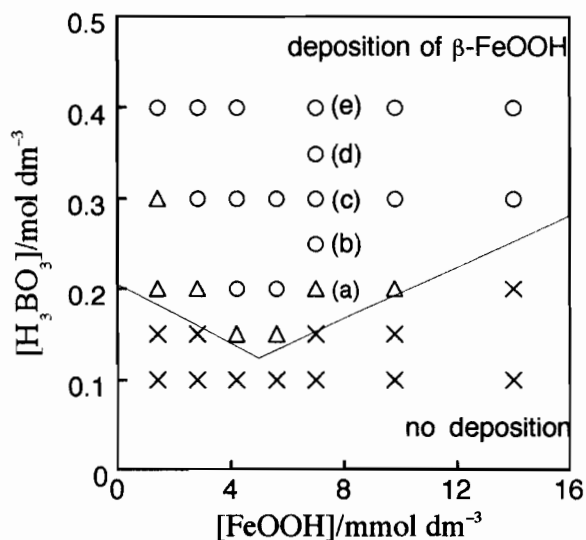


Figure 6.1. Relationship between aspect of the deposited film and the concentrations of FeOOH and H_3BO_3 . ○: Transparent β -FeOOH, △: hazy β -FeOOH, ×: no deposition. Reaction time: 20 h.

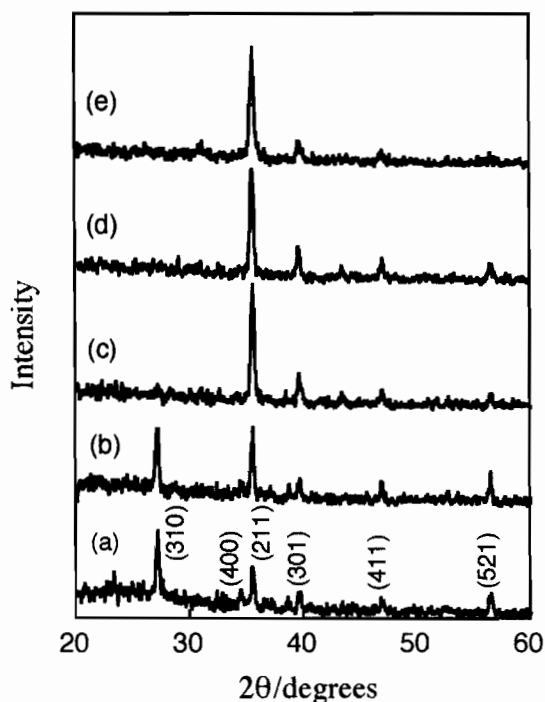


Figure 6.2. X-ray diffraction patterns of the films formed at each point which are indicated in Fig. 6.1. $[\text{FeOOH}]$: 7.0 mmol dm^{-3} . $[\text{H}_3\text{BO}_3]$: (a) 0.20, (b) 0.25, (c) 0.30, (d) 0.35, and (e) 0.40 mol dm^{-3} . Reaction time: 20 h.

β -FeOOH, but the intensity distributions of diffraction peaks are different according to the concentration of H_3BO_3 in the treatment solution. At the concentration of H_3BO_3 was 0.20 mol dm^{-3} (at the point (a)), the intensity distribution of diffraction peaks was agree with reported value for randomly oriented polycrystalline β -FeOOH powder, but the intensity of diffraction from (211) plane of β -FeOOH increased for the film deposited at the concentration of H_3BO_3 was 0.25 mol dm^{-3} (at the point (b)). When the concentration of H_3BO_3 was more than 0.30 mol dm^{-3} (at the points (c), (d), and (e)), the diffraction from (310) plane has disappeared completely, and very intense diffraction peak from (211) plane was observed. It indicates that the films, which deposited at the concentration of H_3BO_3 are more than 0.30 mol dm^{-3} , are preferentially oriented to the [211] direction. Surface morphologies of the

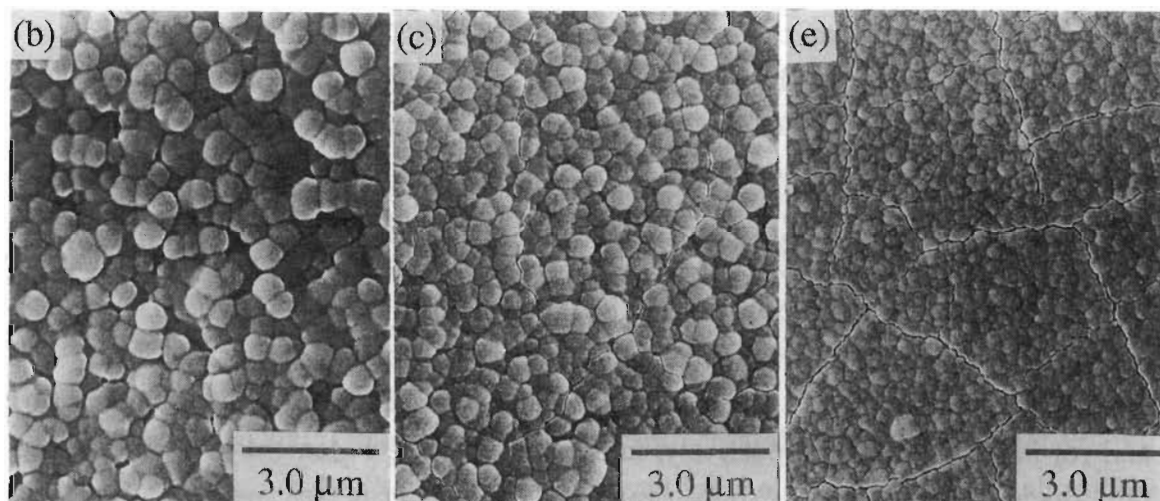
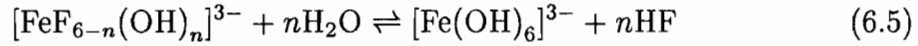
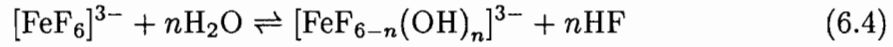


Figure 6.3. SEM photograph of the films formed at each point which are indicated in Fig. 6.1. $[\text{FeOOH}]$: 7.0 mmol dm^{-3} . $[\text{H}_3\text{BO}_3]$: (b) 0.25 , (c) 0.30 , and (e) 0.40 mol dm^{-3} . Reaction time: 20 h.

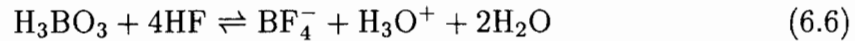
films formed at each point which are indicated in Fig. 6.1 are shown in Fig. 6.3. The films were constructed of particles which were several hundreds of nanometers in diameter. Particle size was decreased with increasing concentration of H_3BO_3 . Those were around 200 nm for the film formed at the point (b), around 150 nm at the point (c), and around 100 nm at the point (e), respectively.

For the formation of β -FeOOH thin films by the LPD method, the author proposes following deposition mechanism. The LPD method consists of ligand-exchange (hydrolysis) equilibrium reaction of metal-fluoro complex ion and F^- consuming reaction by boric acid of F^- scavenger [1, 2]. Iron ion in the treatment solution exists as Fe^{III} , and it may be coordinated by fluorine ions like $[\text{FeF}_6]^{3-}$. Following F^-

releasing reaction proceeds on the film formation process:



The ligand-exchange (hydrolysis) equilibrium reactions (6.4) and (6.5) are shifted to the right-hand side under the low of mass action by the addition of boric acid solution which readily reacts with F^- and forms stable complex as follows:



The addition of boric acid in the treatment solution leads to consumption of non-coordinated F^- and accelerates the ligand-exchange of $[\text{FeF}_6]^{3-}$ and $[\text{FeF}_{6-n}(\text{OH})_n]^{3-}$. Consequently, dehydration reaction occurs among $[\text{Fe}(\text{OH})_6]^{3-}$ species on the surface of the substrate, and iron oxyhydroxide thin film forms on the substrate.

It is well known that the presence of Cl^- or F^- ions during hydrolysis of Fe^{III} results in formation of β -FeOOH instead of α -FeOOH [4, 5, 6]. A large number of investigations related to the formation of β -FeOOH by hydrolysis of FeCl_3 aqueous solution have been made by many researchers. According to these investigations, the crystal structure of β -FeOOH has tunnel parallel to *c*-axis, in which water molecules and Cl^- ions were accommodated [6, 7, 8, 9]. In the case of F^- ion, same discussion is accepted, that is, F^- ions were accommodated in the tunnel of β -FeOOH. From XPS studies, F contents were 14.8 and 14.7 % F/Fe for the films formed at the points (b) and (c) in the Fig. 6.1, respectively, indicating that the F content in the deposited film was independent on the concentration of H_3BO_3 in the treatment solution. The unit cell of β -FeOOH has eight Fe atoms. If one F^- ion is accommodated in the unit cell of β -FeOOH, the F content is $1/8 = 12.5$ % F/Fe [8]. In the present case, F content was *ca.* 15 % F/Fe which is larger than 12.5 % F/Fe. It is considered that some F^- ions existed at the surfaces of the crystals which consist of the film.

Figure 6.4 shows XRD patterns of the films which were heat-treated at various temperatures for 1 h. The films were formed at the point (c) in Fig. 6.1, that is the as-deposited film was oriented β -FeOOH. As shown in Fig. 6.4, transformation into α - Fe_2O_3 upon heat treatment was observed. On the heat treatment at 100 °C, the intensities of the diffraction peaks were reduced, but there is no change in crystal phase. Only one broad and low-intensity diffraction peak was observed for the film heat-treated at 200 to 500 °C. The diffraction peak was assigned to α - Fe_2O_3 . On the heat treatment at 600 °C, the film was completely transformed into α - Fe_2O_3 . Ishikawa *et al.* [7, 8] reported that β -FeOOH, which obtained by hydrolysis of FeCl_3 , changes to an amorphous mixture of β -FeOOH and α - Fe_2O_3 in the temperature

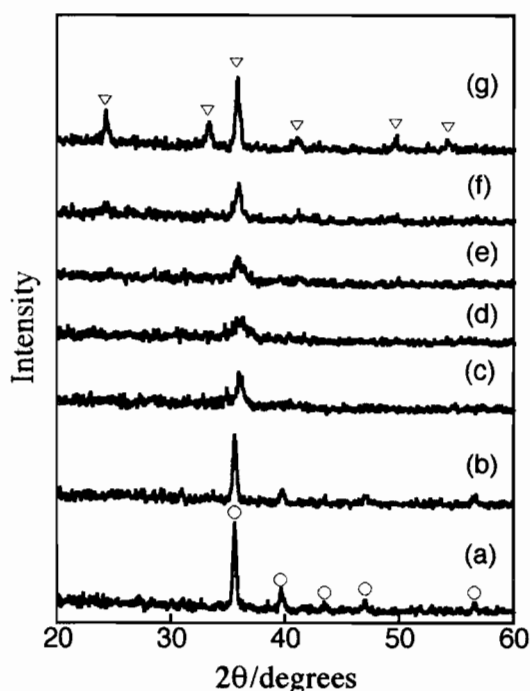


Figure 6.4. X-ray diffraction patterns of the deposited films heat-treated at various temperatures. (a): As-deposited film, (b) to (g): films heat-treated at 100, 200, 300, 400, 500, and 600 °C. \circ : β -FeOOH, ∇ : α -Fe₂O₃. [FeOOH]: 7.0 mmol dm⁻³. [H₃BO₃]: 0.3 mol dm⁻³. Reaction time: 20h.

range from 200 to 300 °C, and is transformed into crystalline α -Fe₂O₃ above 400 °C. In the present case, α -Fe₂O₃ phase was observed for the film heat-treated above 200 °C, however the crystallinity was low even heat-treated at 500 °C. The crystallite size which calculated using Scherrer's equation [3] for the diffraction peak at *ca.* 35° (diffraction from (211) plane for β -FeOOH and that from (110) plane for α -Fe₂O₃) is shown in Fig. 6.5. The crystallite size decreased with increasing heat-treatment temperature up to 300 °C, thereafter it increased. The decrease of the crystallite size is due to destruction of the structure of β -FeOOH, and the increase of the crystallite size is due to the crystal growth of α -Fe₂O₃ phase. The intensity distribution of the diffraction peaks of the film heat-treated at 600 °C is different from that of randomly oriented powder of α -Fe₂O₃. The diffraction from (110) plane is particularly intense, indicating that the film is partially oriented to [110] direction.

Figure 6.6 shows SEM photographs of the films heat-treated at various temperatures. Any morphological change was not observed upon the heat treatment.

Figure 6.7 shows the F/Fe atomic ratio of the films formed at the point (c) in Fig. 6.1 as a function of heat treatment temperature. The F content in the deposited

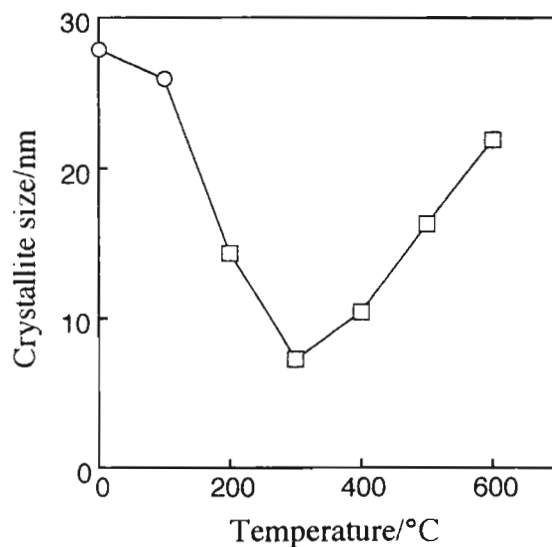


Figure 6.5. Relationship between the crystallite size and heat-treatment temperature. ○: Calculated for the diffraction peak from (211) plane of β -FeOOH and □: calculated for (111) plane of α -Fe₂O₃. [FeOOH]: 7.0 mmol dm⁻³. [H₃BO₃]: 0.3 mol dm⁻³. Reaction time: 20h.

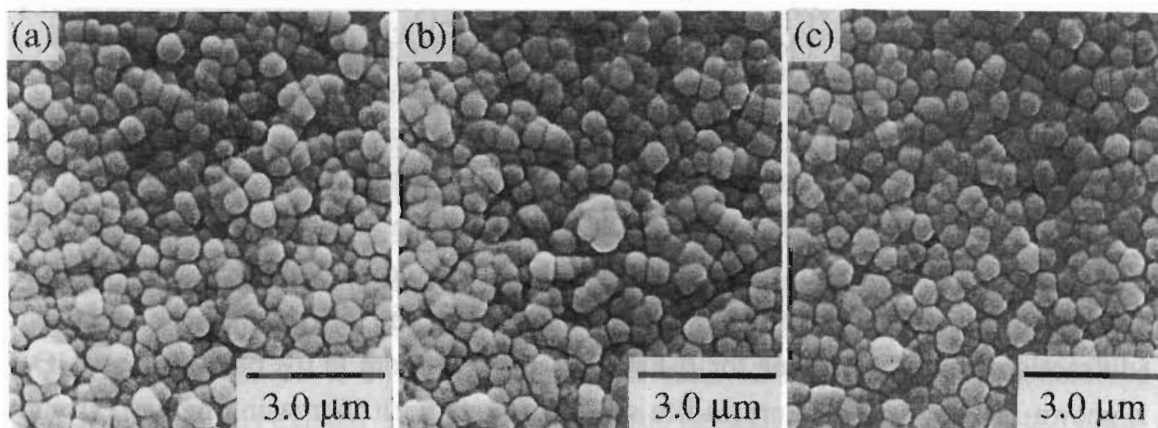


Figure 6.6. SEM photograph of the films heat-treated at various temperatures in an air flow. Films heat-treated at 200 (a), 400 (b), and 600 °C (c). [FeOOH]: 7.0 mmol dm⁻³, [H₃BO₃]: 0.3 mol dm⁻³. Reaction time: 20 h.

film is constant below 100 °C, decreased rapidly with increasing temperature in the range 100–300 °C and then decreased gently with temperature up to 600 °C. It is presumed that β -FeOOH contains two kinds of F⁻ ions, one of which can be readily removed and the other which strongly bound to Fe. The formers are presumably existed on the surfaces of the crystals and the latters are accommodated in the tunnel of β -FeOOH [10]. The F content of the film heat-treated at 600 °C was

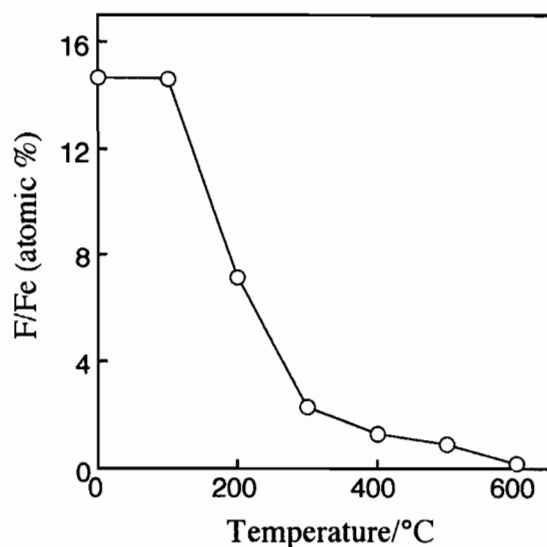


Figure 6.7. F contents in the deposited films heat-treated at various temperatures. $[\text{FeOOH}]$: 7.0 mmol dm^{-3} . $[\text{H}_3\text{BO}_3]$: 0.3 mol dm^{-3} . Reaction time: 20h.

0.19 % F/Fe.

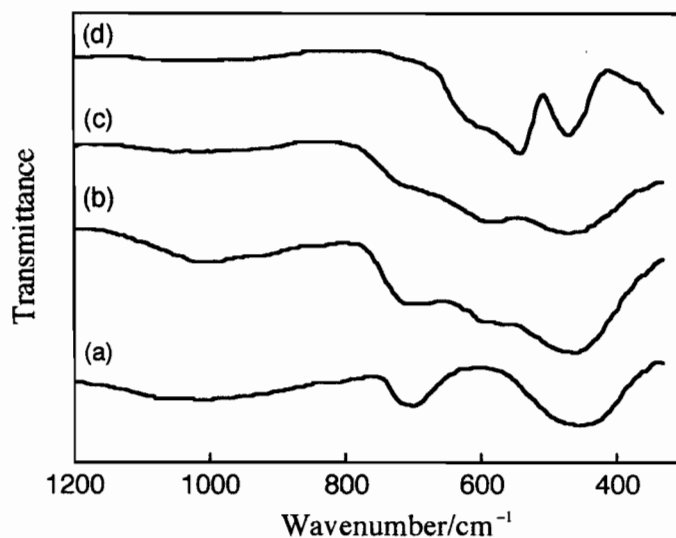


Figure 6.8. IR absorption spectra of the deposited films heat-treated at various temperatures. (a): As-deposited film, (b) to (d): films heat-treated at 200, 400, and 600 °C. $[\text{FeOOH}]$: 7.0 mmol dm^{-3} , $[\text{H}_3\text{BO}_3]$: 0.3 mol dm^{-3} . Reaction time: 20 h.

IR absorption spectra of the deposited films heat-treated at various temperatures are shown in Fig. 6.8. The spectra were measured by conventional KBr method for the films which scratched out from the substrates. IR absorption spectrum of the

as-deposited film has absorption bands at 700 and 450 cm^{-1} . Müller [11] reported that β -FeOOH prepared from FeCl_3 solution has IR absorption bands at 840 and 690 cm^{-1} due to the deformation mode of Fe-OH groups. Ishikawa and Inouye [8] reported that β -FeOOH has absorption bands at 840, 690, and 640 cm^{-1} which are assigned the deformation mode of Fe-OH groups. And the absorption bands at 840 and 640 cm^{-1} diminished with removal of Cl^- ions contained within the tunnels of β -FeOOH crystal. Ishikawa *et al.* [12, 13] accounted the diminution of the absorption bands at 840 and 640 cm^{-1} as follow. In the β -FeOOH, Fe-OH groups exist in the wall of the tunnels of the crystal. Cl^- ions and water molecules exist in the tunnels, therefore there are two kinds of Fe-OH groups one of which interacts with Cl^- ions and another which interacts with water molecules. The absorption bands at 840 and 640 cm^{-1} which diminished with removal of Cl^- ion are assigned to the deformation band of Fe-OH groups interacting with Cl^- ions. In the present spectra (Fig. 6.8), the bands of 840 and 640 cm^{-1} were not observed. The details are indistinct, but it is considered that differences in interaction with water molecules between Cl^- and F^- cause such difference in IR absorption band.

The absorption band at 450 cm^{-1} is assigned to lattice vibration of β -FeOOH [10]. For the films heat-treated at 200 and 400 $^\circ\text{C}$, the absorption bands became broad and the absorption band at 700 cm^{-1} was disappeared, indicating that the destruction of the structure of β -FeOOH and transformation into α - Fe_2O_3 . IR absorption spectrum of the film heat-treated at 600 $^\circ\text{C}$ showed absorption bands at 540 and 470 cm^{-1} , which are characteristic of α - Fe_2O_3 [10, 14].

6.4 Conclusion

The LPD method was applied to the preparation of iron oxyhydroxide and iron oxide thin films. The crystalline β -FeOOH thin film was formed by the LPD method from a mixed solution of ($\text{FeOOH-NH}_4\text{F}\cdot\text{HF}$) and H_3BO_3 at ambient temperature. F content of the formed film was *ca.* 15 % F/Fe. XRD measurements revealed that the film deposited at higher concentration of H_3BO_3 was oriented to the [211] direction. On the other hand, the formed film was randomly oriented when the concentration of H_3BO_3 was low.

On heat treatment in an air flow, the deposited film (crystalline β -FeOOH) was changed to amorphous, and was transformed into α - Fe_2O_3 completely at 600 $^\circ\text{C}$. F/Fe atomic ratio of the deposited film decreased with increasing heat treatment temperature, and it was 0.19 % for the film heat treated at 600 $^\circ\text{C}$.

The author proposes the following reaction mechanism for the deposition of iron

hydroxide thin films by the LPD method. In the treatment solution, Fe^{III} exists as [FeF₆]³⁻ or partially hydrolyzed species, [FeF_{6-n}(OH)_n]³⁻. The ligand-exchange (hydrolysis) reaction of such species was accelerated by the addition of H₃BO₃ as F⁻ scavenger. Then the dehydration reaction occurs in [Fe(OH)₆]³⁻ at the surface of the substrate. Consequently, iron oxyhydroxide thin film formed on the immersed substrate.

References

- [1] H. Nagayama, H. Honda, and H. Kawahara, *J. Electrochem. Soc.* **135**, 2013 (1988).
- [2] A. Hishinuma, T. Goda, M. Kitaoka, S. Hayashi, and H. Kawahara, *Appl. Surf. Sci.* **48/49**, 405 (1991).
- [3] B. E. Warren, in *X-ray Diffraction*, Dover Publications, New York, p.253 (1969).
- [4] D. Dasgupta and A. Mackay, *J. Phys. Soc. Jpn.* **14**, 932 (1959).
- [5] Y. Ujihira and M. Ohyabu, *J. Phys. Coll. C* **2**, 347 (1979).
- [6] C. M. Flynn, Jr., *Chem. Rev.* **84**, 31 (1984).
- [7] T. Ishikawa and K. Inouye, *Bull. Chem. Soc. Jpn.* **46**, 2665 (1973).
- [8] T. Ishikawa and K. Inouye, *Bull. Chem. Soc. Jpn.* **48**, 1580 (1975).
- [9] J. Bottero, A. Manceau, F. Villieras, and D. Tchoubar, *Langmuir* **10**, 316 (1994).
- [10] K. M. Parida, *J. Mater. Sci.* **23**, 1201 (1988).
- [11] A. Müller, *Arzneimittel Forsch.* **17**, 921 (1967).
- [12] K. Kandori, M. Fukuoka, and T. Ishikawa, *J. Mater. Sci.* **26**, 3313 (1991).
- [13] T. Ishikawa, T. Takeda, and K. Kandori, *J. Mater. Sci.* **27**, 4531 (1992).
- [14] C. J. Serna, J. L. Rendon, and J. E. Iglesias, *Spectrochim. Acta* **38A**, 797 (1982).

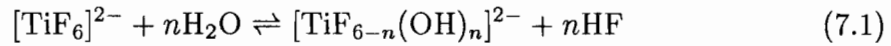
Chapter 7

Gold-Dispersed Titanium Oxide Thin Films Prepared by Liquid-Phase Deposition

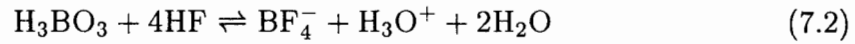
7.1 Introduction

Microcrystals of metals and semiconductor-doped glasses have been studied in detail due to their large optical nonlinearity [1, 2, 3, 4, 5]. These glasses are expected to be used in optical logic devices in an optical information context. Generally, these metal-dispersed glass films or thin layers are prepared by r.f. sputtering [1], ion-implantation [2], and the sol-gel method [3].

In the Chapter 2, the author described a very simple wet process for the preparation of TiO₂ thin films, the Liquid-Phase Deposition (LPD) method. In this process, transparent anatase thin films form directly on the substrates which are immersed in a mixed solution of ammonium hexafluorotitanate [(NH₄)₂TiF₆] and boric acid (H₃BO₃). In the solution, following ligand-exchange (hydrolysis) equilibrium reaction of (NH₄)₂TiF₆ is presumed:



This equilibrium reaction is shifted to the right-hand side by the addition of boric acid which readily reacts with F⁻ and forms stable complex ion as follows:



The addition of H₃BO₃ leads to consumption of non-coordinated F⁻ ions and accelerates the ligand-exchange (hydrolysis) reaction (7.1). Consequently, titanium oxide thin films form on the substrates immersed in the solution. This process is readily applied to the preparation of thin films on substrates which have a complex morphologies and large surface areas without special equipment, because the LPD process is performed in an aqueous solution system. Multi-component oxide thin films can be formed by the addition of the objective metal ion to the treatment solution.

In this chapter, preparation and characterization of Au-dispersed TiO₂ thin film using the LPD method by adding tetrachloroauric acid (HAuCl₄) solution to the mixed solution of (NH₄)₂TiF₆ and H₃BO₃ is described. The as-deposited film contained Au^{III} and following heat treatment or photoirradiation produced dispersed Au metal particles. The films deposited were characterized by X-ray diffraction, X-ray photoelectron spectroscopy, transmission electron microscopy, and optical absorption spectroscopy.

7.2 Experimental

7.2.1 Liquid-phase deposition process

As parent solutions, $(\text{NH}_4)_2\text{TiF}_6$ (Kishida Chemical Co. Ltd.) and H_3BO_3 (Nacalai Tesque Inc.) were dissolved in distilled water at concentrations of 0.5 mol dm^{-3} , and HAuCl_4 (Wako Pure Chemical Industries Ltd.) was dissolved in distilled water at a concentration of 2.4 mmol dm^{-3} . These solutions were mixed at various compositions and used as the treatment solution for deposition. The films were formed at a concentration of 0.1 mol dm^{-3} for $(\text{NH}_4)_2\text{TiF}_6$ and of 0.2 mol dm^{-3} for H_3BO_3 . This solution composition is that corresponding to the concentration at which the transparent anatase thin film was formed (*cf.* Chapter 2). The concentration of HAuCl_4 in the treatment solution was varied from 0.1 to 1.0 mmol dm^{-3} . Most of the experiments were performed with the concentration of HAuCl_4 at $0.29 \text{ mmol dm}^{-3}$. Non-alkali glass (Corning, # 7059) was used as the substrate. After being degreased and washed ultrasonically, the substrate was immersed in the treatment solution and suspended therein vertically for 20 h. The substrate was then removed from the solution, washed with distilled water and dried at ambient temperature. Heat treatment was carried out in an air flow for 1 h at various temperatures from 100 to $600 \text{ }^\circ\text{C}$. Photoirradiation of the deposited films were carried out by a 100 W high-pressure mercury lamp USH-102D (Ushio Denki Co.) with a power supply HB-101A (Ushio Denki Co.) at ambient temperature for 20 to 120 min. The irradiated films were stored in the dark at ambient temperature.

7.2.2 Characterization of the deposited films

The atomic ratios of Au/Ti in the deposited films were determined by inductively coupled plasma atomic emission spectroscopic analysis (ICP-AES, Seiko Instruments Inc., SRS 1500VR) of the solutions produced by dissolving the films with dilute hydrochloric acid. X-ray photoelectron spectroscopic (XPS) analyses of the deposited films were carried out on a Shimadzu ESCA 750 instrument. X-ray diffraction (XRD) studies of the deposited films were measured on a Rigaku RINT 2100 diffractometer with thin film attachment, using $\text{Cu-K}\alpha$ radiation (40 kV, 40 mA). Crystallite sizes of the dispersed gold were calculated using Scherrer's equation, $L = 0.94\lambda/\beta \cos\theta$, where L is the mean dimension of the crystallites, β is the full width in radians subtended by the half maximum intensity width of the diffraction peak, θ is the diffraction angle, and λ is the wavelength of the $\text{Cu-K}\alpha$ radiation (1.54 \AA) [6]. In order to calculate the crystallite size, the intensities were accu-

mulated by repeating the measurement 10 times. Optical absorption spectra were measured with a UVIDE C 660 (Japan Spectroscopic Co. Ltd.). Particle sizes of the dispersed Au metal were measured directly on a Hitachi H-7100TE transmission electron microscope (TEM).

7.3 Results and Discussion

The deposited film was colourless, transparent, and showed strong adherence to the substrate.

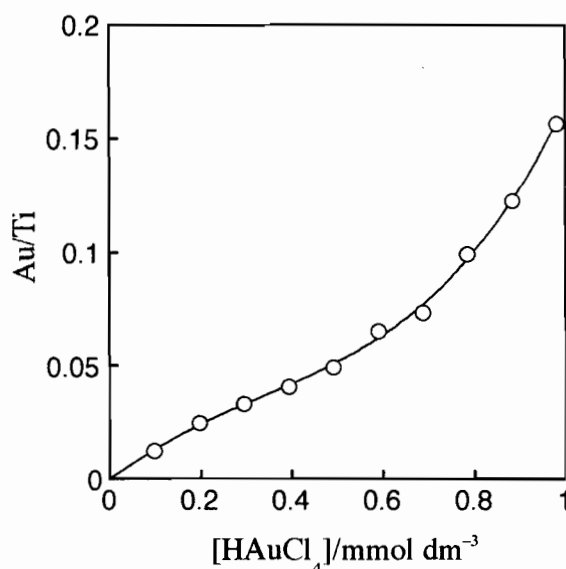


Figure 7.1. Relationship between the Au/Ti atomic ratio of the deposited film and the concentration of HAuCl₄ in the treatment solution. Concentration of (NH₄)₂TiF₆: 0.1 mol dm⁻³ and of H₃BO₃: 0.2 mol dm⁻³. Reaction time: 20 h.

Figure 7.1 shows the relationship between the concentration of HAuCl₄ in the treatment solution and the Au/Ti atomic ratio of the deposited films. The Au content of the deposited film increased up to *ca.* 0.16 with increasing HAuCl₄ concentration in the treatment solution. This indicates that the Au content of the film is controllable over a wide range by controlling the concentration of HAuCl₄ in the treatment solution. In the X-ray photoelectron spectrum of the as-deposited film, the binding energy of Au 4f_{7/2} was 86.3 eV which is close to that of Au^{III} [7], indicating that gold exist as Au^{III} ionic species in the as-deposited film.

7.3.1 Heat treatment of the deposited films

The film changed from colourless to purple on heat treatment, indicating the formation of Au metal particles in the film. In the X-ray photoelectron spectrum of the film heat-treated at 600 °C, the binding energy of Au 4f_{7/2} was 84.3 eV which is close to that of Au metal [7].

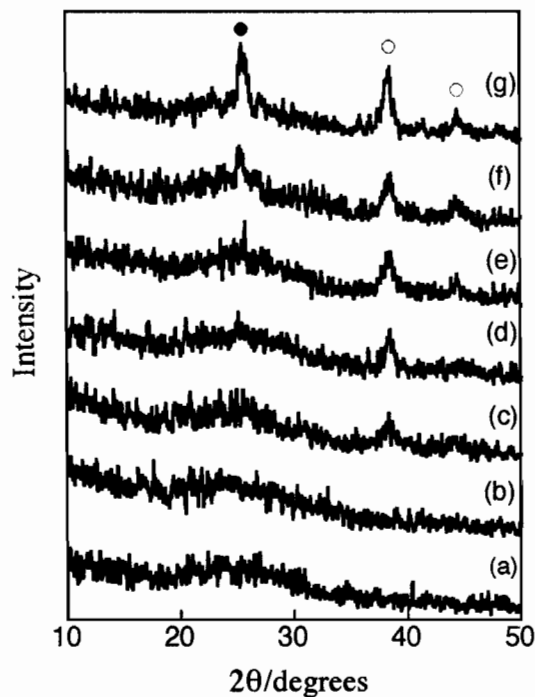


Figure 7.2. X-ray diffraction patterns of the deposited films heat-treated at various temperatures for 1 h. (a): As-deposited film, (b) to (g): films heat-treated at 100, 200, 300, 400, 500, and 600 °C, respectively. ○: Au, ●: TiO₂ (anatase). Concentration of (NH₄)₂TiF₆: 0.1 mol dm⁻³, of H₃BO₃: 0.2 mol dm⁻³, and of HAuCl₄: 0.29 mmol dm⁻³. Reaction time: 20 h.

The XRD patterns of the deposited films which were heat-treated at various temperatures for 1 h are shown in Fig. 7.2. The measurements were made at an X-ray incidence angle of 1°. The as-deposited film and the film heat-treated at 100 °C were amorphous without any significant diffraction peak. The diffraction peaks assigned to Au metal were observed for the deposited films after heat-treated above 200 °C. The decomposition of Au^{III} ionic species with formation of Au micro crystals occurred in the temperature range 100 to 200 °C. The full-width at half-maximum of the diffraction peaks of Au (111) decreased as the heat-treatment temperature increased, indicating that the Au metal crystals aggregated and grew in crystallite size during the heat treatment. The crystallite sizes calculated using Scherrer's

equation [6] for the diffraction line from Au (111) are summarized in Table 7.1. For the films heat-treated above 400 °C, diffraction peaks assigned to anatase as the matrix phase of the film were also observed. This indicates that the oxide phase as the matrix was transformed from amorphous to crystalline anatase by the heat treatment simultaneously with formation and aggregation of the Au metal particles.

Table 7.1. Crystallite and mean particle sizes of the dispersed Au metal particles in the films heat-treated at various temperatures.

heat-treatment temperature/°C	crystallite size/nm	mean particle size/nm
200	8.5	–
300	11.5	–
400	12.4	14.6
500	14.0	17.4
600	14.0	15.6

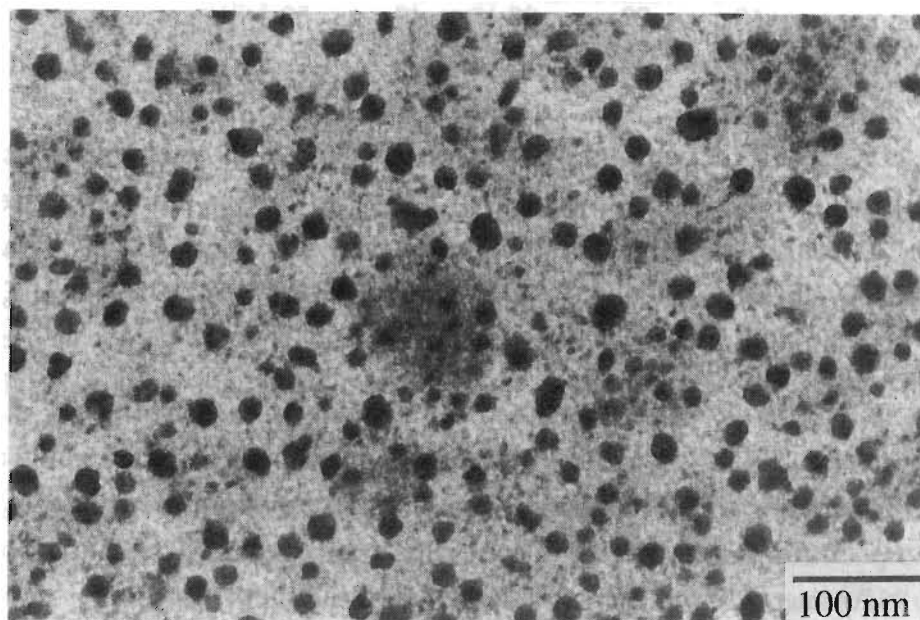


Figure 7.3. TEM photograph of the deposited film heat-treated at 400 °C for 1 h. Concentration of $(\text{NH}_4)_2\text{TiF}_6$: 0.1 mol dm^{-3} , of H_3BO_3 : 0.2 mol dm^{-3} , and of HAuCl_4 : $0.29 \text{ mmol dm}^{-3}$. Reaction time: 20 h.

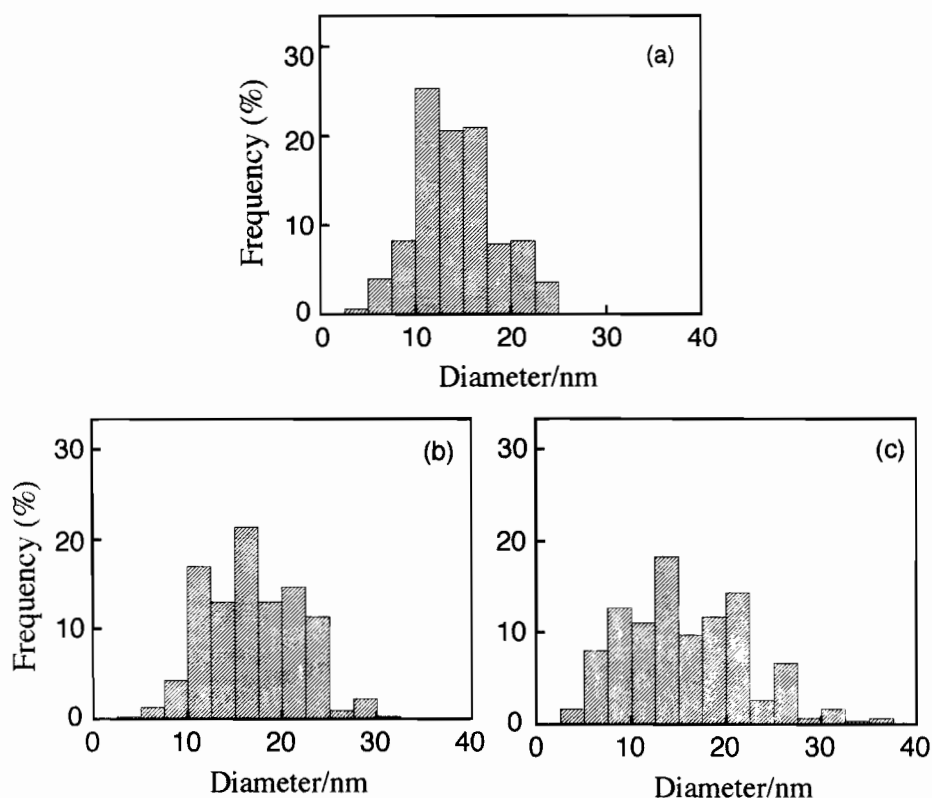


Figure 7.4. Size distributions of dispersed Au metal particles in the deposited films heat-treated at 400 (a), 500 (b), and 600 °C (c). Concentration of $(\text{NH}_4)_2\text{TiF}_6$: 0.1 mol dm^{-3} , of H_3BO_3 : 0.2 mol dm^{-3} , and of HAuCl_4 : $0.29 \text{ mmol dm}^{-3}$. Reaction time: 20 h.

A TEM photograph of the deposited film after heat-treated at 400 °C is shown in Fig. 7.3. In order to study them with the TEM, gold-dispersed thin films were removed from the substrates by exposure to hydrogen fluoride (HF) vapour. The Au metal particles are spherical and uniformly dispersed in the film. Particle-size distributions of the dispersed Au metal for the films heat-treated at 400, 500, and 600 °C are shown in Fig. 7.4. 300 Particles were counted to obtain the distributions shown. The size distributions became broad as the heat-treatment temperature increased. The mean particle sizes of dispersed Au metal are summarized in Table 7.1.

The optical absorption spectra of the deposited films after heat treatment for 1 h are shown in Fig. 7.5. The absorption spectrum of the as-deposited film showed no absorption bands except for that below 400 nm due to the interband transition of the TiO_2 matrix. The absorption bands due to the surface plasmon resonance of the Au metal fine particles were observed for the deposited films heat-treated above 200 °C. The plasmon band increased in intensity and shifted toward longer

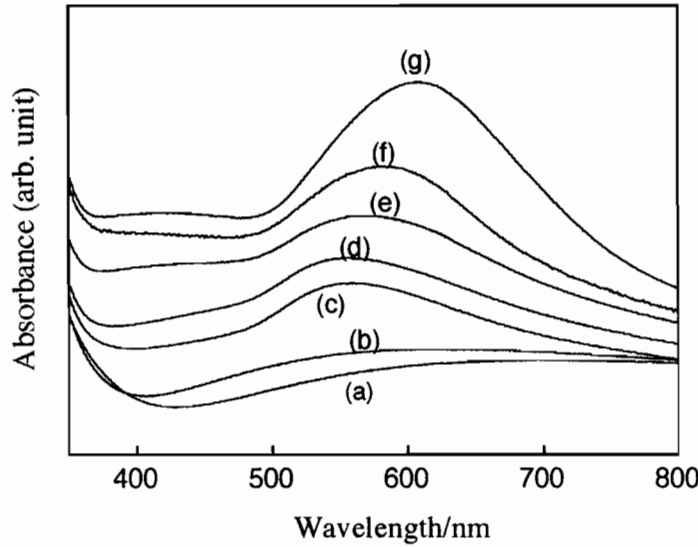


Figure 7.5. Optical absorption spectra of the deposited films heat-treated at various temperatures for 1 h. (a): As-deposited film, (b) to (g): films heat-treated at 100, 200, 300, 400, 500, and 600 °C, respectively. Concentration of $(\text{NH}_4)_2\text{TiF}_6$: 0.1 mol dm^{-3} , of H_3BO_3 : 0.2 mol dm^{-3} , and of HAuCl_4 : $0.29 \text{ mmol dm}^{-3}$. Reaction time: 20 h.

wavelengths from 555 to 608 nm, with increasing heat-treatment temperature. The change of the absorption peak position of the deposited films heat-treated at various temperatures is shown in Fig. 7.6. The peak wavelength shifted slightly to longer wavelengths up to 300 °C, then shifted markedly with increasing heat-treatment temperature. For other gold-dispersed glasses, similar red shifts have been reported [1, 2, 8]. The plasmon band is affected by the dispersed metal particle size, relative permittivity of the surrounding matrix, and the aggregation of the metal particles [8, 9, 10, 11, 12]. For colloidal gold particles in water, Bloemer *et al.* [11] reported that the peak wavelength of the surface plasmon resonance shifted *ca.* 12.5 nm toward longer wavelengths with increasing particle size from 5 to 30 nm. In our samples, the peak wavelength shifted by *ca.* 55 nm towards longer wavelengths with increasing the heat-treatment temperature, although the mean particle sizes of the dispersed gold are almost constant around 15 nm for the films heat-treated above 400 °C (Table 7.1). The absorption coefficient, α , of the plasmon band of gold-dispersed glass is expressed as follows [2]:

$$\alpha = p \frac{\omega}{nc} |f_1|^2 \epsilon_m'' \quad (7.3)$$

$$f_1(\omega) = \frac{3\epsilon_d}{\epsilon_m(\omega) + 2\epsilon_d} \quad (7.4)$$

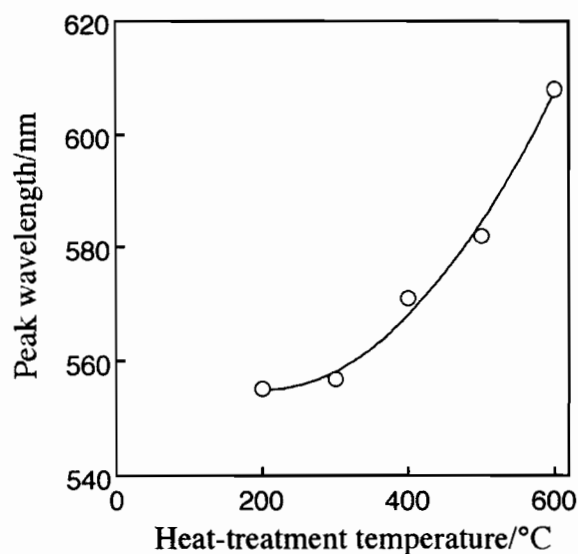


Figure 7.6. Relationship between the peak wavelength of the surface plasmon band of dispersed Au metal particles in the film and the heat-treatment temperature of the film. Concentration of $(\text{NH}_4)_2\text{TiF}_6$: 0.1 mol dm^{-3} , of H_3BO_3 : 0.2 mol dm^{-3} , and of HAuCl_4 : $0.29 \text{ mmol dm}^{-3}$. Reaction time: 20 h.

Where $\epsilon_m(\omega) = \epsilon'_m + i\epsilon''_m$ is the relative permittivity of the gold particles, ϵ_d is the relative permittivity of the matrix, p is the volume fraction of gold particles, ω is the wavelength, n is the refractive index of the matrix, c is the velocity of light, and f_1 is the local field factor. The maximum absorption given by

$$\epsilon_m' = -2\epsilon_d \quad (7.5)$$

The peak wavelength of the plasmon resonance depends on the relative permittivity of the dispersed gold particles, which depends on the particle size [2], and that of the matrix. As shown in Fig. 7.6, the peak wavelengths shifted markedly towards longer wavelengths for the films heat-treated above $300 \text{ }^\circ\text{C}$. From the XRD studies of the films (Fig. 7.2), the TiO_2 as matrix phase was transformed from amorphous to crystalline by heat-treatment above $300 \text{ }^\circ\text{C}$. Based on these results, the author concludes that the shift of the plasmon band toward longer wavelengths by the heat treatment was caused by the change in relative permittivity of the matrix due to the crystallization of TiO_2 .

7.3.2 Photoirradiation of the deposited films

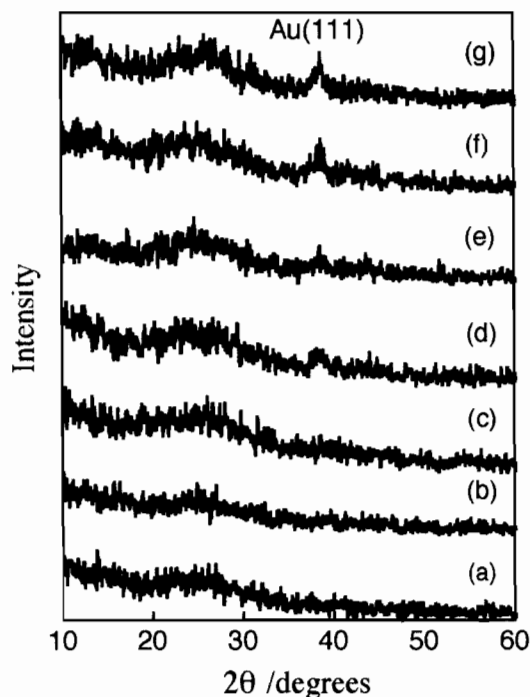


Figure 7.7. X-ray diffraction patterns of the deposited films irradiated for various time. (a): As-deposited film, (b) to (g): films irradiated for 20, 40, 60, 80, 100, and 120 min, respectively. Concentration of $(\text{NH}_4)_2\text{TiF}_6$: 0.1 mol dm^{-3} , of H_3BO_3 : 0.2 mol dm^{-3} , and of HAuCl_4 : $0.29 \text{ mmol dm}^{-3}$. Reaction time: 20 h.

In the previous section, Au^{III} ionic species in the as-deposited film were reduced to Au metal by heat treatment in an air flow. In this section, the author tried to reduce Au^{III} to Au metal by photoirradiation of the deposited film at ambient temperature.

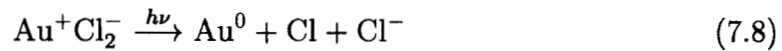
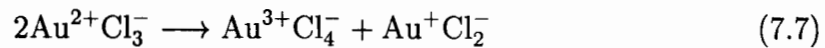
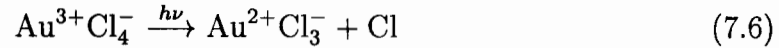
The XRD patterns of the deposited films which were irradiated for various time are shown in Fig. 7.7. The as-deposited film and the films irradiated for 20 and 40 min were amorphous without any significant diffraction peak. On the other hand, the diffraction peaks assigned to Au metal were observed for the films after irradiation for more than 60 min. The intensity of the diffraction peak at 38.1° which is assigned to (111) reflection line of cubic Au was increased as the irradiation time increased. As previously reported (*cf.* Section 7.3.1), heat treatment of the deposited film produces the dispersed Au metal particles accompanied by the crystallization of TiO_2 as matrix. For the present case, photoreduction of Au^{III} to Au metal, titanium oxide as matrix remains amorphous phase. The crystallite sizes of the dispersed Au metal particles which were calculated using Scherrer's equation [6] for the diffraction line from Au(111) are *ca.* 6 nm.

TEM photographs of the as-deposited film and the film irradiated for 20 and 100 min are shown in Fig. 7.8. In order to investigate with the TEM, thin films were scratched out from the substrates. As shown in Fig. 7.8 (a), any particles were not observed for the as-deposited film. For the irradiated films, Au metal particles dispersed in the film were observed. Content of the Au metal particles of the film irradiated for 100 min was more than that irradiated for 20 min. The Au particles were almost spherical and sizes of the dispersed Au particles were around 15 nm for the film irradiated for 20 min. Two kinds of particles were observed for the film irradiated for 100 min (Fig. 7.8 (c) and (d)). One is the smaller than the other. The sizes of the Au particles were around 10 to 50 nm and the size distribution of the dispersed Au particles seemed to be large. Both of the particles of the film irradiated for 100 min were not spherical, and they were constructed of several particles.

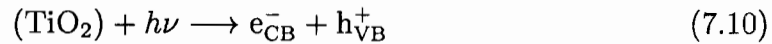
The optical absorption spectra of the deposited films after irradiated for various time are shown in Fig. 7.9. The irradiated films were kept in the dark for 48 h at ambient temperature before the spectra measurements. The absorption over 500 nm for the as-deposited film result from the interference of the light. The absorption band below 450 nm due to the interband transition of the matrix were observed for every sample. The absorption over the visible region increased by the irradiation of the film. Figure 7.10 shows the differential absorption spectra which subtracted the spectrum of the as-deposited film from that of the irradiated film. The absorption bands due to the surface plasmon resonance of the Au metal fine particles were observed around 550 nm, indicating the formation of Au metal particles upon the photoirradiation. The plasmon band increased in intensity and shifted toward longer wavelengths with increasing irradiation time. The change of the absorption peak position of the deposited films irradiated for various time is shown in Fig. 7.11. The peak wavelength shifted slightly toward longer wavelengths from 537 to 556 nm with increasing irradiation time. As mentioned in Section 7.3.1, the plasmon band is affected by the relative permittivity of the dispersed gold particles and of the surrounding matrix, and the volume fraction of the gold metal particles [8, 9, 10, 11, 12]. According to the Eqs. (7.3) and (7.5), the surface plasmon band intensified with increasing volume fraction of gold particles, and the peak wavelength depends on the relative permittivity of the dispersed gold particles, which depends on the particle size, and that of the matrix. The increasing of the absorbance due to the surface plasmon resonance with increasing irradiation time may be caused by the increasing of volume fraction of the dispersed gold particles. In the case of photoirradiated film, it is considered that the TiO_2 as the matrix does not change in the relative permittivity. Thus the shift of the peak wavelength is due to the change

of the dispersed particle size, that is, the change of the relative permittivity of the dispersed Au metal particles.

For the preparation of Au-dispersed silica gel by photoreduction of AuCl_4^- , Tanahashi and Tohda [13] proposed similar mechanisms to the photoreduction of AuCl_4^- ions in water and in microemulsions [14, 15]. According to them, AuCl_4^- ions have absorption at 320 nm and are photoreduced as follows:



In the present case, most of the photons lower than 450 nm may be absorbed by TiO_2 as the matrix (Fig 7.9). It is well known that the TiO_2 absorbed photon energy larger than the band gap, generating electrons in the conduction band (e_{CB}^-) and holes in the valence band (h_{VB}^+) as follows:



The generated charges then trapped by appropriate sites, as illustrated in Eqs. (7.11) and (7.12).



The subscript tr represents a trap. Au^{III} ions in the TiO_2 were reduced by such electrons according to



On the other hand, the trapped holes may react with H_2O or other species which contained in the film. The author therefore concludes that the reduction of Au^{III} species in the as-deposited film may occurred by both photochemically and photocatalytically.

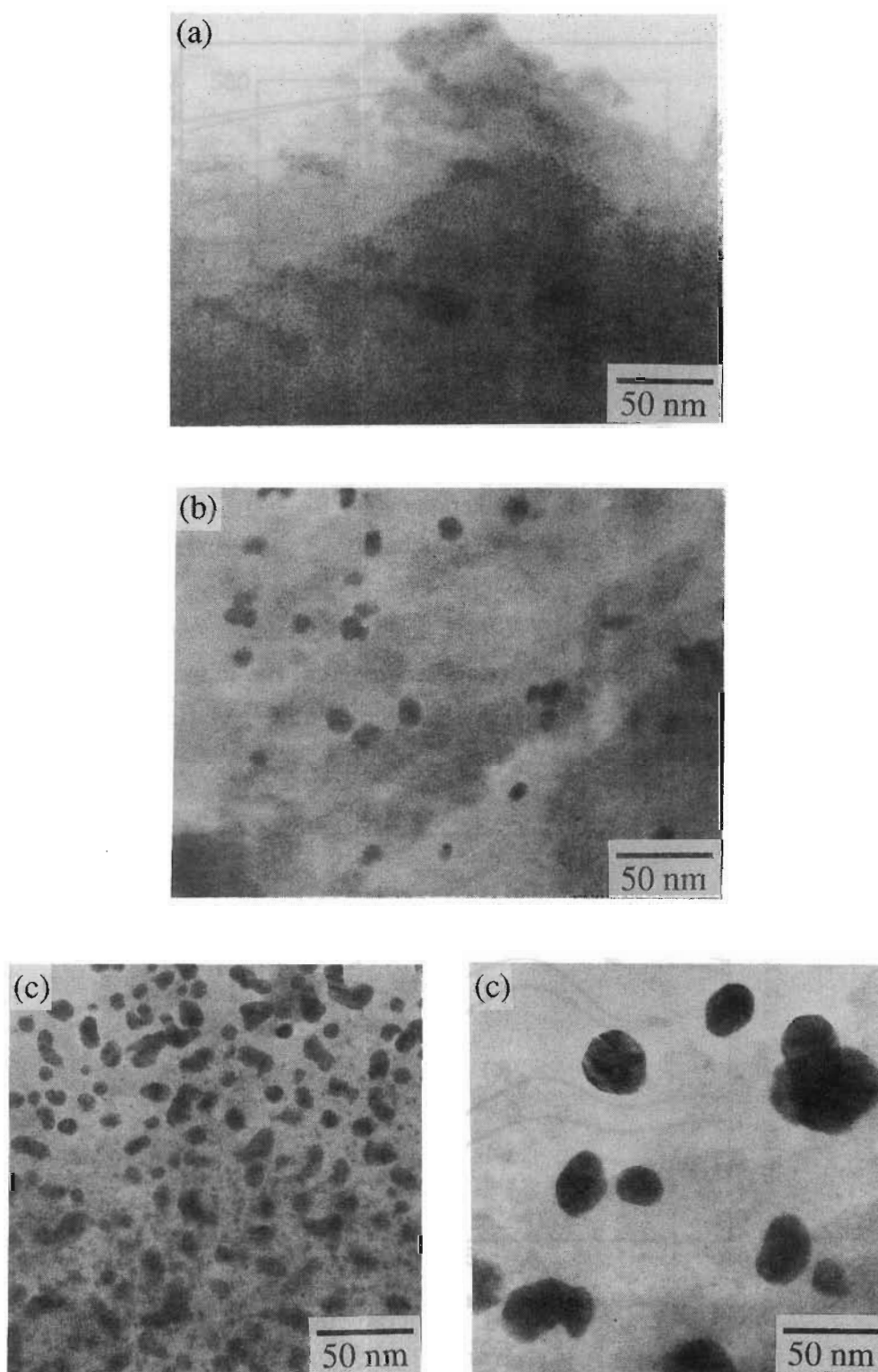


Figure 7.8. TEM photographs of the deposited film before irradiation (a) and after irradiation for 20 min (b) and 100 min (c). Concentration of $(\text{NH}_4)_2\text{TiF}_6$: 0.1 mol dm^{-3} , of H_3BO_3 : 0.2 mol dm^{-3} , and of HAuCl_4 : $0.29 \text{ mmol dm}^{-3}$. Reaction time: 20 h.

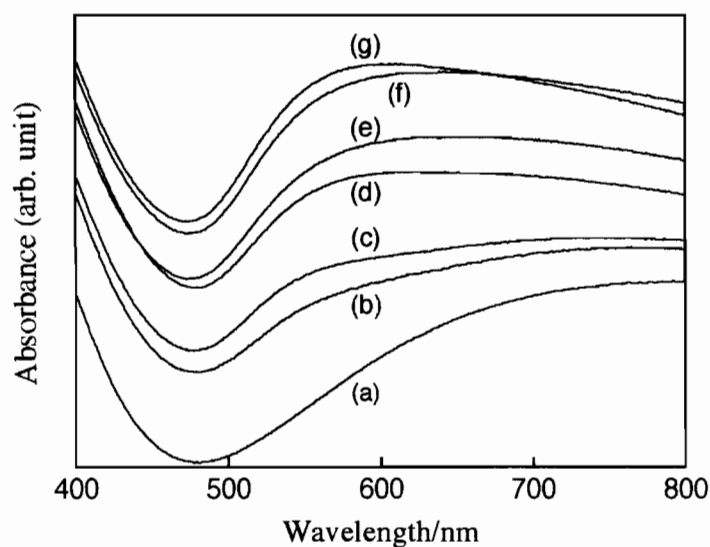


Figure 7.9. Optical absorption spectra of the deposited films irradiated for various time. (a): As-deposited film, (b) to (g): films irradiated for 20, 40, 60, 80, 100, and 120 min, respectively. Before spectra measurements, the films were kept in the dark for 48 h. Concentration of $(\text{NH}_4)_2\text{TiF}_6$: 0.1 mol dm^{-3} , of H_3BO_3 : 0.2 mol dm^{-3} , and of HAuCl_4 : $0.29 \text{ mmol dm}^{-3}$. Reaction time: 20 h.

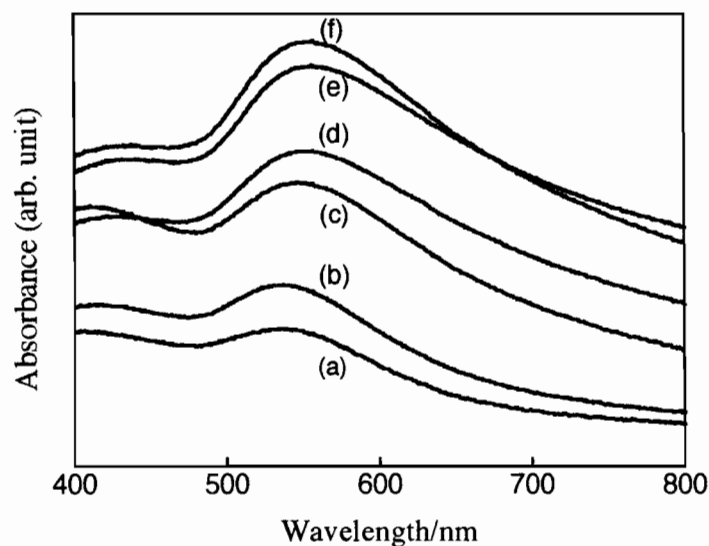


Figure 7.10. Differential optical absorption spectra of the deposited films irradiated for various time. (a) to (f): Films irradiated for 20, 40, 60, 80, 100, and 120 min, respectively. Before spectra measurements, the films were kept in the dark for 48 h. Concentration of $(\text{NH}_4)_2\text{TiF}_6$: 0.1 mol dm^{-3} , of H_3BO_3 : 0.2 mol dm^{-3} , and of HAuCl_4 : $0.29 \text{ mmol dm}^{-3}$. Reaction time: 20 h.

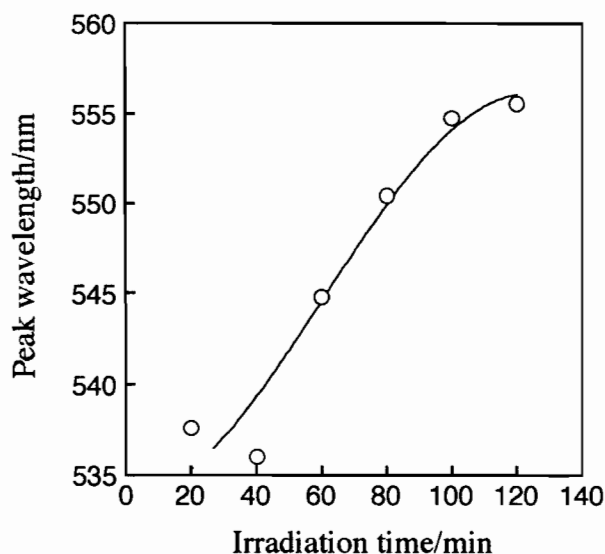


Figure 7.11. Relationship between peak wavelength of surface plasmon band of dispersed Au metal particles in the film and irradiation time. Concentration of $(\text{NH}_4)_2\text{TiF}_6$: 0.1 mol dm^{-3} , of H_3BO_3 : 0.2 mol dm^{-3} , and of HAuCl_4 : $0.29 \text{ mmol dm}^{-3}$. Reaction time: 20 h.

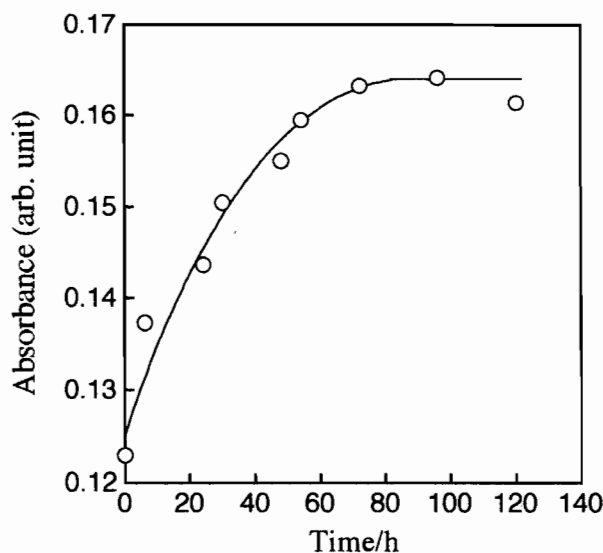


Figure 7.12. Time course of absorbance at 550 nm after irradiation for 120 min. Concentration of $(\text{NH}_4)_2\text{TiF}_6$: 0.1 mol dm^{-3} , of H_3BO_3 : 0.2 mol dm^{-3} , and of HAuCl_4 : $0.29 \text{ mmol dm}^{-3}$. Reaction time: 20 h.

Figure 7.12 shows the time course of absorbance at 550 nm, which is the peak wavelength of the surface plasmon band, of the film after irradiation of 100 min. The films were stored in the dark at ambient temperature before the spectra measurements. The peak wavelength did not change with elapsed time. As shown in Fig. 7.12, the absorbance of surface plasmon band increased with elapsed time until 72 h after the irradiation and then became constant. The details are indistinct, but it suggests that the increasing the number of dispersed gold particles and/or the growth of dispersed gold particles may occur in the dark. Further investigation is necessary to determine the mechanism of photoreduction of Au^{III} ions in titanium oxide.

7.4 Conclusion

We have developed a very simple process for the preparation of Au-dispersed TiO₂ thin films. The TiO₂ thin film containing Au^{III} ions was formed by the LPD method from a mixed solution of (NH₄)₂TiF₆, H₃BO₃, and HAuCl₄ at ambient temperature and atmosphere. The Au content in the film was controlled easily by controlling the concentration of HAuCl₄ in the treatment solution.

Heat treatment of the deposited film above 200 °C produced Au metal particles which were *ca.* 15 nm in diameter. The size distribution of the dispersed Au particles became broad as the heat-treatment temperature increased. Crystallization of TiO₂ as the matrix occurred simultaneously with formation of Au metal particles during the heat treatment. Surface plasmon resonance bands were observed for the films heat-treated above 200 °C. The peak wavelength shifted by *ca.* 55 nm towards longer wavelengths following the heat treatment. The shift of the peak position is caused by the change of the relative permittivity of the TiO₂ as the matrix crystallized.

Photoirradiation of the deposited film also produced dispersed Au particles. Particle size of the dispersed Au metal became large as irradiation time increased. The size distribution of the particles seemed to be large. Surface plasmon resonance bands due to the dispersed Au particles were observed for the photoirradiated films. The surface plasmon band intensified with increasing irradiation time, indicating that the volume fraction of dispersed Au metal particles in the film increased as irradiation time. The shift of the surface plasmon band with increasing irradiation time, which due to the change of the dispersed Au particle size, that is the change of the relative permittivity of dispersed Au, was observed. Photoreduction of Au^{III} ionic species in the as-deposited film to Au metal may occurred by both photochemically and photocatalytically.

References

- [1] T. Kineri, M. Mori, K. Kadono, T. Sakaguchi, M. Miya, H. Wakabayashi, and T. Tsuchiya, *J. Ceram. Soc. Jpn.* **101**, 1340 (1993).
- [2] K. Fukumi, A. Chayahara, K. Kadono, T. Sakaguchi, Y. Horino, M. Miya, K. Fujii, J. Hayakawa, and M. Satou, *J. Appl. Phys.* **75**, 3075 (1994).
- [3] J. Matsuoka, R. Mizutani, S. Kaneko, H. Nasu, K. Kamiya, K. Kadono, T. Sakaguchi, and M. Miya, *J. Ceram. Soc. Jpn.* **101**, 53 (1993).
- [4] H. Shinojima, J. Yumoto, and N. Uesugi, *Appl. Phys. Lett.* **60**, 298 (1992).
- [5] B. L. Justus, M. E. Seaver, J. A. Ruller, and A. J. Campillo, *Appl. Phys. Lett.* **57**, 1381 (1990).
- [6] B. E. Warren, in *X-ray Diffraction*, Dover Publications, New York, p.253 (1969).
- [7] J. J. Pireaux, M. Liehr, P. A. Thiry, J. P. Delrue, and R. Caudano, *Surf. Sci.* **141**, 221 (1984).
- [8] U. Kreibig, *J. Phys. Coll. C* **2**, 97 (1977).
- [9] U. Kreibig and L. Genzel, *Surf. Sci.* **156**, 678 (1985).
- [10] R. H. Doremus, *J. Chem. Phys.* **40**, 2389 (1964).
- [11] M. J. Bloemer, J. W. Haus, and P. R. Ashley, *J. Opt. Soc. Am. B* **7**, 790 (1990).
- [12] G. W. Arnold, *J. Appl. Phys.* **46**, 4466 (1975).
- [13] I. Tanahashi and T. Tohda, *J. Am. Ceram. Soc.* **79**, 796 (1996).
- [14] K. Kurihara, J. Kizling, P. Stenius, and J. H. Fendler, *J. Am. Chem. Soc.* **105**, 2574 (1983).
- [15] Y. Yonezawa, T. Sato, M. Ohno, and H. Hada, *J. Chem. Soc., Faraday Trans. 1* **83**, 1559 (1987).

Chapter 8

Summary

In the present thesis, preparation, characterization, and properties of metal oxide thin films by the Liquid-Phase Deposition (LPD) method were studied. The results were summarized as follows.

In Chapter 2, titanium (IV) oxide (anatase) thin films have been prepared from an aqueous solution system of $(\text{NH}_4)_2\text{TiF}_6$ and H_3BO_3 by the LPD method. The aspects and chemical composition of the formed films were different according to the concentrations of $(\text{NH}_4)_2\text{TiF}_6$ and H_3BO_3 . At low concentration range of $(\text{NH}_4)_2\text{TiF}_6$, hazy or transparent TiO_2 (anatase) thin film was formed, and at high concentration of $(\text{NH}_4)_2\text{TiF}_6$, micro-crystalline of NH_4TiOF_3 was deposited. Thickness of the deposited TiO_2 film increased linearly with reaction time. Crystallinity of the deposited TiO_2 thin film was improved upon the heat treatment. The heat treated film showed photoelectrochemical behavior. Photocurrent due to the decomposition of water increased with increasing heat treatment temperature.

In Chapter 3, the QCM technique was applied to the monitoring thin film formation by the LPD method. This is the first attempt to monitor the growth of thin film by the LPD method with QCM technique. The linear relationship was observed between the thickness measured by the QCM technique and that measured by the direct observation with a SEM, indicating that it is possible to monitor the growth of thin film by the LPD method with QCM technique. In Chapter 3, The effects of the concentration of free F^- , $(\text{NH}_4)_2\text{TiF}_6$, and H_3BO_3 on the titanium oxide thin film formation were studied. The initial stage of the deposition reaction, the induction period, free F^- ions in the treatment solution preferentially react with H_3BO_3 . The induction time depended on the concentration of free F^- , and the film formation rate depended on the concentration of free F^- . The film formation rate increased and induction period decreased with increasing H_3BO_3 concentration. As $(\text{NH}_4)_2\text{TiF}_6$ concentration increased, the film formation rate decreased, and the dependence of the induction period on $(\text{NH}_4)_2\text{TiF}_6$ concentration was small.

In Chapter 4, the LPD method was applied to the preparation of vanadium oxide thin films. $(\text{V}_2\text{O}_5\text{-HF})$ solution was used as the treatment solution, and aluminum metal was used as F^- scavenger. The as-deposited film was amorphous and consisted of reduced state vanadium ions. The film was crystallized and oxidized upon the heat treatment. The film heat-treated at $300\text{ }^\circ\text{C}$ consisted of mixed compounds of V_3O_7 and V_2O_5 , and the film heat-treated at $400\text{ }^\circ\text{C}$ was V_2O_5 . The vanadium oxide was formed through the ligand-exchange (hydrolysis) reaction of $[\text{VOF}_n]^{2-n}$ which was accelerated by the addition of aluminum metal as F^- scavenger. The crystallized film showed reversible color change when lithium ion was electrochemically intercalated and deintercalated, that is electrochromism. On injected charge

by applying an external voltage with the polarity of the V_2O_5 film negative, the optical absorption above 650 nm increased. The absorbance was increased linearly with charge injection, and it decreased gently with charge extraction. Although the whole injected charges extracted from the colored film, the absorbance was not agree with that of the initial state. It suggests that the positive charges which do not act the coloring process are extracted during the bleaching process.

In Chapter 5, VO_2 thin film has been prepared by heat treatment of the vanadium oxide thin film obtained by the LPD method in an N_2 atmosphere. Monoclinic VO_2 thin film was obtained upon the heat treatment above 400 °C in an N_2 atmosphere. No other phases were detected by XRD studies. The obtained VO_2 thin film was partially oriented to the [001] direction. The obtained VO_2 thin film exhibited metal-to-semiconductor transition behavior around 70 °C. The transition behavior depended on the preparation condition of the film.

In Chapter 6, the LPD method was applied to the preparation of iron oxide thin films. The crystalline β - $FeOOH$ thin film was formed by the LPD method from a mixed solution of $FeOOH \cdot NH_4F \cdot HF$ and H_3BO_3 at ambient temperature. XRD measurements revealed that the film deposited at higher concentration of H_3BO_3 was oriented to the [211] direction. On the other hand, the formed film was randomly oriented when the concentration of H_3BO_3 was low. On heat treatment in an air flow, the deposited film (crystalline β - $FeOOH$) was changed to amorphous, and was transformed into α - Fe_2O_3 completely at 600 °C. The iron hydroxide thin film was formed through the ligand-exchange (hydrolysis) reaction of $[FeF_6]^{3-}$ or partially hydrolyzed species, $[FeF_{6-n}(OH)_n]^{3-}$ which was accelerated by the addition of H_3BO_3 as F^- scavenger.

The LPD method can be applied readily to the preparation of multi-component oxide thin films by the addition of the objective metal ion to the treatment solution, because it is performed in an aqueous solution system which is a typical homogeneously mixing system. In Chapter 7, Au-dispersed TiO_2 (anatase) thin films have been prepared by the LPD method. The titanium oxide thin film containing Au^{III} ions was formed from mixed solution of $(NH_4)_2TiF_6$, H_3BO_3 , and $HAuCl_4$ by the LPD method. The Au content in the film was controlled easily by controlling the concentration of $HAuCl_4$ in the treatment solution. Heat treatment of the deposited film above 200 °C in an air flow produced dispersed Au metal particles, accompanied by the crystallization of titanium oxide as a matrix. The optical absorption band due to the surface plasmon resonance of dispersed Au metal particles shifted toward longer wavelengths with increasing heat treatment temperature. This shift is caused by the change of the relative permittivity of the matrix crystallized. Photoir-

radiation of the as-deposited film also produced dispersed Au metal particles. The surface plasmon resonance band intensified and shifted toward longer wavelengths as irradiation time increased. The increasing of absorbance was caused by the increasing of the volume fraction of the dispersed Au, and the shift was due to the change of dispersed Au particle size. Photoreduction of Au^{III} may occurred both photochemically and photocatalytically.

The LPD method is a very simple process to preparation of metal oxide thin films. The metal oxide or multi-component oxide thin films form directly on the substrate from an aqueous solution system. This process is milder and more cost-effective than the conventional methods such as vacuum evaporation, sputtering, chemical vapor deposition, and sol-gel method, because it does not require special equipment and expensive reagents. There are, however, several problems. Several advantages and problems are summarized in Table. 8.1. The author is of the opinion that such problems are possible to improve.

Advantages	Problems
<ul style="list-style-type: none"> • Operation is easy. • Operation temperature is low. • Substrate is unrestricted (material, area, and morphology). • Does not require special apparatus and high energy. • Multi component oxide films are obtained readily and composition control is easy. 	<ul style="list-style-type: none"> • Processing time is long. • Containing fluorine as impurity. • Remaining water. • Generating cracks when drying or heat treatment procedure (depends on product). • Treatment of fluoride is uneasy. • By-product precipitates in bulk (depends on product).

Table 8.1. Characteristics of the LPD method.

In the present study, the LPD method was applied to the preparation of several metal oxide thin films, and characterization of the formed films were studied. Figure 8.1 shows the possibility of preparing oxide thin films by the LPD method so far. It may be possible to preparation of other metal oxide and multi-component oxide thin films by the LPD method. In the future, further studies with respect to the mechanism of the formation of thin films by the LPD method are necessary to establish the LPD method as more well-defined process. The author expects that the LPD method is utilized widely.

	1	2	3	4	5	6	7	8	9	10	11	12	13	14	15	16	17	18
1	1 H																	2 He
2	3 Li	4 Be											5 B	6 C	7 N	8 O	9 F	10 Ne
3	11 Na	12 Mg											13 Al	14 Si	15 P	16 S	17 Cl	18 Ar
4	19 K	20 Ca	21 Sc	22 Ti	23 V	24 Cr	25 Mn	26 Fe	27 Co	28 Ni	29 Cu	30 Zn	31 Ga	32 Ge	33 As	34 Se	35 Br	36 Kr
5	37 Rb	38 Sr	39 Y	40 Zr	41 Nb	42 Mo	43 Tc	44 Ru	45 Rh	46 Pd	47 Ag	48 Cd	49 In	50 Sn	51 Sb	52 Te	53 I	54 Xe
6	55 Cs	56 Ba	57-71 La-Lu	72 Hf	73 Ta	74 W	75 Re	76 Os	77 Ir	78 Pt	79 Au	80 Hg	81 Tl	82 Pb	83 Bi	84 Po	85 At	86 Rn
7	87 Fr	88 Ra	89-103 Ac-Lr	104	105	106	107											

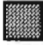

 oxide or oxy-hydroxide
 oxy-fluoride

Figure 8.1. Possibility of preparation of oxide thin films by the LPD method.

Publication list

Chapter 2

S. Deki, Y. Aoi, O. Hiroi, and A. Kajinami

“Titanium (IV) oxide thin films prepared from aqueous solution”

Chem. Lett., 433 (1996).

Chapter 3

S. Deki, Y. Aoi, Y. Asaoka, A. Kajinami, and M. Mizuhata

“Monitoring the growth of titanium oxide thin films by liquid-phase deposition method with the quartz crystal microbalance”

J. Mater. Chem., submitted.

Chapter 4

S. Deki, Y. Aoi, Y. Miyake, A. Gotoh, A. Kajinami, and Y. Kanaji

“Vanadium oxide and vanadium-titanium oxide thin films prepared from aqueous solution”

Proc. Symp. Electrochemically Deposited Thin Films, **93-26**, 402 (1993).

S. Deki, Y. Aoi, Y. Miyake, A. Gotoh, and A. Kajinami

“Novel wet process for preparation of vanadium oxide thin film”

Mater. Res. Bull. **31**, 1399 (1996).

Chapter 5

S. Deki, Y. Aoi, and A. Kajinami

“Novel wet process for preparation of vanadium dioxide thin film”

J. Mater. Sci., submitted.

Chapter 6

S. Deki, Y. Aoi, J. Okibe, H. Yanagimoto, A. Kajinami, and M. Mizuhata

“Preparation and characterization of iron hydroxide and iron oxide thin films by a liquid-phase deposition method”

in preparing.

Chapter 7

S. Deki, Y. Aoi, H. Yanagimoto, K. Ishii, K. Akamatsu, M. Mizuhata, and

A. Kajinami

“Preparation and characterization of Au-dispersed TiO₂ thin films by a liquid-phase deposition method”

J. Mater. Chem. **6**, 1879 (1996).

S. Deki, Y. Aoi, H. Yanagimoto, K. Ishii, K. Akamatsu, M. Mizuhata, and

A. Kajinami

“Photo-assisted preparation of Au-dispersed TiO₂ thin films by a liquid-phase deposition method”

in preparing.

Oral presentation list

1. S. Deki, O. Hiroi, Y. Aoi, A. Kajinami, and Y. Kanaji
“Thin film formation by using the equilibrium reaction in the aqueous solution”
'91 Autumn Meeting of the Electrochemical Society of Japan
Nagoya, October 1991.
2. S. Deki, Y. Aoi, A. Kajinami, and Y. Kanaji
“Electrical conductivity of vanadium oxide thin film prepared by liquid-phase deposition”
59th General Meeting of the Electrochemical Society of Japan
Hachioji, April 1992.
3. S. Deki, Y. Aoi, A. Kajinami, and Y. Kanaji
“Photoelectrochemical properties of TiO₂ thin films prepared by the liquid-phase deposition method”
60th General Meeting of the Electrochemical Society of Japan
Tokyo, April 1993.
4. S. Deki, Y. Aoi, A. Gotoh, A. Kajinami, and Y. Kanaji
“Vanadium oxide and vanadium-titanium oxide thin films prepared from aqueous solution”
The Electrochemical Society 183rd Meeting
Honolulu, May 1993.
5. S. Deki, Y. Aoi, A. Kajinami, and Y. Kanaji
“Iron oxide thin film prepared by the liquid-phase deposition method”
65th National Meeting of the Chemical Society of Japan
Tokyo, March 1993.
6. S. Deki, Y. Aoi, Y. Miyake, A. Gotoh, A. Kajinami, and Y. Kanaji
“Preparation of vanadium oxide thin films from aqueous solution and their electrochromic properties”
60th General Meeting of the Electrochemical Society of Japan
Sendai, April 1994.
7. S. Deki, Y. Aoi, S. Yamahira, and A. Kajinami
“Electrochemical behavior of vanadium oxide thin film deposited from aqueous solution”
'95 Asian Conference on Electrochemistry
Suta, May 1995.

8. S. Deki, Y. Aoi, and A. Kajinami
“Preparation of vanadium oxide thin films from aqueous solution and their metal-semiconductor transition”
'95 Autumn Meeting of the Electrochemical Society of Japan
Kofu, September 1995.
9. Y. Aoi, A. Kajinami, and S. Deki
“Metal oxide thin films prepared from aqueous solution”
MRSJ symposium
Kawasaki, December 1995.
10. S. Deki, H. Yanagimoto, Y. Aoi, and A. Kajinami
“Preparation of Au/TiO₂ composite thin film from aqueous solution”
70th National Meeting of the Chemical Society of Japan
Tokyo, March 1996.
11. S. Deki, Y. Aoi, and A. Kajinami
“Preparation of Au/MO_x (M =Ti, Fe) composite thin films from aqueous solution”
63th General Meeting of the Electrochemical Society of Japan
Tokyo, April 1996.
12. S. Deki, Y. Aoi, S. Miyano, Y. Matsuura, and A. Kajinami
“Preparation of titanium oxide thin films from aqueous solution and their photocatalytic properties”
63th General Meeting of the Electrochemical Society of Japan
Tokyo, April 1996.
13. S. Deki, Y. Aoi, and A. Kajinami
“Preparation of metal-dispersed oxide thin films by liquid-phase deposition”
57th Meeting of the Japan Society of Applied Physics
Fukuoka, September 1996.